2013

TISSUE ENGINEERING COMPOSITE BIOMIMETIC GELATIN SPONGES FOR BONE REGENERATION

Isaac Rodriguez
Virginia Commonwealth University

School of Engineering
Virginia Commonwealth University

This is to certify that the dissertation prepared by Isaac Anthony Rodríguez entitled Tissue Engineering Composite Biomimetic Gelatin Sponges for Bone Regeneration has been approved by his committee as satisfactory completion of the dissertation requirement for the degree of Doctor of Philosophy in Biomedical Engineering

Gary L. Bowlin, Ph.D., Director of Dissertation, School of Engineering

Peter C. Moon, Ph.D., School of Dentistry

Hu Yang, Ph.D., School of Engineering

Christopher A. Lemmon, Ph.D., School of Engineering

Parthasarathy Madurantakam, D.D.S., M.D.S., Ph.D., School of Dentistry

Matthew J. Beckman, Ph.D., Pharmacology and Toxicology

Scott A. Sell, Ph.D., Parks College of Engineering, Aviation and Technology, St. Louis University

Gerald E. Miller, Ph.D., Chair of Biomedical Engineering, School of Engineering

Barbara D. Boyan, Ph.D., Dean, School of Engineering

F. Douglas Boudinot, Ph.D., Dean of the School of Graduate Studies

May 2013

TISSUE ENGINEERING COMPOSITE BIOMIMETIC GELATIN SPONGES FOR BONE REGENERATION

A dissertation submitted in partial fulfillment of the requirements for the degree of Doctor of Philosophy in Biomedical Engineering at Virginia Commonwealth University.

by

ISAAC ANTHONY RODRIGUEZ
Bachelor of Science, University of Virginia, 2007
Master of Science, Virginia Commonwealth University, 2010

Director: GARY L. BOWLIN, PH.D.
Professor, Biomedical Engineering

Virginia Commonwealth University
Richmond, Virginia
May 2013

Acknowledgement

First of all I would like to thank Dr. Gary Bowlin for giving me the opportunity to work in his lab. He has been an exceptional mentor always setting high goals for me. I also wanted to thank my advisors and committee members: Dr. Peter Moon, Dr. Hu Yang, Dr. Matthew Beckman, Dr. Scott Sell. Dr. Parth Madurantakam, and Dr. Christopher Lemmon for their support and guidance throughout this project.

Bone tissue engineering is a field I was always interested in and this has been a great experience and opportunity. I want to acknowledge Dr. Parthasarathy Madurantakam who was the one who gave me the opportunity to work with him and trained me in the lab. Without his guidance I would not be where I am today. I also want to thank my current/former lab colleagues Dr. Michael McClure, Dr. Patricia Wolfe, Dr. Koyal Garg, Jennifer McCool, Yas Maghdouri Moghaddam, Andrew Spence, Daniel Abebayehu, Gunjan Saxena, and Ryan Clohessy for their assistance and for making lab a fun environment to work in. Special thanks to Gunjan and Scott who assisted with this project.

Last but not least I would like to thank my family. None of this would be possible without their love and support. I specifically want to recognize my Mom (Becky), Dad (Jose), sister (Kayla), stepmom (Kristi), and girlfriend (Pamela) for always believing in and encouraging me. I also consider my fraternity, La Unidad Latina, Lambda Upsilon Lambda Fraternity, Inc. my family and want to thank my Hermanos for their support.

Table of Contents

List of Tables

List of Figures

Abstract

TISSUE ENGINEERING COMPOSITE BIOMIMETIC GELATIN SPONGES FOR BONE REPAIR

By Isaac Anthony Rodríguez, M.S.

A Dissertation submitted in partial fulfillment of the requirements for the degree of Doctor of Philosophy in Biomedical Engineering at Virginia Commonwealth University.

Virginia Commonwealth University, 2013

Major Director: Dr. Gary L. Bowlin
Professor, Biomedical Engineering

The field of tissue engineering aims to develop viable substitutes with the ability to repair and regenerate the functions of damaged tissue. Common practices to supplement bone regeneration in larger defects include bone graft biomaterials such as autografts, allografts, xenografts, and synthetic biomaterials. Autologous bone grafting is the current gold-standard procedure used to replace missing or damaged bone. However, these grafts have disadvantages such as donor site morbidity, limited availability, and the need for a secondary surgery. The focus of this study is to tissue engineer a lyophilized gelatin composite sponge composed of hydroxyapatite (HA), chitin whiskers (CW), and preparations rich in growth factors (PRGF) to provide sufficient structural support to the defect site while enhancing the body's own reparative capacity, ultimately eliminating the need for autologous tissue harvesting or repeat operations.

The present study investigates several *in vitro* evaluations on multiple compositions of modified gelatin sponge scaffolds for use in bone graft applications. Gelatin sponges were fabricated via freeze-drying, enhanced with PRGF, HA, and/or CW, and cross-linked with 50 mM 1-Ethyl-3-(3-dimethylaminopropyl)carbodiimide hydrochloride (EDC) either during or post gelation. Initial evaluation of all scaffold combinations indicated that scaffolds released contents up to 90 days, EDC cross-linking during gelation allowed for more protein release, and had the ability to swell. Since the incorporation of PRGF, HA, and CW increased cell infiltration, and production of cell-created mineral matrix over 90 days in culture, these scaffolds were further characterized. Freeze-dried gelatin sponges enhanced with PRGF, HA, and CW and cross-linked during gelation with EDC (PHCE) were mineralized (M) in 5x revised simulated body fluid (r-SBF) for 1 hour to create a bone-like mineral surface. Gelatin EDC scaffold controls (GE), GE-M, PHCE, and PHCE-M scaffolds were characterized for their ability to swell, mineralizing potential, surface morphology, growth factor incorporation and release, uniaxial compression properties, and cell attachment, proliferation, infiltration, and protein/cytokine secretion.. After mineralization, scanning electron microscopy showed sparse clusters of mineral deposition for GE-M scaffolds while PHCE-M scaffolds exhibited a more uniform mineral deposition. Both GE and PHCE scaffolds were porous structures that swelled up to 50% of their original volume upon hydration. Over 21 days incubation, PHCE-M scaffolds cumulatively released about 30% of their original protein content, significantly more than all other scaffolds. Multiplex Luminex assays confirmed the successful incorporation of PRGF growth factors within PRGF sponges. For acellular uniaxial compression testing,

PHCE-M scaffolds reported lower Young's modulus values (1.3 - 1.6 MPa) when compared to GE and GE-M scaffolds (1.6 – 3.2 MPa). These low modulus values were comparable to values of tissue found in early stages of bone healing. DAPI (4',6-diamidino-2-phenylindole) staining and imaging showed an increase in initial cell attachment and infiltration of PHCE and PHCE-M scaffolds on day 1. GE-M scaffolds also appeared to attach more cells than the GE control. MTS cell proliferation assay results indicated that on days 4 and 7, PHCE scaffolds increased cell proliferation (compared to GE controls). MTS also illustrated that the addition of a mineral coating increases and decreases cell proliferation on GE-M and PHCE-M scaffolds, respectively. Multiplexer analysis of MG-63 protein/cytokine secretion suggests that cells are responding in a bone regenerative fashion on all scaffolds, as evidence of osteocalcin secretion. Little to no secretion of osteopontin, IL-1β, and TNF-α demonstrates that scaffolds are not influencing cells to secrete factors associated with bone resorption. The compressive mechanical properties of cellularized scaffolds did not differ much from acellular scaffolds. The collective results indicated increased cellular attachment, infiltration, and bone regenerative protein/cytokine secretion by cells on GE-M scaffolds, which support the addition of a bone-like mineral surface on GE scaffolds. Cellularized PHCE and PHCE-M scaffolds report similar advantages as well as Young's modulus values in the range of native tissues present in the early stages of bone healing. The results of this study propose that the developed PHCE and PHCE-M scaffolds exhibit good cellular responses and mechanical properties for use in early bone healing applications.

1. ALTERNATIVE BONE GRAFTS – A CLINICAL NEED

1.1. INTRODUCTION

Healthy bone has the unique ability to spontaneously regenerate. However, bone injuries, particularly large bone defects/injuries, lack the ability to heal and have a severely limited reparative capacity ultimately requiring surgical intervention and replacement. Autologous bone grafting is the current gold-standard procedure used to replace missing or damaged bone and has been used for the regeneration of bone for multiple applications: dental implants (restore area of a missing tooth), spinal fusion, and repairing broken bones (that have bone loss or have not yet healed). Currently, there are more than 500,000 bone grafting surgeries performed in the United States each year, averaging between $33,860 to $37,227 per procedure, not including other expenses such as surgeon/anesthesiologist fees and hospital/medication charges [1, 2]. Although autologous bone grafting produces satisfactory results, these grafts carry the risk of donor site morbidity as well as limited availability. Other grafting options such as synthetic materials (metals and ceramics) elicit a foreign body response and are not biodegradable. The increasing number of bone grafts performed in the U.S. annually, combined with the drawbacks of autografts, has created a shortage of cadaver allografts and a need to increase musculoskeletal tissue donation. As a result, there has been an increase in corporate interest in regards to developing alternative bone grafting substitutes which include (but are not limited to) the use of natural, synthetic, human, and animal-derived biomaterials. The sales of bone grafts and bone-graft substitutes in the US have increased from 0.3 to 1.5 billion dollars from 1999 – 2009 with

increased spending on bone substitutes, platelet concentrators, bone morphogenetic proteins, and more [1]. This dissertation will particularly focus on tissue engineering a lyophilized (or freeze-dried) gelatin sponge enhanced with concentrated platelet-derived growth factors and bone extracellular matrix (ECM) factors which may provide sufficient structural support to the defect site while enhancing the body's own reparative capacity, ultimately eliminating the need for autologous tissue harvesting or repeat operations.

1.2. CURRENT TREATMENT OPTIONS FOR BONE GRAFTS

Common practices to supplement bone regeneration in larger defects include bone graft biomaterials such as autograft (patient's own bone), allograft (human cadaver bone), xenograft (animal bone), and synthetic biomaterials (i.e. ceramics, cements, glasses, metals, polymers, and composites) [2-6]. The most common hard tissue graft is an autograft, whereby bone is taken from the patient's own body and reimplanted into the defect site. Autologous bone grafts harvested from patient donor sites are osteoconductive (provide a scaffold where bone cells can proliferate), osteoinductive (induce proliferation of undifferentiated cells and their differentiation into osteoblasts), and osteogenic (provide a reservoir of skeletal stem and progenitor cells that can form new bone) [3]. Autografts are the best material for bone repair because of their supreme histocompatibility without the risk of disease transfer [4]. However, their limited availability, additional invasive surgery, and significant donor site morbidity (as shown in Table 1.1) are all drawbacks which encourage the development of alternative bone substitutes [3, 5-10]. The most frequently used donor site for autologous bone grafts is cancellous iliac bone. Alternative

donor sites have been explored [11, 12], however even these suffer the same drawbacks mentioned above.

Table 1.1 – Reported complication rates of harvesting iliac crest bone for autografts [10]. Reprinted with permission from Springer.

Complication	Reported rate of occurrence
Minor complications	10–39 %
Superficial infections	
Superficial seromas	
Superficial hematomas	
Major complications	5.8–10 %
Herniation	
Vascular injuries	
Deep infections at the donor site	
Neurologic injuries	
Deep hematoma formation requiring OR	
Iliac wing fractures	
Chronic donor site pain (>24 months)	25–60 %
Reoperation due to wound complications	2–5 %
Poor appearance of graft site	5–16 %
Harvest site numbness	24 %
Pain, paresthesias, hematoma, infection	Up to 50 %
Difficulty in daily activities at 36 mo post-op	18–19 %

Allografts are an option for bone grafting because they are harvested from cadaver donors which means they are readily available, can be prepared in various shapes/sizes and there is no need to compromise or sacrifice the patient's own bone (no donor site morbidity or secondary surgery for harvesting). The main disadvantage of allografts is the potential for disease transfer. Although, the allograft providers do their best to inactivate viruses,

there is still the possibility that not all infectious contents (such as blood and cellular components) were sufficiently destroyed. Even if the processing and irradiation protocols are successful in removing any threats for disease transfer, it is still possible for these procedures to compromise the graft's biomechanical and biochemical properties. The overall challenge with allografts is to prepare well cleaned, sterile, and free of virus implants, while maintaining the natural biologic and biomechanical properties of the tissue [1, 13].

Xenografts are grafts derived from another species other than the host. For humans, the most common xenografts are harvested from bovine bone [14]. Before implantation in humans, the organic components of the graft are completely removed (to ideally eliminate human rejection by the immune response) leaving only the inorganic portions which serve as the natural architecture matrix and a source of calcium [15]. The disadvantages of xenografts include potential disease transfer (similar to allografts), infection, and rejection by the host immune system [16].

The field of tissue engineering "aims to restore function to or replace damaged or diseased tissues through the application of engineering and biological principles" [17]. Given that each of the above mentioned grafts has their own distinct disadvantages, synthetic biomaterial scaffolds that are biocompatible, biodegradable, porous, bioactive, and mechanically stable have been the focus of research as alternative bone substitutes. The use of polymeric scaffolds and tissue engineering techniques can achieve bone repair while eliminating the need for autologous grafts. Most research has centered on developing some form of a mineralized biomimetic scaffold that is biocompatible, mechanically

stable, has a moderate degradation rate over several months, and is osteogenic. These biomimetic structures are typically composed of synthetic/natural polymers and some form of calcium phosphates (usually hydroxyapatite, HA). Although many of these structures contain the basic ECM components of bone, they lack enhancing osteogenic promoting proteins and true three-dimensionality. Chapter 2 will provide a review of alternative bone graft substitutes within the field of bone tissue engineering.

2. BACKGROUND INFORMATION

2.1. BONE: STRUCTURE AND REMODELING

Bone is a natural composite of collagenous organic matrix reinforced by an inorganic mineral phase of HA whose structure is ultimately responsible for its functional properties. Other components of bone include calcium phosphates, water, proteins, etc. [18]. Natural bone is a complex and highly organized structure of parallel collagen nanofibrils, and carbonated apatite (HA nanocrystals) located within the fibrils and precipitated on their surface [18, 19]. These HA nanocrystals can be either platelet or spindle shaped and up to about 200 nm long which creates a large surface area for effective mineral exchange [20]. Type I collagen is the main organic component (composing about 90%) of mineralized ECM and is the foundation upon which minerals are deposited. The ECM is the framework of each tissue which provides cues to promote cellular adhesion, migration, differentiation, and proliferation. Cells continually produce, secrete, and modify ECM components which attribute to a unique ECM structure and composition for each tissue. Ultimately, the biomechanical properties and biological function is attributed to this organic-inorganic nanocomposite bone ECM [21].

Bone undergoes continuous yet subtle remodeling in order to achieve its function. The mineral components, such as calcium phosphates and HA are responsible for the hardness of bone. The toughness and visco-elasticity is attributed to the soft organic collagenous matrix [22]. At the cellular level, osteoblasts reside on the surfaces of bone

and are involved in the secretion of the osteoid (unmineralized organic matrix, mainly type I collagen) and subsequent formation, mineralization, and organization of bone ECM. Osteoblasts are also differentiated forms of progenitor cells (such as mesenchymal stem cells and stromal cells) that are recruited to the site in need of bone rebuilding [23]. Once mature osteoblasts rebuild the area in need they either undergo apoptosis or become integrated within the deposited matrix and become osteocytes which maintain the bone matrix by controlling the activity of osteoblasts and osteoclasts [24]. Osteoclasts are large, multinucleated phagocyte-like cells formed from the fusion of macrophages, which adhere to the bone surface and are responsible for mineral dissolution and the degradation of the organic phase (bone resorption) [21]. It is known that bone remodeling is regulated through an osteoblast-osteoclast coupling system in which both cell types signal each other to maintain the balance of bone rebuilding and resorption at the appropriate sites. Any imbalance of this system can cause diseases, such as osteoporosis. Specifically with bone rebuilding, little is known about the role of osteoclasts with regards to signaling osteoblast recruitment. It has been reported that platelet-derived growth factor bb (PDGF-bb) is one such factor released by osteoclasts that control osteoblast chemotaxis [25]. Within the last five years, a new bone cell type has been identified and studied. Like most tissues, the bone-lining tissues (endosteum and periosteum) contain a population of resident tissue macrophages (OsteoMacs) that are likely to play a role in bone healing and bone homeostasis (through regulating osteoblast function). OsteoMacs are a significant population within the osteal microenvironment (constitute about one sixth of the total cell population) confirming that cells other than osteoblasts reside on the bone surface [26-28].

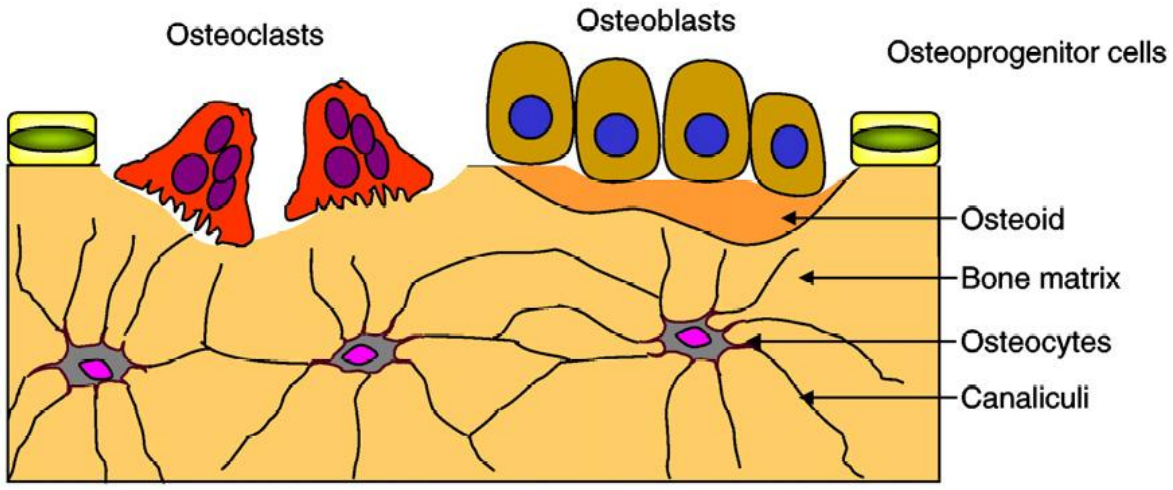

Figure 2.1 – The basic multicellular unit of bone remodeling [21]. Reprinted with permission from Elsevier.

Mineralization of bone first occurs at nucleation sites located within the hole zone regions of the organic matrix of bone (collagen fibrils). This region is a volume of space where mineral crystals (calcium phosphates, Ca-P) are deposited from the extracellular fluid. Since mineralization occurs in these hole zones, it suggests that the three-dimensional geometry and the composition of the fibrils (mineral-filled collagen) are factors in mineralization; specifically suggesting that nucleation sites are located in the collagen fibrils within the hole zone regions [29]. This initial nucleation process occurs at independent sites within the collagen fibrils and does not damage or disrupt the matrix structure. After the initial nucleation, there is continuous formation of Ca-P crystals due to secondary nucleation of the already formed crystals. Also during this stage, primary nucleation sites within the hole zone which did mineralize are still able to nucleate Ca-P crystals. Throughout the mineralization process Ca-P undergo a phase transformation from

a solution (extracellular fluid) to a solid phase (Ca-P crystals). It is important to note that the increase in mineralization is due to the increase in the number of crystals rather than the increase in the size of the crystals already formed [29]. Mineralization of a polymer scaffold occurs in the same manner as described above for native bone. Mineral nucleation occurs first on the polymer surface and then mineral crystals multiply on the nucleated mineral [30]. This native mineralization process is the underlying principles behind biomimetic mineralization described later.

2.2. NORMAL BONE HEALING

The process in which normal bone healing occurs is divided into three main stages: inflammatory, repair, and remodeling. To initiate the inflammatory stage, a hematoma is developed at the injury site. This fibrin clot provides the framework for inflammatory cells (such as monocytes and macrophages) and fibroblasts to infiltrate the site of injury which results in granulation tissue formation, vascularization, and migration/differentiation of mesenchymal stem cells (MSCs) [31]. It is known that a variety of growth factors contribute to the migration and differentiation of MSCs into bone building cells (osteoblasts). These growth factors are supplied by multiple sources, including the various migrating cells and the platelets from the clot [23]. The repair stage begins within 1 to 2 weeks by removing damaged cells and replacing the weak fibrin clot with a more mechanically stable structure (callus). During the repair stage, cartilage and collagen are formed and subsequently mineralized. Eventually the callus ossifies (endochondral ossification) and becomes woven bone (newly formed bone only present in early

development or during bone repair) [23, 31, 32]. In the remodeling stage, the bone is restored to its original shape, structure, and mechanical strength. Here, the woven bone is remodeled into lamellar bone via osteoclast and osteoblast coupling as previously described. A popular area of bone tissue engineering is the focus on the repair and remodeling stage, specifically the differentiation of MSCs into osteoblasts and the osteoblasts ability to attach and produce organic-inorganic matrix.

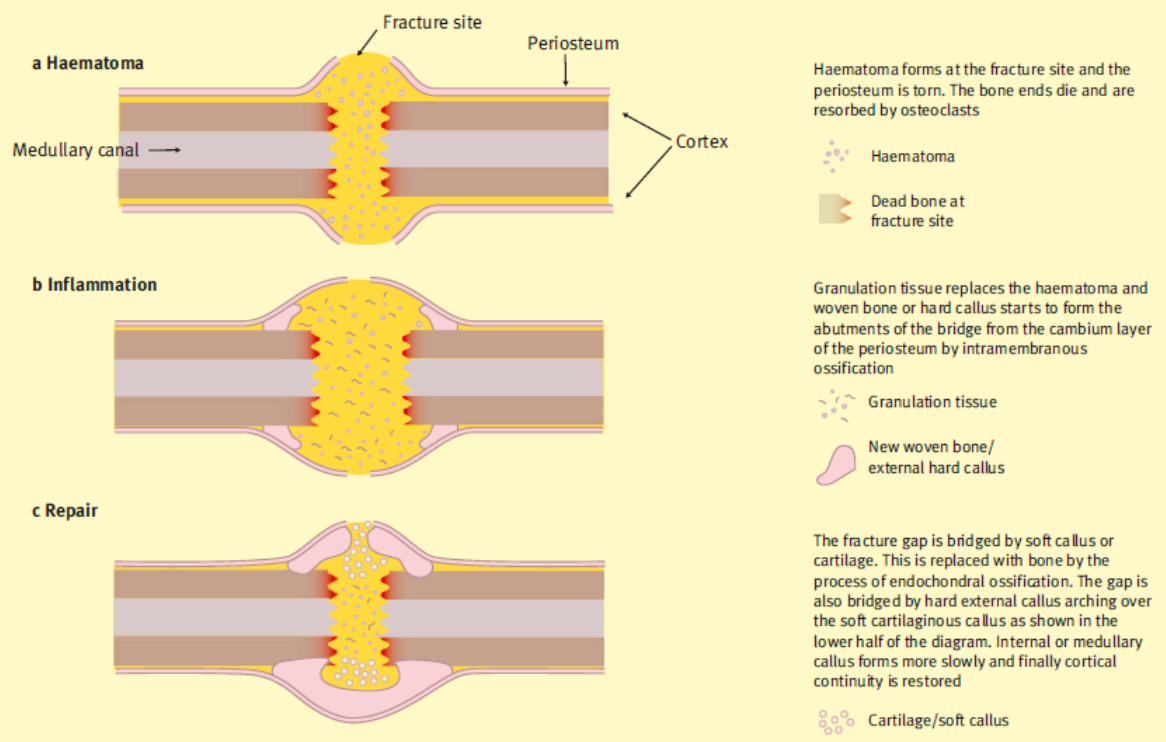

Figure 2.2 - Fracture healing: inflammatory and repair stages. Although remodeling is a stage of fracture healing, it is also a process that is continuously occurring in the body at all times and therefore is not included in the immediate healing diagram above [32]. Reprinted with permission from Elsevier.

Intuitively, as the stages of bone healing progress, the mechanical properties of the tissue increases. As displayed in Figure 2.3, Leong *et al.* reported the changes in mechanical properties of bone fracture calluses in rats, specifically recording the indentation modulus of granulation tissue (0.55 ± 0.04 MPa), cartilage (1.36 ± 0.078 MPa), newly formed woven bone (36.5 ± 5.84 MPa), and cortical bone (7.2 ± 0.61 GPa). Although this study reports the indentation modulus and not elastic modulus, the general relationship of mechanical properties of healing bone can be extracted. For rat femur fracture callus healing cortical bone was approximately 200x, 5,300x, and 13,000x higher modulus values than woven bone, cartilage, and granulation tissue, respectively. Fabrication of scaffolds for this dissertation will cater to the lower mechanical properties of the early stages of bone healing (granulation tissue and cartilage) rather than newly formed or mature bone since the goal is to create a scaffold that mimics early healing and promotes osteoblast matrix deposition.

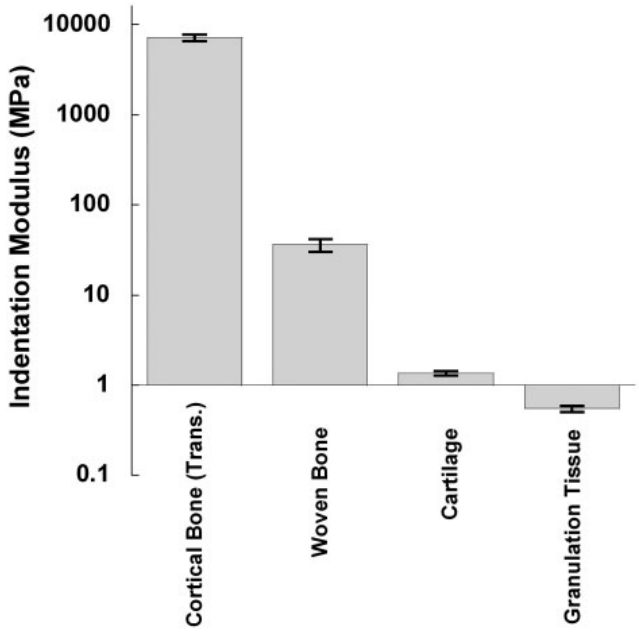

Figure 2.3 - Measurement of indentation modulus of rat fracture calluses at progressive stages in bone healing [33]. Reprinted with permission from Oxford University Press.

2.3. BONE TISSUE ENGINEERING

Tissue engineering focuses on developing viable substitutes that are able to repair and regenerate the functions of damaged tissue [34]. Specifically, bone tissue engineering requires a scaffold to temporarily support cell adhesion and direct their growth into bone tissue until the scaffold is completely replaced by the new tissue [35]. Cells respond to environmental cues such as composition, topographical structure, mechanical properties, and presence of biological factors. Therefore, within tissue engineering, cellular response and subsequent tissue growth are dependent on the characteristics of the scaffolding system. Since cellular growth depends on the characteristics of the scaffolding system, it is

important to fabricate scaffolds that mimic the structure and composition of natural bone ECM [36].

Several scaffold fabrication techniques for tissue engineering applications have been developed using biodegradable synthetic and/or natural polymers with the potential to incorporate bioactive molecules. Some of these include freeze-drying [18], solvent casting/particulate leaching [30, 37], gas foaming/particulate leaching [5, 7, 9], plates/meshes [38], solvent casting/salt leaching [39], salt leaching/solid-liquid phase separation [40], and electrospinning [8, 21, 36, 41-47]. Important factors in the success of bone tissue engineering scaffolds include biocompatibility, degradability, porosity, osteoconductivity, and mechanical stability. Biocompatibility and degradability can be controlled by the polymer(s) used. Osteoconductivity and mechanical stability can potentially be enhanced by the growth of a bone-like mineral (BLM) on the scaffold surface prior to cell seeding [37]. Porosity can be controlled by altering parameters during different scaffold fabrication techniques. Porosity is an important design criterion for scaffolds, as a highly porous scaffold will allow for neovascularization throughout the construct [48]. It has been demonstrated that scaffolds with increased pore size enhance osteoblast proliferation and differentiation throughout the scaffold as a result of increased oxygen and nutrient transport, and neovascularization [49-51].

Polymers (both natural and synthetic) are a promising category of potential biomaterials used for bone tissue engineering [3]. Natural polymers attract special interest in tissue engineering since they have high mineralization potential, are highly bioactive, biocompatible, biodegradable, and natural substrates where cells can attach, proliferate,

and function [52]. One main criticism of natural polymers is that (when used alone) they lack mechanical integrity and are more quickly degraded. Synthetic polymers have been specifically fabricated for medical applications because they are versatile and free of potential contamination [53]. The advantage of using synthetic polymers for scaffolding is that they are more mechanically stable and able to undergo chemical modifications in order to improve cell adhesion, cell function, and mineralization. However, synthetic polymers generally lack bioactivity without these modifications which led to interest in developing composite scaffolds combining osteoconductive materials with polymer-based materials [3].

There has also been widespread use of Ca-P (such as HA) for bone tissue engineering applications [5]. The major advantages of HA include (i) it is the major inorganic component of bone matrix, (ii) they have affinity to many adhesive proteins, and (iii) they are osteoconductive materials directly involved in bone cell differentiation and mineralization process [22, 46]. Even though inorganic HA materials have many advantages, they have limited use as tissue engineering scaffolds because they are brittle [42]. However, combining the bone-bioactivity of the inorganic materials with the structural integrity of the organic polymers introduces an organic-inorganic composite scaffold specifically tailored for bone tissue engineering. Composite organic-inorganic scaffolds have the potential to satisfy the complex scaffold designs criteria such as material composition, architecture, structural mechanics, surface properties, and degradation properties and products [22].In addition, calcium-based ceramics undergo a phase transformation and precipitate on the surfaces as Ca-P crystals. This sequence of events

leads to the formation of a carbonate-containing BLM layer on the surface which enhances osteoconductivity and is essential in creating a bond with the living host bone [54-56].

Collagen and HA are popular materials when investigating bone scaffolds since their composites mimic the ECM of natural bone [18, 57-60]. More recently, gelatin (denatured collagen) has been used as a replacement for collagen since it is less expensive, easier to obtain, and contains similar functional groups which enhance cellular response [61]. Gelatin also contains specific binding domains, such as the RGD sequence, which are related to cell attachment [62]. Freeze-dried gelatin sponges have many advantages because they can be designed to fit any size defect/injury site, have the ability to swell and fill a void space, degrade controllably in a range of rates (due to various cross-linking methods) to ensure drug release and mechanical stability, and can be easily modified by incorporating various osteoconductive/osteoinductive materials (i.e. minerals, growth factors, proteins, etc.). These porous scaffolds are fabricated without the use of harsh organic solvents which addresses one of the drawbacks of alternative scaffold fabrication methods. The addition of bioactive inorganic HA to freeze-dried gelatin sponges creates a bone-like ECM scaffold which allows a more controlled drug delivery system and increases cellular attachment, proliferation, alkaline phosphatase activity, and osteocalcin production [63-65]. HA also has the ability to bind to a variety of molecules, including proteins. As a result, scaffolds incorporated with HA provide a more favorable environment through increased adsorption of serum adhesion proteins such as fibronectin and vitronectin [66]. Enhanced cellular responses have also been observed with the addition of other minerals (β-tricalcium phosphate, dicalcium phosphate dihydrate),

polymers (gellan, poly-lactide-co-glycolide) and proteins (bone morphogenetic protein, Wnt1 inducible signaling pathway protein) in combination with HA [67-69].

Other additions such as chitin whiskers (CW, i.e. chitin nanocrystals) and platelet-rich plasma (PRP) have been used to increase the mechanical integrity (CW), bioactivity (CW and PRP), and osteogenic potential of scaffolds (PRP) [70-72]. Chitin is the second most abundant biopolymer next to cellulose and possesses many favorable properties such as non-toxicity, high crystallinity, biocompatibility and biodegradability. Acid-treatment of chitin can dissolve regions of low lateral order, resulting in elongated rod-like nanocrystals, termed "whiskers". CW are an emerging and novel nanofiller that have been shown to bring about reinforcing effects on both synthetic and natural polymeric structures. The biocompatibility and biodegradability also make it one of the most promising nanofillers. In recent years, experiments studying CW have increased due to its availability, nontoxicity, and ability to mechanically reinforce polymer nanocomposites and enhance cell proliferation [70, 73-77].

Platelet-rich plasma (PRP) is a simple and cost-effective method for collecting and concentrating autologous platelets for the purpose of activating and releasing their growth factor-rich alpha and dense granules. Upon collecting PRP, platelet-poor plasma (PPP) can also be obtained simultaneously. PPP contains little to no amounts of growth factors and high concentrations of fibrinogen. Results of numerous studies have demonstrated the versatility and effectiveness of PRP within wound healing, skin engineering, ligament/tendon engineering, cartilage repair, bone regeneration, and more [71, 78-83]. Particularly with bone regeneration, the addition of PRP has been reported to increase bone

density/mineralization, vascularization, and osteogenesis [71, 72, 84-86]. Preparation rich in growth factors (PRGF, a bioactive lyophilized version of PRP) contains high concentrations of growth factors such as platelet-derived growth factor (PDGF), transforming growth factor-β (TGF-β), insulin-like growth factor-1 (IGF-1), vascular endothelial growth factor (VEGF), epidermal growth factor (EGF), fibroblast growth factor (FGF), hepatocyte growth factor (HGF), and more [87-89]. PRGF also contains cell adhesive proteins such as fibronectin and vitronectin. Many of these factors are known for their angiogenic potential, however, their ability to enhance bone repair has also been studied. In relation to bone remodeling, these growth factors and proteins elicit a favorable cellular response which supports the incorporation of PRGF within scaffolds intended for bone tissue engineering [90-98]. The bone remodeling functions for some of these molecules are summarized in Table 2.1. PRGF can be easily incorporated into scaffolds at desired concentrations which ultimately allow consistent reproducible bioactive scaffolds. The incorporation of PRGF within gelatin sponges, the general combination of CW and PRGF, and the combination of PRGF with HA and/or CW in gelatin sponges are all areas that have yet to be explored.

Table 2.1 - Role of PRGF components in bone remodeling [87-94, 97-104].

	Function
PDGF	MSC and progenitor cell recruitment, proliferation, migration and differentiation into osteoblasts
TGF-β	MSC differentiation, increased production of collagen and mineral matrix
IGF-1	Osteoblast proliferation and differentiation
VEGF	Angiogenesis, endochondral ossification
HGF	Angiogenesis, osteoblast proliferation, increases osteoblast BMP-2 production
EGF	MSC migration and osteoblast differentiation
FGF	Angiogenesis, osteoprogenitor cell proliferation, differentiation, and expression of osteogenic markers and mineralization
Fibronectin, Vitronectin	Enhance formation of focal adhesions by osteoblasts, osteoblast migration

Several cell types can be used for *in vitro* evaluation of bone tissue engineering. Some include undifferentiated osteoprogenitor cells (mesenchymal stem cells, stromal cells, and periosteal cells) and already differentiated osteoblasts. For this dissertation, MG-63 cells were used to evaluate *in vitro* cellular response. MG-63 cells are human osteoblast-like cells derived from an osteosarcoma. These cells behave similar to osteoblasts with their attachment, migration, proliferation, and organic-inorganic matrix production. MG-63 cells are commonly used for evaluation of biocompatibility and cellular response to bone regenerative environmental cues, such as scaffolds [65, 67, 105-109].

2.4. BIOMIMETIC MINERALIZATION

As previously mentioned, a BLM layer formed on the surface of biomaterials is an essential requirement for the material to bond to the living bone and enhance osteoconductivity. In 1990, Kokubo et al. developed an acellular solution, simulated body fluid (SBF), with ionic concentrations approximately equal to those of human blood plasma [110]. The most commonly used SBF is conventional (c-SBF). Oyane et al. revised the c-SBF and prepared new SBFs that were closer to the ionic concentration of blood plasma. The SBFs developed were revised (r-SBF), ionic (i-SBF), and modified (m-SBF) [111]. Of these, r-SBF has the overall closest ionic concentrations to that of total blood plasma (Table 2.2).

Table 2.2 - Ionic concentrations of blood plasma [112]. Reprinted with permission from John Wiley and Sons.

Ion	Concentration (mM)				
	Total blood plasma	c-SBF	r-SBF	i-SBF	m-SBF
Na^+	142.0	142.0	142.0	142.0	142.0
Cl^-	103.0	147.8	103.0	103.0	103.0
HCO_3^-	27.0	4.2	27.0	27.0	10.0
K^+	5.0	5.0	5.0	5.0	5.0
Ca^{2+}	2.5	2.5	2.5	1.6	1.5
Mg^{2+}	1.5	1.5	1.5	1.0	1.5
HPO_4^{2-}	1.0	1.0	1.0	1.0	1.0
SO_4^{2-}	0.5	0.5	0.5	0.5	0.5

SBF is used to induce mineral nucleation, creating a BLM layer on the surface of materials [110]. This technique can be used for complex porous scaffolds since the apatite crystals are generated from an aqueous solution. Immersion of scaffolds in SBF is an easy task and does not require any special equipment. It has been found that the BLM

(carbonated HA) layer generated resembles natural bone mineral in its nano-crystal size and low crystallinity [40]. SBF has been widely used for biomimetic BLM coating on bioinert materials to directly mimic the process of mineralization in native bone and to predict the *in vivo* bioactivity of the material [9, 30, 37, 38, 41, 43, 45, 113]. It has been found that if a material is able to form a BLM layer in short periods when immersed in SBF, then it will bond to living bone in short periods [114].

The overall focus of this study was to characterize the first attempts of a tissue engineered freeze-dried gelatin composite sponge enhanced with PRGF, HA, and CW to provide sufficient structural support to the defect site while enhancing the body's own reparative capacity, ultimately eliminating the need for autologous tissue harvesting or repeat operations. Composite gelatin sponges were further modified via mineralization and characterized to understand scaffold release, cell response, and mechanical properties. The central hypothesis of this study is that a biodegradable lyophilized gelatin composite sponge will serve as a bioactive structure to facilitate osteoblast attachment, migration, and matrix secretion while exhibiting controlled release and stable mechanical properties in the range of tissues present in early bone healing.

3. A PRELIMINARY EVALUATION OF LYOPHILIZED GELATIN SPONGES ENHANCED WITH PLATELET-RICH-PLASMA, HYDROXYAPATITE, AND CHITIN WHISKERS

Isaac A. Rodriguez [1,†], Scott A. Sell [2,†], Jennifer M. McCool [1], Gunjan Saxena [1], Andrew J. Spence [3] and Gary L. Bowlin [1,*]

[1] Department of Biomedical Engineering, Virginia Commonwealth University, 401 West Main St, P.O. Box 843067, Richmond, VA 23284, USA; E-Mails: rodriguezia@vcu.edu (I.A.R.); mccooljm2@vcu.edu (J.M.M.); saxenag@vcu.edu (G.S.); glbowlin@vcu.edu (G.L.B.)

[2] Department of Biomedical Engineering, Parks College of Engineering, Aviation, and Technology, Saint Louis University, 3507 Lindell Blvd, St. Louis, MO 63103, USA; E-Mail: ssell@slu.edu

[3] Department of Biology, Virginia Commonwealth University, 1000 West Cary St, Room 126, Richmond, VA 23284, USA; E-Mail: spenceaj@vcu.edu

† These authors contributed equally to this manuscript.

Preface: The following chapter is compiled from a manuscript accepted on April 14, 2013 for publication in the Journal, *Cells*, doi:10.3390/cells10x000x

3.1. ABSTRACT

The purpose of this study was to perform a number of preliminary *in vitro* evaluations on an array of modified gelatin gel sponge scaffolds for use in a bone graft application. The gelatin gels were modified through the addition of a number of components which each possess unique properties conducive to the creation and regeneration of bone: a PRGF, HA, and CW. PRP therapy is an emerging practice that has proven effective in a number of clinical applications, including enhancing bone repair through improved deposition of new bony matrix and angiogenesis. As such, the inclusion of PRGF in our gelatin scaffolds was intended to significantly enhance scaffold bioactivity, while the addition of HA and CW were anticipated to increase scaffold strength. Additionally, the gelatin sponges, which readily dissolve in aqueous solutions, were subjected to 1-Ethyl-3-(3-dimethylaminopropyl)carbodiimide hydrochloride (EDC) cross-linking either during or post gelation to control their rate of degradation. Scaffolds were evaluated *in vitro* with respect to compressive strength, change in mass, protein release, and MG-63 cellular interaction, with results demonstrating the potential of the gelatin sponge scaffold for use in the regeneration of bone.

3.2. INTRODUCTION

As previously mentioned, healthy bone has the unique ability to spontaneously regenerate. However, if the diseased or damaged area exceeds a certain size, bone grafting is needed to regenerate the tissue [115]. Common practices to supplement bone

regeneration in larger defects include bone graft biomaterials such as autografts, allografts, xenografts, and synthetic biomaterials (i.e. ceramics, cements, glasses, metals, polymers, and composites) [3, 116-119]. Since each of the above mentioned grafts have their own distinct disadvantages, synthetic biomaterial scaffolds that are biocompatible, biodegradable, porous, bioactive, and mechanically stable have been the focus of research as alternative bone substitutes.

The present study aimed to evaluate the release kinetics, difference in mass, mechanical properties, and cellular responses of multiple combinations of composite freeze-dried gelatin sponges. PRGF, CW, and/or HA were incorporated into the gelatin sponges and cross-linked during gelation or after lyophilization to increase the scaffolds' overall compatibility as a bone tissue engineering substitute. The goal of this study is to create a scaffold that mimics the microenvironment of early bone healing. In turn, this will foster a hospitable environment for osteoblast attachment, migration, and secretion of bone matrix, which will lead to woven bone formation and remodeling.

3.3. MATERIALS AND METHODS

3.3.1. Fabrication of gelatin composite sponges

All scaffolds were fabricated with a base solution of 30 mg/ml gelatin (Type B from Bovine skin, Sigma) in deionized (DI) water. For composite scaffolds, a total amount of 10 mg/ml of PRGF, HA, and/or CW were weighed, added to the 30 mg/mL gelatin solution, then sonicated if necessary (Table 3.1). Materials included HA nanopowder

(particle size < 200 nm (BET), Sigma-Aldrich), CW (prepared by following a published protocol [74]), PRGF (created using published protocol [88]), and1-Ethyl-3-(3-dimethylaminopropyl)carbodiimide hydrochloride (EDC, Thermo Scientific). To create PRGF, fresh human whole blood from 3 donors was purchased, combined, and centrifuged (SmartPReP® 2) to create PRP. PRP then underwent a freeze (-70°C) – thaw (37°C) – freeze (-70°C) cycle to ensure platelet lysis and activation. Frozen PRP was then lyophilized to obtain a dry PRGF powder to be weighed and incorporated within the gelatin solution [88].

4 mL of the prepared gelatin or gelatin composite solution was pipetted into a 35 x 10 mm Petri dish, refrigerated at 4°C overnight to gel, and then slowly frozen at -15°C overnight, -20°C for 4 hours, and -70°C for 4 hours. Frozen gel composites were lyophilized for 24 hours then cross-linked for 18 hours at room temperature in 50 mM EDC in ethanol [120-123]. To analyze the effect of an alternative cross-linking method, another set of solutions were made and 50 mM EDC was added directly to the composite solution before gelation. This process allowed for simultaneous gelation and cross-linking (scaffolds denoted as +EDC). After gelation, scaffolds were frozen and lyophilized as previously described. Using a Miltex biopsy punch, 6 mm discs were punched and used for all experiments.

Table 3.1 - Scaffold components and fabrication concentrations.

	amount (mg/mL) added to gelatin solution	**sonicated**
+HA	10	yes
+CW	10	yes
+HA+CW	5 (HA) and 5 (CW)	yes
+PRGF	10	no
+PRGF+HA	5 (PRGF) and 5 (HA)	yes (HA) then PRGF added
+PRGF+CW	5 (PRGF) and 5 (CW)	yes (CW) then PRGF added
+PRGF+HA+CW	3.33 (PRGF), 3.33 (HA), and 3.33 (CW)	yes (HA+CW) then PRGF added

3.3.2. Mass loss

Two 6 mm scaffold punches were weighed as a unit for initial dry mass. Scaffolds were then disinfected (30 minutes ethanol followed by three 10 minute washes of 1x Phosphate Buffered Saline, PBS – Quality Biological, Inc., pH 7.4) and transferred to a 48-well plate (two discs per well, n=3). 500 µL of Dulbecco's modified Eagle's medium (DMEM, HyClone) high glucose containing 10% fetal bovine serum (FBS, Atlanta Biologicals) and 1% penicillin/streptomycin (HyClone) was added to each well. The two scaffolds per well were incubated in media at 37°C and 5% CO_2 with media changes every 7 days. Scaffolds were removed and weighed as a unit every 7 days up to 90 days. Hydrated scaffolds were massed and compared to original dry weights as a percentage to determine percent increase in scaffold mass. Scaffolds were air-dried post 90 day culture and compared to original dry weights to determine overall mass loss.

3.3.3. Protein release

To determine total protein content of each 6 mm scaffold disc, triplicates of one non cross-linked 6 mm discs of each scaffold type was immersed in 500 µL of 1x PBS. Uncross-linked scaffolds completely degraded within minutes at room temperature. Since scaffolds are primarily comprised of gelatin, the released components are detectable using a general protein assay. Protein was quantified using a Pierce BCA Protein Assay (Thermo Scientific) with 8 serial dilutions of bovine serum albumin as standards (from 2 to 0 mg/mL). Briefly, 25 µL of PBS containing the degraded scaffold contents was added to 200 µL of working reagent in a 96-well plate. The well plate was then incubated at 37°C for 30 minutes, cooled to room temperature, and absorbance measured at 562 nm using a SpectraMax Plus 384 Microplate Spectrophotometer (Molecular Devices).

Scaffold release kinetics was studied by quantifying protein release from each scaffold over a period of 90 days. Triplicates of one 6 mm disc of each cross-linked scaffold type were incubated in 500 µL of 1x PBS at 37°C with PBS replaced every 3 days. After 1, 4, 7, 10, 14, 21, 28, 56, and 90 days the PBS containing released scaffold contents in each well was analyzed for protein content using the Pierce BCA Protein Assay described above.

3.3.4. Cell attachment, migration and matrix production

Triplicates of 6 mm discs of each scaffold composition were seeded with 50,000 osteoblast-like cells (MG-63 cells from a human osteosarcoma) and incubated at 37°C and 5% CO_2 in DMEM high glucose media containing 10% FBS and 1%

penicillin/streptomycin with media changes every three days. After 1, 28, and 90 days, scaffolds were fixed in 10% Buffered Formalin Acetate (Fisher Scientific) and stored at 4°C until preparation for scanning electron microscopy (SEM) and fluorescent staining. For uniaxial compression testing, scaffolds were tested directly after being removed from the incubator.

Scanning electron microscopy

Scaffolds were removed from formalin, briefly rinsed in PBS and water, and then subjected to ethanol dehydration (10 minute soaks in 30, 50, 70, 90, and 100 % ethanol, subsequently). Samples were air dried overnight, mounted on aluminum stubs, sputter coated in gold for 70 seconds, and examined using a JEOL JSM-5610LV scanning electron microscope.

DAPI staining

Scaffolds were removed from formalin, immersed in a 30% sucrose solution in DI water for 48 hours at 4°C to ensure displacement of all air bubbles, suspended in premium frozen section compound (VWR), and frozen at -70°C overnight. 60 µm slices were cryosectioned using a Cryostat (Thermo) and transferred to microscope slides. Cryosectioned samples were then stained with 4'-6-diamidino-2-phenylindole (DAPI) stain for 5 minutes and imaged using a UV fluorescent microscope to display the location of cell nuclei.

Alizarin Red S staining

Alizarin Red S (ARS) is a dye that selectively binds to calcium salts. ARS staining was used to quantify scaffold mineral content by modifying a published protocol [112]. ARS was performed on the 6 mm scaffold punches after 1, 28, and 90 days incubation in media with and without cells. After incubation scaffolds were stained with 40 mM Alizarin Red (Sigma-Aldrich) for 30 minutes then washed with DI water to remove any unbound stain. Scaffolds were then transferred to a 2 mL microcentrifuge tube containing 1.5 mL of 50% acetic acid to destain for 1 hour at room temperature. 500 µL of the solubilized stain was added to 600 µL of 1 M NaOH to adjust the pH to 4.1. 200 µL of this solution was pipetted into a 96-well plate and absorbance read at 550 nm using a SpectraMax Plus 384 Microplate Spectrophotometer.

3.3.5. Uniaxial compression testing

Uniaxial compression testing was performed on acellular and cellularized 6 mm scaffold discs after 1, 28, and 90 days incubation in media. Mechanical testing was conducted by attaching an indenter (cylindrical, 2 mm diameter, plane-ended, stainless steel) to a MTS Bionix 200 Mechanical Testing System instrument with a 100 N load cell (MTS Systems Corp., USA, Figure 3.1). Indentation was performed perpendicular to the scaffold surface at the center of each scaffold disc. The discs were placed on a flat metal surface and kept hydrated with PBS. The indenter was lowered to the surface of the scaffolds and the following parameters were used: test speed of 0.5 mm/min, data acquisition rate of 10 Hz, a preload of 0.015 N, and a max indenter displacement of 90% of

the scaffold thickness. Peak load was calculated by the MTS software TestWorks 4.0. Many scaffolds at later time points did not register a preload until later in the testing which resulted in the indenter moving through the entire scaffold until reaching the maximum load of 100 N when the intender contacted the metal plate. In these instances, the maximum peak load plateau, just before the maximum load was reached, was extracted from the graph and reported.

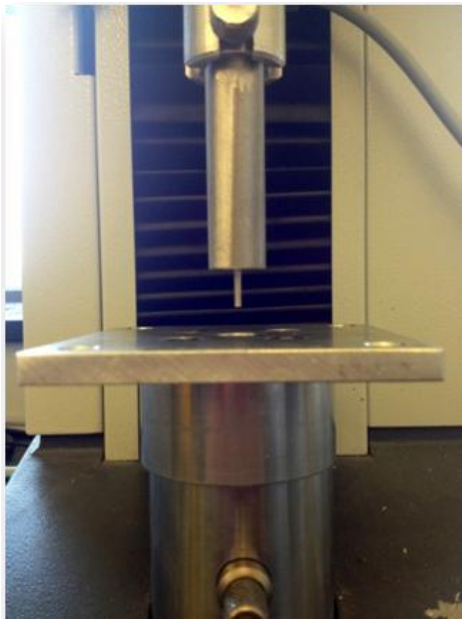

Figure 3.1 - Compressive mechanical testing set up with indenter.

3.3.6. Statistical analysis

Statistical analysis was performed using JMP IN 9 statistical software (SAS Institute) to determine significant differences. Analysis of the data was based on a Kruskal-Wallis one-way analysis of variance on ranks and a Tukey-Kramer pairwise multiple

comparison procedure. The results are presented in mean ± standard deviation (SD). Unless otherwise specified all samples were run at a minimum of triplicate (n=3) to ensure statistical significance ($p<0.05$).

3.4. RESULTS AND DISCUSSION

3.4.1. Mass loss

Figure 3.2 below shows the percent difference in mass between original dry scaffold weight, days 1, 28, 90, and dry post-culture scaffold weight. When comparing the two methods of cross-linking, scaffolds cross-linked post-fabrication absorbed more media and gained more mass (between 1500-2800 %) than scaffolds that were cross-linked during gelation (+EDC, between 500-1600 %). Upon comparing post cross-linked scaffolds at days 1, 28, and 90, the gelatin scaffolds showed significantly higher ($p<0.05$) mass increase than any other scaffold type. Also, CW and all scaffolds containing PRGF showed statistically significant ($p<0.05$) increases in mass at day 90 when compared to day 1, suggesting that these scaffolds continuously absorbed media throughout the culture period. For +EDC scaffolds, most scaffold types reached their maximum weight after day 1 and did not increase in mass over 90 days incubation. Only CW and PRGF+HA+CW scaffolds showed significant ($p<0.05$) mass increases. On days 1 and 28, HA scaffolds had significantly higher ($p<0.05$) percent differences in mass than all other scaffolds except for HA+CW and PRGF+HA+CW scaffolds, respectively. After 90 days, the percent difference in mass of HA scaffolds was only significantly higher than gelatin, PRGF, and PRGF+CW

scaffolds. Overall, the post cross-linked scaffolds swelled and absorbed more media than the +EDC scaffolds.

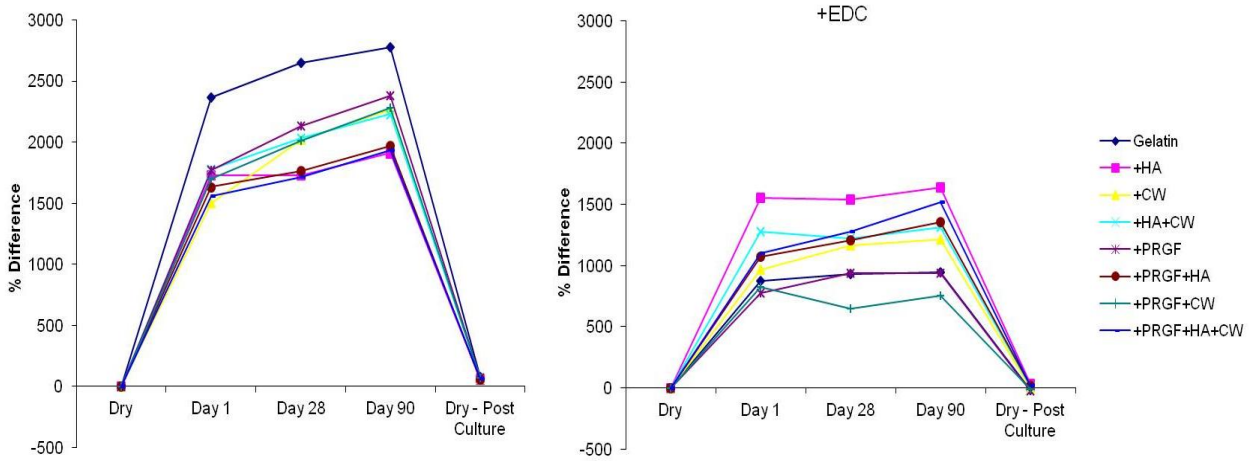

Figure 3.2 - Percent difference in mass.

Table 3.2 below compares the original dry pre-culture mass (Pre) to the dry, post 90 day culture mass (Post) of each scaffold type for both cross-linking methods. All scaffolds that were cross-linked post-fabrication significantly increased in dry mass after culture. For +EDC scaffolds, all scaffolds containing HA showed significant increases in mass while PRGF scaffolds significantly decreased in dry mass. The reason for this increase in mass following a 90 day culture period is not completely understood, especially since each scaffold demonstrated protein release throughout its culture duration that would be indicative of an overall mass loss. It is hypothesized that the gelatin sponges absorbed FBS-resident proteins present in the complete media in which they were incubated, which, upon subsequent drying and removal of any liquid prior to the post-culture massing remained trapped within the scaffold's structure. The swelling and media absorption seen

when dry scaffolds were introduced into culture media demonstrated that the gelatin scaffolds had a tremendous hygroscopic potential, thereby making it feasible that large amounts of FBS-resident proteins could be introduced and retained within the scaffold's structure. Since the post cross-linked scaffolds absorbed more media than the +EDC scaffolds, the increase in mass for these scaffolds could be attributed to the higher absorption of media resulting in increased resident protein integration with the scaffolds. The post dry mass increase observed in +EDC scaffolds containing HA may be attributed to increased resident protein integration as well, considering that HA is a bioactive nanofiller with the capability of increasing binding sites for proteins, minerals, and cells.

Table 3.2 - Mass (mg) of dry scaffolds pre/post-incubation. * denotes post-culture mass is statistically different ($p<0.05$) than pre-culture mass.

			+EDC	
	Pre	**Post**	**Pre**	**Post**
Gelatin	7.97 ± 0.57	14.27 ± 1.51*	7.53 ± 1.40	6.20 ± 1.71
+HA	12.17 ± 0.61	19.10 ± 0.78*	8.17 ± 0.67	11.00 ± 1.31*
+CW	10.67 ± 0.98	17.13 ± 9.29*	11.23 ± 0.95	10.63 ± 1.45
+HA+CW	11.20 ± 0.70	19.13 ± 8.39*	7.23 ± 0.29	7.93 ± 0.95
+PRGF	10.83 ± 0.99	18.53 ± 1.60*	9.40 ± 0.53	7.13 ± 0.81*
+PRGF+HA	11. 07 ± 0.45	17.43 ± 0.47*	8.13 ± 0.76	9.47 ± 0.21*
+PRGF+CW	9.63 ± 1.01	16.10 ± 0.27*	8.33 ± 0.50	7.73 ± 0.31
+PRGF+HA+CW	11.33 ± 0.65	18.23 ± 0.40*	8.10 ± 0.26	9.47 ± 0.25*

3.4.2. Protein release

Original total protein content of all scaffolds was between 1500 and 2100 µg. The +HA and +PRGF+HA scaffolds contained lower amounts of original protein when compared to other +PRGF scaffolds while all other scaffolds were not statistically different ($p<0.05$) from each other (Figure 3.3).

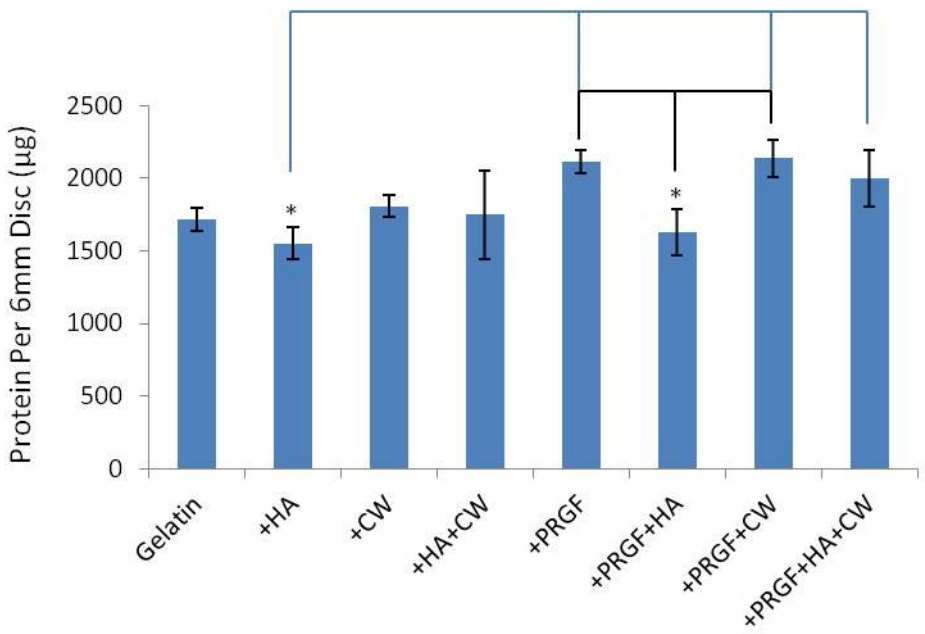

Figure 3.3 - Original protein content of scaffolds. * denotes statistical differences ($p<0.05$). The black and blue lines show statistical difference of +PRGF+HA and +HA, respectively.

The protein release kinetics of different cross-linking methods and scaffold compositions are compared over a 90 day incubation period and shown in Figure 3.4 A and B. All +EDC scaffolds released higher amounts of protein after 1 day incubation than their post-gelation cross-linked counterparts. The protein released from each +EDC scaffold ranged between 40 and 185 µg while the post-gelation cross-linked scaffolds only released a maximum of 35 µg. All +EDC scaffolds followed the same trend of protein release; a high release on day 1, a steady decline throughout 14 days, a jump at day 21, then declined to little/no release after 90 days. Throughout 56 days, the +EDC gelatin and +HA scaffolds showed consistently higher and lower release, respectively. Post-gelation cross-linked scaffolds had more variety in trends, however, the overall protein release remained low in

comparison to the +EDC scaffolds. Graphs C and D in Figure 3.4 show the cumulative protein released from scaffolds over 90 days. These graphs show the same trends as graphs A and B; however, it provides a better perspective on overall protein release.

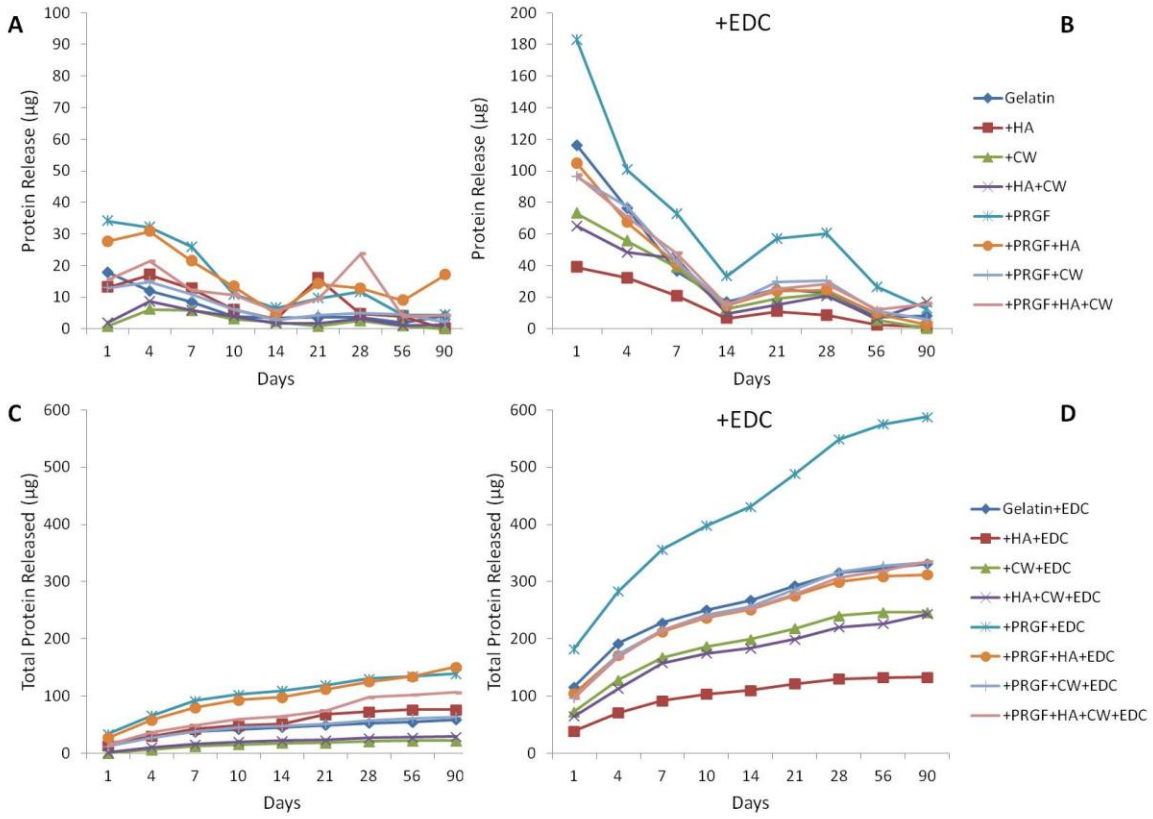

Figure 3.4 - (A & B) Protein release of scaffolds per time point. (C & D) cumulative protein release over 90 days.

Total protein released from each scaffold after 90 days (Figure 3.4 C and D) was compared to the original protein content of the scaffolds (Figure 3.3) to compute a percentage of total protein released for each scaffold type after 90 days incubation. Table

3.3 lists these percentages in descending order. The overall trend was that scaffolds cross-linked during gelation (+EDC) released more protein over 90 days than post-gelation cross-linked scaffolds. These results indicate that the method of cross-linking has a significant impact on the release kinetics of the scaffolds. In this study, where EDC concentrations were identical between the two cross-linking methods (pre or post-gelation) and the only difference was when the cross-linker was applied, it was apparent that the pre-gelation +EDC group were faster degrading than the post-gelation group. It is hypothesized that the post EDC scaffolds degrade slower as a result of their stronger surface cross-linking since these scaffolds were submerged in an EDC solution. However, the +EDC scaffolds were allowed to cross-link during gelation most likely resulting in more uniform cross-linking throughout the interior of the scaffold. The lower amounts of cross-linking on the surface could make the scaffold susceptible to faster degradation. While a quick rate of degradation may not be ideal for a bone graft scaffolding material, it may be appropriate in an orthopedic drug delivery scenario where a more rapid, yet still controlled release of protein may be ideal. It should be noted that in this study, for the sake of simplicity, only a single concentration of EDC was utilized. The ability to increase or decrease the concentration of the EDC cross-linker allows users to truly tailor the rate of protein release from the scaffold by effectively increasing or decreasing the degree to which the scaffold is cross-linked.

Table 3.3 - Percent total protein released after 90 days.

	% Released
+PRGF+EDC	27.79
Gelatin+EDC	19.30
+PRGF+HA+EDC	19.18
+PRGF+HA+CW+EDC	16.75
+PRGF+CW+EDC	15.62
+HA+CW+EDC	13.94
+CW+EDC	13.66
+PRGF+HA	9.29
+HA+EDC	8.61
+PRGF	6.59
+PRGF+HA+CW	5.32
+HA	4.95
Gelatin	3.43
+PRGF+CW	2.98
+HA+CW	1.68
+CW	1.23

3.4.3. Cell attachment, migration and matrix production

Scanning electron microscopy

Scaffold characterization, cell attachment, and matrix production was first analyzed via scanning electron microscopy (Figures 3.5 and 3.6). Visually, all the acellular scaffolds appeared similar in structure: a flaky surface with large pores. Differences were noticed when observing MG-63 cell attachment after day 1. For post-gelation cross-linked scaffolds, the addition of HA and any scaffold containing PRGF appeared to have more cells attached (small dots in image). The same trend was observed for +EDC scaffolds with the exception of +PRGF+HA+CW. As previously mentioned, PRGF contains cell adhesive

proteins such as fibronectin and vitronectin. In addition, HA has the ability to adsorb these and other cell adhesion proteins either from the serum once incubated or from the PRGF pre-scaffold fabrication. The presence (in PRGF and serum) and/or adsorption (of HA) of these cell adhesive proteins allow the scaffolds containing HA and/or PRGF to increase in bioactivity and ultimately attach more cells, compared to the gelatin controls. After 28 days, little to no matrix was produced by the cells on the post-gelation cross-linked scaffolds, however, the +HA, +HA+CW, +PRGF, and +PRGF+HA+CW +EDC scaffolds showed mineral matrix production by the cells. After 90 days, cells on the post cross-linked scaffolds appeared to produce a more collagen bundle-like morphology matrix rather than a bone-like mineral substance. Cells on +EDC scaffolds for 90 days appeared to have produced more mineral matrix on the surface when compared to post cross-linked scaffolds. By visual inspection of the SEM images, cells produced desired bone-like mineral formation on the +HA, +HA+CW, +PRGF, and +PRGF+HA+CW +EDC scaffolds suggesting these scaffolds to be conducive to bone formation.

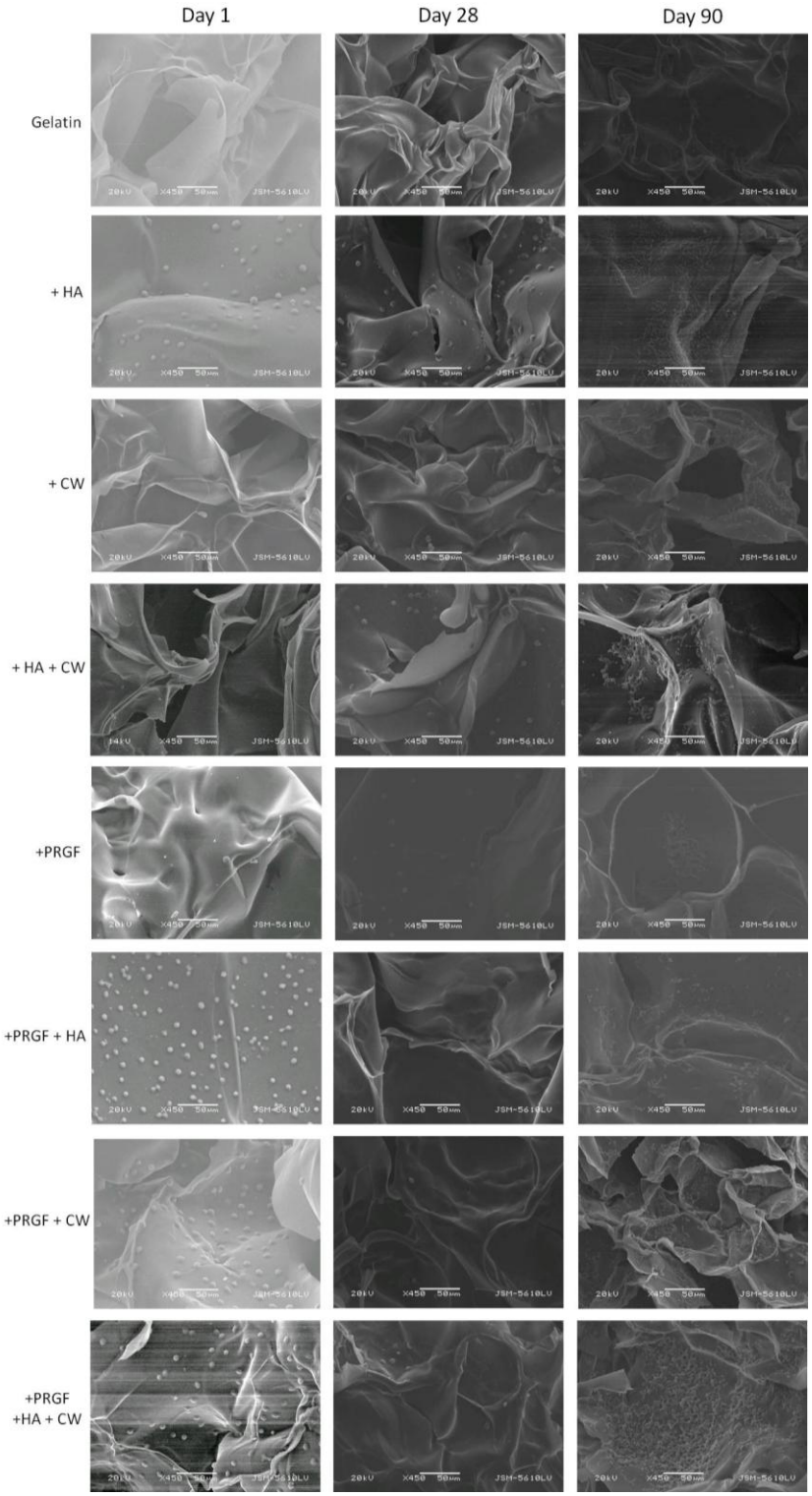

Figure 3.5 - SEM of post cross-linked scaffolds seeded with MG-63 cells for 1, 28, and 90 days. Magnification at 450x and scale bars at 50 µm.

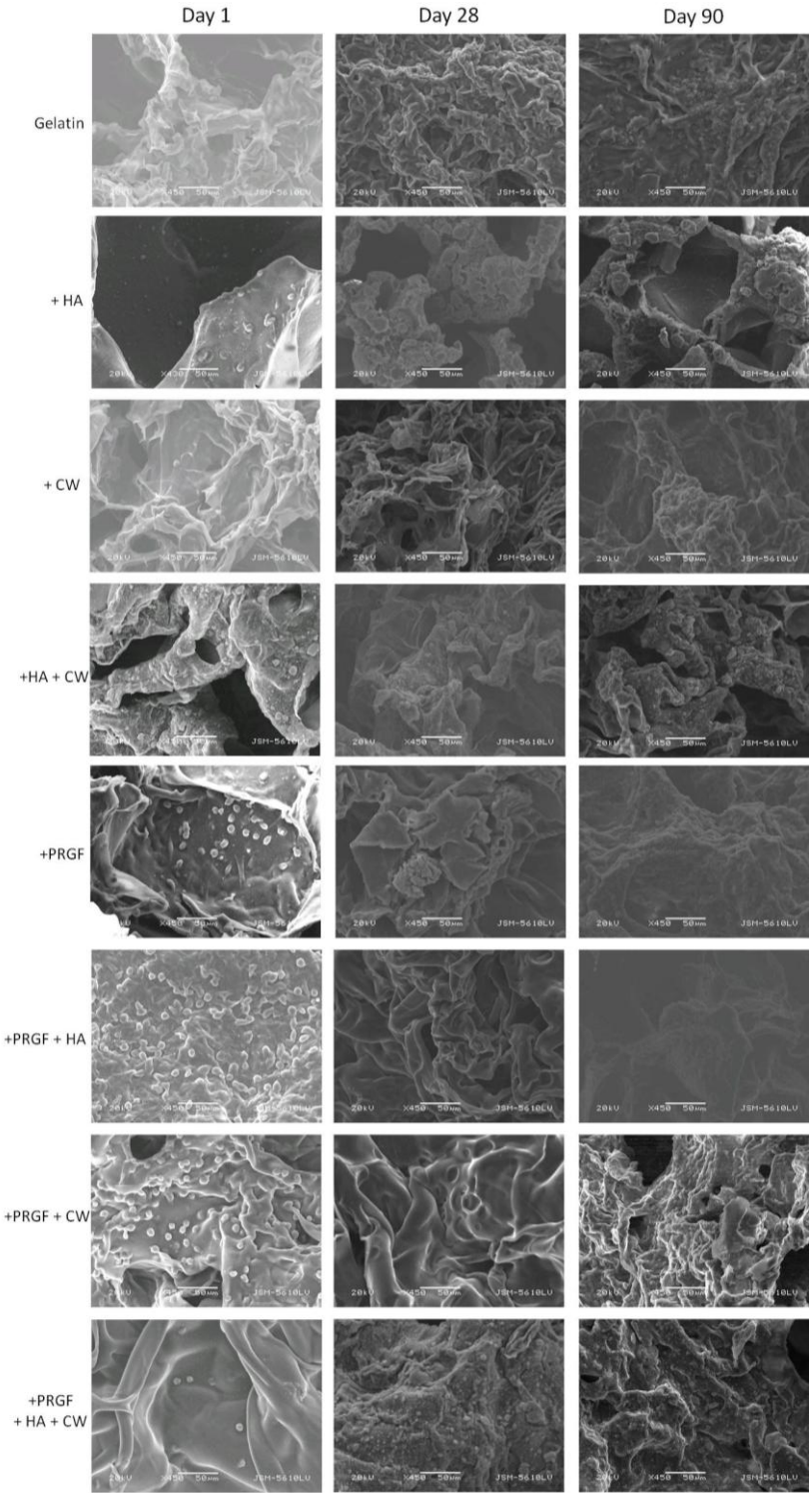

Figure 3.6 - SEM of +EDC cross-linked scaffolds seeded with MG-63 cells for 1, 28, and 90 days. Magnification at 450x and scale bars at 50 µm.

Alizarin Red S staining

Absorbance was measured to compare the relative mineral content of the cellular and acellular composite gelatin sponges incubated for 90 days (Figure 3.7). Each scaffold composition was compared to itself at each day to determine if the addition of MG-63 cells significantly increased or decreased ($p<0.05$) overall scaffold mineral content. Scaffolds were only compared to themselves and not to other compositions since the initial amount of mineral per scaffold varied (i.e. all scaffolds containing +HA had higher absorbance values than scaffolds without +HA). For post cross-linked scaffolds, gelatin, +CW, and +PRGF showed a significant decrease ($p<0.05$) in absorbance after 90 days with cells when compared to 90 days without cells. The only post cross-linked scaffold that had a significant increase ($p<0.05$) in mineral content as a result of cells was +PRGF +HA at day 28. For +EDC scaffolds, the addition of cells resulted in significant decreases ($p<0.05$) in mineral content in gelatin (day 90), +PRGF (day 90), and +PRGF +CW (day 28 and 90) scaffolds. However, there were more +EDC scaffolds that recorded higher absorbance values as a result of the cells producing mineral matrix: +CW (day 28), +HA (day 28 and 90), +PRGF +HA (day 28 and 90), and +PRGF +CW +HA (day 28).

While the ARS results were not consistent for a specific group, the fact that a number of groups exhibited statistically significant increases in mineral matrix production was seen as a positive result indicative of the potential *in vitro* formation of new bone. The statistically significant decreases between day 90 acellular scaffolds and day 90 cellularized scaffolds could be attributed to the previous mention of acellular scaffolds continuously absorbing media (and in conjunction, resident proteins and calcium ions

within the media) over 90 days. Alternatively, cells seeded on scaffolds remodel the constructs as the cells migrate, proliferate, and produce matrix. The ARS stain may have a higher affinity to these adherent resident proteins and calcium than a partially degraded scaffold covered with cells, resulting in a higher ARS absorbance for acellular scaffolds. It has been shown that Alizarin Red S has the ability to also bind to human serum albumin (HSA) [124]. HSA is the most abundant protein in whole blood; as such it is present in PRGF. In addition, bovine serum albumin is present in the cell culture media and can potentially have binding affinity to ARS. In either instance there may be confounding variables when using ARS on samples that have components of blood or that have been exposed to culture media. Overall, the very nature of the ARS procedure (multiple staining/de-staining and washing steps) makes it difficult to obtain truly accurate quantifications of mineral production of cells on scaffolds. However, for the preliminary nature of this study the ARS stain and its fairly positive results proved adequate in demonstrating the osteoinductive potential of the modified gelatin sponges tested here.

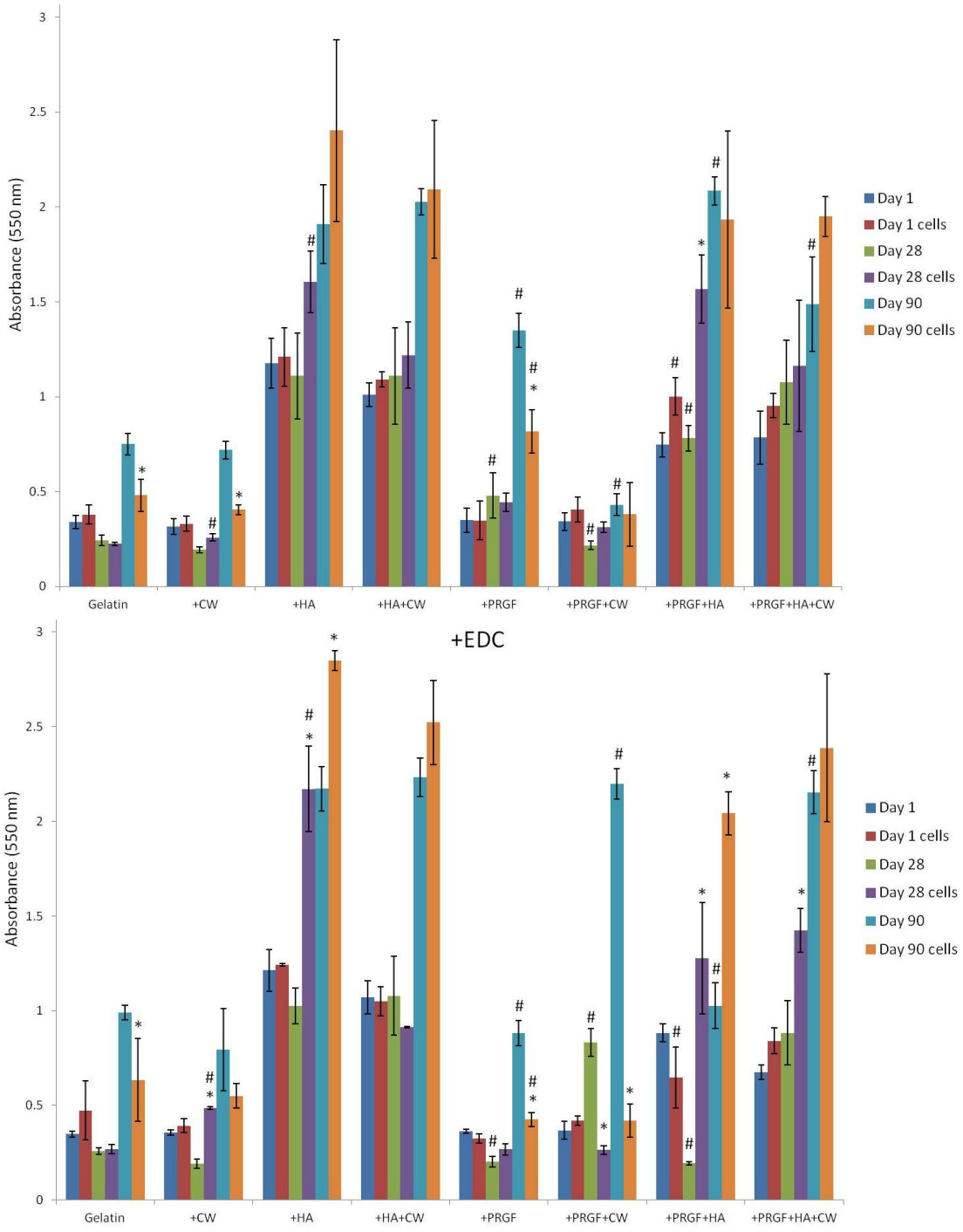

Figure 3.7 - ARS of acellular and cellular scaffolds over 90 days incubation. * denotes a statistical difference ($p<0.05$) between cells and no cells for a specific day and scaffold composition. # denotes a statistical difference ($p<0.05$) when comparing cross-linking methods of each condition.

Statistical analysis was also performed between the two graphs to determine if there were any significant differences in absorbance for a given scaffold on a particular time point. A total of six post cross-linked scaffolds and five +EDC scaffolds showed significant increases in absorbance values when compared to their cross-linked counterparts (Table 3.4).

Table 3.4 - Scaffolds with significant increases ($p<0.05$) in absorbance values when comparing cross-linking methods.

	post cross-linked	**+EDC**
Day 1 cells	+PRGF +HA	
Day 28	+PRGF +PRGF +HA	+PRGF +CW
Day 28 cells		+CW +HA
Day 90	+PRGF +PRGF +HA	+PRGF +CW +PRGF +HA +CW
Day 90 cells	+PRGF	

DAPI staining

The SEM images provided an overview of how cells attached and produced matrix on the surface of gelatin composite sponges. Cell attachment and more importantly, infiltration into the scaffold, was analyzed via DAPI staining. Not all images are reported due to spatial constraints; however, the pure gelatin scaffolds (controls) are compared to three other scaffold compositions that facilitated a more pronounced infiltration of cells. In Figure 3.8, post cross-linked gelatin scaffolds are compared to +PRGF, +PRGF +HA, and

+PRGF +HA +CW. After day 1, cells attached along the surface of the pure gelatin scaffold while the other scaffolds promoted cell infiltration and attachment (as evidence of blue cell nuclei visible throughout the cross section of the scaffold). With post cross-linked scaffolds, it appears that the addition of PRGF enhanced the attachment and infiltration of cells when compared to the gelatin control. The milieu of growth factors and cytokines contained within PRGF (some listed in Table 3.1) are known to be highly chemotactic as well as have the ability to induce cellular attachment, proliferation, and migration in a number of cell types. While the presence and release of PRGF derived biomolecules was not specifically investigated in this study, it can be assumed that the growth factors and cytokines contained within the PRGF are being eluted from the scaffolds based upon previous studies conducted with the incorporation of PRGF into electrospun scaffolds [87, 125]. These results suggest that these molecules remain active post-scaffold fabrication and ultimately increase the bioactivity of the scaffolds.

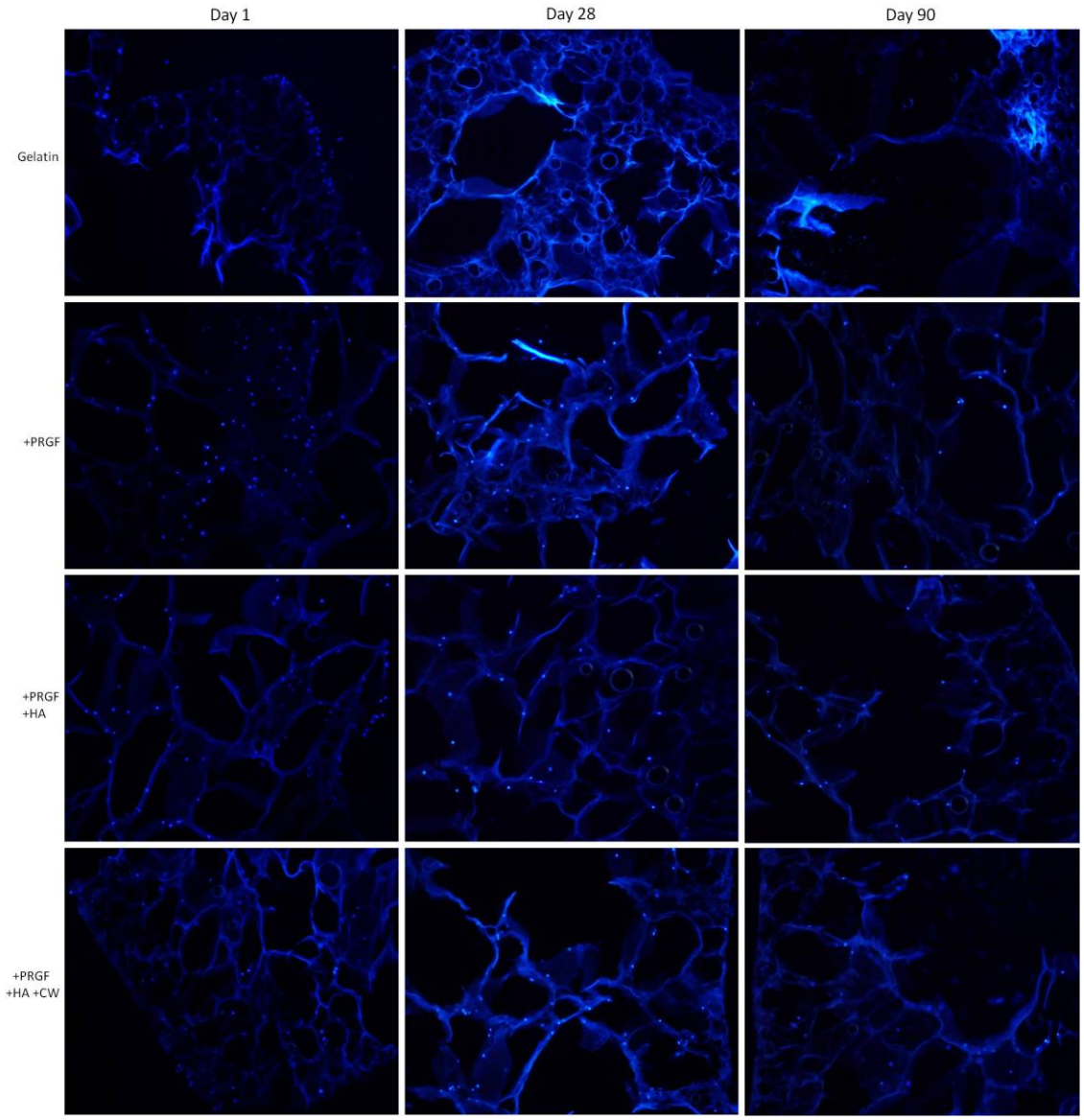

Figure 3.8 - DAPI staining of post cross-linked scaffolds with MG-63 cells for 1, 28, and 90 days. Images taken at 20x magnification.

Figure 3.9 compares the gelatin +EDC control to +CW, +PRGF, and +PRGF +CW +EDC. A similar trend was noticed with the +EDC scaffolds in that cells attached mainly to the control gelatin scaffold surface while the other scaffold compositions showed

enhanced cell infiltration after day 1. However, it appears that more cells penetrated and attached to +EDC scaffolds when compared to post cross-linked scaffolds. By day 28 and 90, it became increasingly difficult to distinguish fluoresced cell nuclei on any scaffolds, independent of cross-linking methods. There appeared to be an abundance of newly created cell matrix at days 28 and 90, especially with +EDC scaffolds. This newly deposited matrix may have interfered with the staining, which commonly produced a uniform fluoresced scaffold making it difficult to discern individual cell nuclei and analyze day 28 and 90 DAPI images. With +EDC scaffolds, the addition of CW and/or PRGF appeared to promote cell attachment and penetration when compared to the gelatin +EDC control.

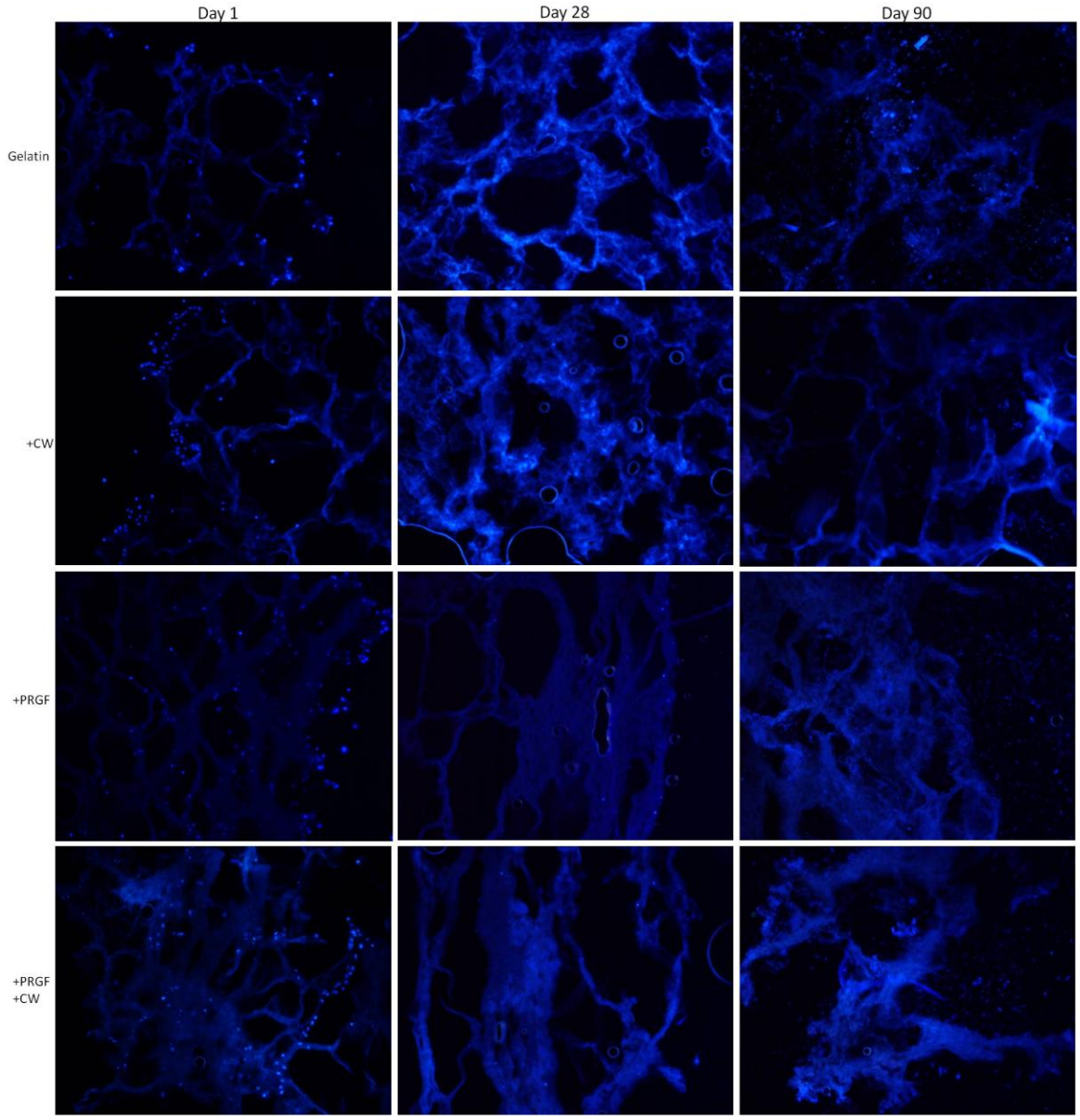

Figure 3.9 - DAPI staining of +EDC cross-linked scaffolds with MG-63 cells for 1, 28, and 90 days. Images taken at 20x magnification.

3.4.4. Uniaxial compression testing

Peak load was recorded to determine the compressive strength of the cellular and acellular composite gelatin sponges incubated for 90 days (Figure 3.10). Each scaffold composition was compared to itself at each day to determine if the presence of cultured cells strengthened or weakened the scaffold over the duration of culture. Most of the post-gelation cross-linked scaffolds did not record a significant difference ($p<0.05$) between cellularized and acellular scaffolds, meaning that the addition of cells did not significantly affect the scaffolds compressive strength positively or negatively. However, significant increases ($p<0.05$) in peak load as a result of culturing cells were observed for +PRGF +HA +CW (day 1 and 28), +CW (day 28), and +PRGF +CW (day 28) post-gelation cross-linked scaffolds. Many of the scaffolds cross-linked during fabrication (+EDC) also did not record significant differences ($p<0.05$) between cells and no cells when comparing scaffolds to themselves at a specific day. Significant increases ($p<0.05$) in compressive strength were recorded for +HA (day 28) and +CW +HA (day 28) scaffolds suggesting the addition of cells improved scaffold strength.

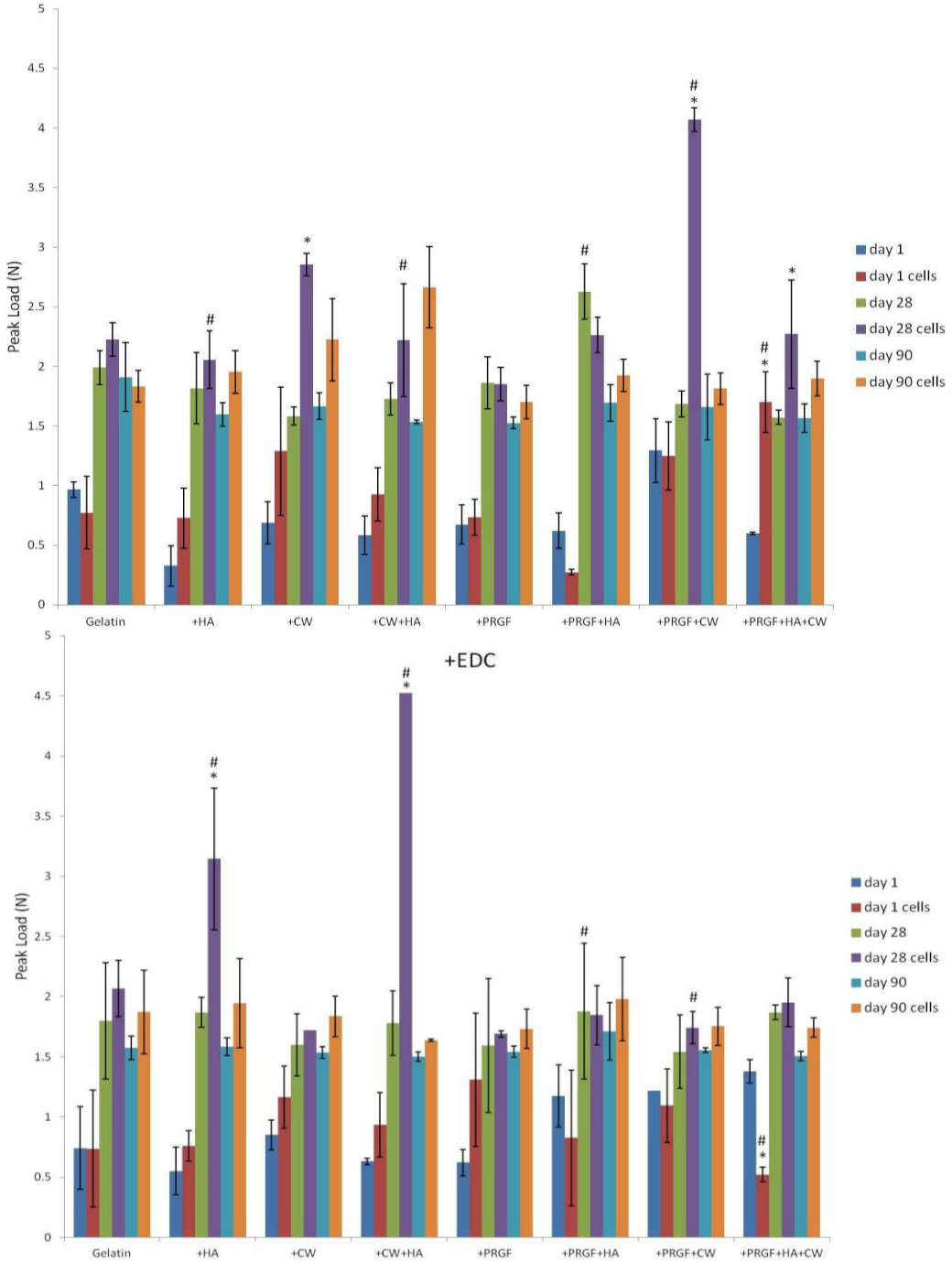

Figure 3.10 - Peak load (N) of acellular and cellular scaffolds over 90 days incubation. *denotes a statistical difference ($p<0.05$) between cells and no cells for a specific day and scaffold composition. # denotes a statistical difference ($p<0.05$) when comparing cross-linking methods of each condition.

Upon comparing peak load between cross-linking methods, it was noticed that for the majority of the scaffolds, the method of cross-linking had no significant effect ($p<0.05$) on the compressive strength for a specific scaffold on a particular day. Cross-linking during scaffold fabrication (+EDC) significantly increased ($p<0.05$) the compressive strength of +HA (day 28 cells) and +CW +HA (day 28 cells) scaffolds. On the other hand, +EDC scaffolds showed significant decreases in peak load for +PRGF +HA (day 28 no cells), +PRGF +CW (day 28 cells), and +PRGF +HA +CW (day 1 cells) scaffolds.

While the nano-indentation for compressive mechanical properties produced satisfactory results, future experiments will use a platen system for testing. Although the nano indenter was within the appropriate size in diameter (2 mm) when compared to the sample diameter (6 mm), there still remains the possibility of local variations in material properties [126]. The platen system compresses the sample using two flat platens (larger that the sample size) instead of a smaller indenter to measure mechanical properties.

3.5. CONCLUSION

In this study it was demonstrated that a lyophilized gelatin gel sponge, modified through the addition of PRGF, HA, and CW, demonstrated clear osteogenic potential when cultured with an MG-63 osteoblast-like cell line. These scaffolds, further modified through EDC cross-linking during gelation, were able to remain intact after 90 days in culture while exhibiting a controlled protein release. This tailorable rate of degradation is critical in a bone repair scaffold, where scaffold breakdown needs to match the ingrowth of new bony matrix to prevent catastrophic failure or the potential for micromotion or stress-

shielding to occur. While this preliminary study failed to determine a clear optimal combination of gelatin and scaffold modifying agents (PRGF, HA, CW) to promote bone regeneration, it demonstrated that the use of a lyophilized gelatin gel sponge with the potential to absorb several times its weight in water was capable of eliciting cell infiltration into the structures as well as promoting the formation of cell-created mineral matrix. However, the +EDC scaffolds containing +PRGF+HA+CW performed well in the preliminary evaluations and need to be further investigated going forward. Further testing must be performed to more accurately determine the cellular interaction with these scaffolds in particular the cellular response inside the structures.

4. MINERALIZATION AND FURTHER CHARACTERIZATION OF LYOPHILIZED GELTIN SPONGES ENHANCED WITH PRGF, HA, AND CW

4.1. ABSTRACT

The application of freeze-dried gelatin sponges as alternative bone grafting substitutes has many advantages which include ability to swell, high porosity, tailorable degradation, and versatile ability to incorporate one or multiple components (proteins, growth factors, inorganic nanofillers, etc.). The previous study demonstrated the enhanced protein release and cell attachment/infiltration in scaffolds cross-linked during gelation (+EDC) and in scaffolds incorporated with biological factors (HA, CW, and PRGF). The purpose of this study was to further characterize freeze-dried gelatin sponges enhanced with PRGF, HA, and CW and cross-linked during gelation (PHCE). Freeze-dried gelatin+EDC (GE) scaffolds were used as a control. Scaffolds were also mineralized (M) in 5x r-SBF to create a bone-like mineral surface. GE, GE-M, PHCE, and PHCE-M scaffolds were characterized for their ability to swell, mineralization (ARS), surface characteristics (SEM), protein release (BCA protein assay), release of PRGF, and uniaxial compression properties (using 2 platens to record modulus and peak load). A growth factor profile of PRGF was also obtained using a human angiogenesis kit and a multiplexer. Growth factors detected in PRGF included VEGF-A, HGF, EGF, FGF-2, VEGF-C, IL-8, and VEGF-D (listed in descending order of concentrations present). Both GE and PHCE scaffolds were porous structures that swelled up to 50% of their original volume upon

hydration. SEM showed sparse clusters of mineral deposition for GE-M scaffolds while PHCE-M scaffolds exhibited a more uniform mineral deposition throughout the surface. ARS was unable to detect any differences between mineralized and non-mineralized scaffolds, however it did show a significant increase in mineral content between GE and PHCE scaffolds which was expected since HA was incorporated within PHCE scaffolds and not present in GE scaffolds. Over 21 days, scaffolds released more of their contents during the first 7 days when compared to later time points. By day 21, PHCE-M scaffolds cumulatively released about 30% of its original protein content, significantly more than all other scaffolds. For uniaxial compression testing of hydrated sponges, PHCE-M scaffolds report lower Young's modulus values (1.3 - 1.6 MPa) when compared to GE and GE-M scaffolds (1.6 – 3.2 MPa). These low modulus values are comparable to values of tissue found in early stages of bone healing. The results of the study demonstrate the enhanced performance of PHCE and PHCE-M scaffolds to serve as bone healing scaffolds. Their potential to release incorporated factors and comparable composition and mechanical properties to tissues developed in the early stages of bone healing make them suitable for further studies evaluating cellular responses.

4.2. INTRODUCTION

There are several properties and characteristics to consider when fabricating an ideal scaffold intended for bone tissue engineering. These include: biocompatibility, degradability (as scaffold degrades, space is created for new bone), porosity (angiogenesis and migration/infiltration of cells to deposit bone within), mechanical integrity (ability to

maintain its structure and mimic mechanical properties found in bone healing microenvironment), osteoconductivity (ability to support bone growth), and osteoinductivity (ability to differentiate osteoprogenitor cells into osteoblasts). A lyophilized gelatin sponge cross-linked with EDC during gelation provides a biocompatible, porous, and degradable scaffold. The addition of PRGF contains many growth factors and cytokines which are known to enhance angiogenesis and osteogenesis (as previously described). The incorporation of HA and CW is also known to enhance osteoconductivity and mechanical integrity. The further acquisition of minerals to a scaffold surface via SBF treatment can further enhance osteoconductivity of scaffolds. The purpose of this study is to characterize acellular cross-linked lyophilized gelatin sponges enhanced with PRGF, HA, and CW (PHCE). The addition of a bone-like mineral surface from SBF treatment created mineralized (M) scaffolds which were also characterized and compared to their non-mineralized counterparts. A growth factor profile of uncross-linked PHC scaffolds and dilutions of PRGF, PRP, and PPP was obtained to identify key growth factors present at different stages. Gelatin controls (GE) were compared to GE-M, PHCE, and PHCE-M in regards to mineralization, protein release, growth factor incorporation, and mechanical properties to determine if these scaffolds appropriately meet the design characteristics of an ideal bone tissue engineering scaffold intended for early bone healing.

4.3. MATERIALS AND METHODS

4.3.1. Fabrication of gelatin composite sponges

Based on the results from Chapter 3, the PRGF+HA+CW+EDC scaffolds exhibited desirable characteristics of a potential bone tissue engineering scaffold and was further studied in this experiment. Gelatin+EDC scaffolds served as the control. Lyophilized gelatin+EDC (GE) and PRGF+HA+CW+EDC (PHCE) sponges were fabricated using the same method as described in Chapter 3, Section 3.3.1. Briefly, a 30 mg/mL gelatin solution in DI water was used as the base solution for creating gels. For GE scaffolds, 50 mM of EDC was added to 4 mL of the gelatin solution, briefly mixed, pipetted into a 35 x 10 mm Petri dish, and stored in a refrigerator at 4°C overnight to gel. For PHCE scaffolds, 3.33 mg/mL of both HA and CW were added to 4mL of the gelatin solution then sonicated. 3.33 mg/mL of PRGF was then added to the gelatin-HA-CW solution and allowed to completely dissolve (about 3 mins). 50 mM EDC was then added to the 4 mL gelatin-PRGF-HA-CW solution, briefly mixed, transferred to a 35 x 10 mm Petri dish, and allowed to gel overnight at 4°C. After gelation of all solutions, gels were slowly frozen to -70°C and lyophilized to obtain the composite porous sponges. 6 mm discs were then punched and used for all studies.

4.3.2. Swelling percent

To quantify the initial swelling capability of the GE and PHCE lyophilized sponges, measurements of the scaffold's dimensions were recorded dry and after 1 day hydration in DMEM high glucose media containing 10% FBS and 1%

penicillin/streptomycin. Volume was calculated using the standard equation for the volume of a cylinder (π * radius^2 * height). The formula (hydrated volume – dry volume) / (dry volume) was used to determine the swelling ratio of each scaffold. This ratio was then multiplied by 100 to calculate the percent increase in volume for each scaffold as a result of hydration (swelling percent).

4.3.3. Scaffold mineralization

The ionic concentrations of the commonly used SBF, conventional SBF (c-SBF), are not exactly equal to those of blood plasma. Oyane *et al.* made revisions to c-SBF and created three new SBFs (revised (r), ionic (i), and modified (m)) that have ionic concentrations equal to, or closer to, those of blood plasma (Table 2.2). The ionic concentrations of the r-, i-, and m-SBFs were formulated to equal those of total blood plasma, dissociated blood plasma, and total blood plasma (except for HCO3-), respectively. Of the compositions, r-SBF is the closest to the concentration of total blood plasma; in fact it is an exact match. For this reason, a r-SBF solution was prepared by following the published protocol for 1x r-SBF and increasing each ion concentration by a factor of 5 [111]. A higher (5x) concentration of SBF was chosen in order to effectively mineralize the scaffolds with minimal incubation time.

Triplicates of 6 mm (diameter) discs were punched from each of the composite gelatin sponges and separately incubated in 1 mL of 5x r-SBF for 1 hour at 37°C and 5% CO_2 atmosphere. Preliminary studies mineralized scaffolds for 1, 6, and 12 hours and determined that 1 hour incubation in 5x r-SBF was sufficient to mineralize the scaffold.

Mineralization was performed under static conditions with the discs completely submerged in SBF. After 1 hour incubation, scaffolds were removed and rinsed with DI water to wash off any minerals that were not bound to the scaffold. To visually inspect surface mineralization, one scaffold disc was dehydrated and used for SEM analysis. For mineral quantification, Alizarin Red S staining was used. GE and PHCE mineralized scaffolds are denoted as GE-M and PHCE-M, respectively.

4.3.4. Scanning electron microscopy

Scanning electron microscopy (SEM) was performed in order to evaluate the scaffold surface characteristics prior to and following mineralization. GE, GE-M, PHCE, and PHCE-M samples were disinfected (30 minutes ethanol followed by three washes of 1x PBS) to simulate preparation for cell studies, air-dried, mounted on an aluminum stub, carbon coated, and examined using a Hitachi SU-70 scanning electron microscope (accelerating voltage at 20 kV).

4.3.5. Alizarin Red S staining

Alizarin Red S (ARS) staining was used to quantify scaffold mineral content by modifying a published protocol as previously described in Chapter 3, Section 3.4.4. [112]. ARS was performed on the 6 mm scaffold punches before and directly after mineralization, and after 21 days incubation in 1x PBS at 37°C and 5% CO_2. At the desired time points, scaffolds were stained with 40 mM Alizarin Red for 30 minutes then washed with DI water to remove any unbound stain. Scaffolds were then transferred to a 2 mL microcentrifuge tube containing 1.5 mL of 50 % acetic acid to destain for 1 hour at room temperature. 500

µL of the solubilized stain was added to 600 µL of 1 M NaOH to adjust the pH to 4.1. 200 µL of this solution was then pipetted into a 96-well plate and absorbance read at 550 nm using a SpectraMax Plus 384 Microplate Spectrophotometer. Absorbance values were compared to each other to determine any change in mineral content as a result of mineralization or degradation.

4.3.6. Scaffold protein release

Release of protein from the scaffolds was measured as one parameter to assess potential degradation. To determine total protein content of each 6 mm scaffold disc, triplicates of non cross-linked 6 mm punch of each scaffold type were immersed in 1 mL of 1x PBS. Non cross-linked scaffolds completely degraded within minutes at room temperature, however scaffolds were left overnight to ensure complete degradation. Since scaffolds are primarily comprised of gelatin, the degraded byproducts are detectable using a general protein assay. Protein was quantified using a Pierce BCA Protein Assay as previously described (in Chapter 3, Section 3.3.3.). Scaffold release kinetics were studied by quantifying protein release from each scaffold over a period of 21 days. Triplicates of one 6 mm disc of each cross-linked scaffold type were incubated in 1 mL of 1x PBS at 37°C with PBS replaced on every analysis point. After 1, 4, 7, 14, and 21 days the PBS containing released scaffold contents in each well was analyzed for protein content using the Pierce BCA Protein Assay.

4.3.7. Growth factor analysis

The same protein release model described in Section 4.3.6 was used to identify and quantify the PRGF growth factors incorporated and released from PRGF containing scaffolds. After 1, 4, 7, 14, and 21 days the 1 mL of 1x PBS containing released PHCE and PHCE-M scaffold contents in each well was analyzed for specific growth factor content. As a control of total growth factors present in each scaffold, triplicates of 6mm discs of uncross-linked gelatin+PRGF+HA+CW (PHC) scaffolds were completely degraded in 1mL of 1x PBS by overnight incubation at 37°C. Dilutions of pure PRGF (100, 50, 10, 1, and 0.1 mg/mL), PRP (1:10 and 1:20), and platelet-poor plasma (PPP, 1:10, 1:20) in DI water were also analyzed to obtain a profile of growth factors present in PRGF, PRP, and PPP alone. This detection and quantification was accomplished by using a Luminex MagPix multiplexer (fluorescent imager) with the MILLIPLEX® MAP human angiogenesis/growth factor magnetic bead panel 1. The Angiogenesis kit contained analytes specific to detecting epidermal growth factor (EGF), granulocyte colony-stimulating factor (G-CSF), fibroblast growth factor-1 (FGF-1), FGF-2, interleukin 8 (IL-8), hepatocyte growth factor (HGF), vascular endothelial growth factor A (VEGF-A), VEGF-C, and VEGF-D. The basic concept behind the Luminex technology is the use of internally color-coded microspheres which are each coated with a specific capture antibody (capable of capturing the analytes above). These microspheres are mixed with the released contents of PHCE and PHCE-M scaffolds where the specific capture antibody can capture the appropriate analyte. After this occurs, a biotinylated detection antibody is introduced followed by the addition and incubation of a reporter/detection molecule to complete the

reaction on the surface of each microsphere. Presence and quantification of analytes are detected based on fluorescent reported signals read by the Magpix system.

4.3.8. Uniaxial compression testing

Uniaxial compression testing was performed on acellular 6 mm scaffold discs after 1, 4, 7, 14, and 21 days incubation in media. Mechanical testing was conducted by using 2 flat metal platens from tension grips (in place of the indenter described in Chapter 3) attached to a Bionix 200 Mechanical Testing System instrument with a 100 N load cell (MTS Systems Corp., USA). The platen system was used to increase accuracy of compressive mechanical testing by increasing the area of compression on the scaffold. The 2 platens spanned the entire 6 mm scaffold disc, while the indenter was only 2 mm in diameter. Platen compression was performed perpendicular to the scaffold surface without any circumferential constraints to allow for free lateral deformation (Figure 4.1). Scaffolds were removed from media, dabbed on a kimwipe to remove excess media/liquid, then placed on the flat metal surface (samples were still hydrated). The upper platen was lowered to the surface of the scaffolds and the following parameters were used: test speed of 0.5 mm/min, data acquisition rate of 10 Hz, and a preload of 0.01 N. Compression was continuous until the scaffold was completely flattened, the platens were compressing against each other, and terminated just before the system maxed out at 100 N. Peak load and Young's modulus for compression were extracted and calculated using the graphical output from the MTS software TestWorks 4.0. Peak load was extracted from the largest

load value before the system began to max out. The compression modulus was calculated using the initial linear region of the stress-strain curve [127].

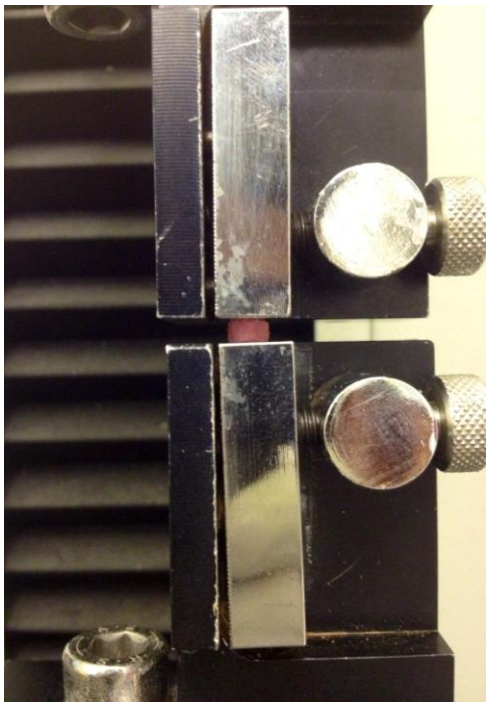

Figure 4.1 - Compressive mechanical testing set up with scaffold between flat platens.

4.3.9. Statistical analysis

Statistical analysis was performed using JMP IN 9 statistical software (SAS Institute) to determine significant differences. Analysis of the data was based on a Kruskal-Wallis one-way analysis of variance on ranks and a Tukey-Kramer pairwise multiple comparison procedure. The results are presented in mean ± standard deviation (SD). Samples were run at least in triplicates (n=3) to ensure statistical significance ($p<0.05$).

4.4. RESULTS AND DISCUSSION

4.4.1. Swelling percent

In Chapter 3, it was discovered that these lyophilized gelatin composite sponges have the ability to absorb the solution they are hydrated in (media and 1x PBS) and significantly increase their mass. By calculating the swelling percent, we are able to further characterize the hygroscopic nature of these sponges and their ability to potentially fill a void space upon implantation. By calculating changes in volume, it was determined that both GE and PHCE lyophilized sponges swelled approximately 50% (Figure 4.2). There was no statistical difference ($p < 0.05$) between the swelling of GE and PHCE scaffolds suggesting that the added components of PRGF, HA, and CW do not enhance nor hinder the swelling ability of the scaffold. The result of no statistical differences in swelling could be attributed to the fact that the 3.33 mg/mL of each PRGF, HA, and CW added to the 30 mg/mL gelatin solution was too low to overcome the natural sweling properties of the gelatin sponge. It would be interesting to study the swelling percentage with increased concentrations of PRGF, HA, and CW to determine if there is a threshold in which the scaffold can no longer swell.

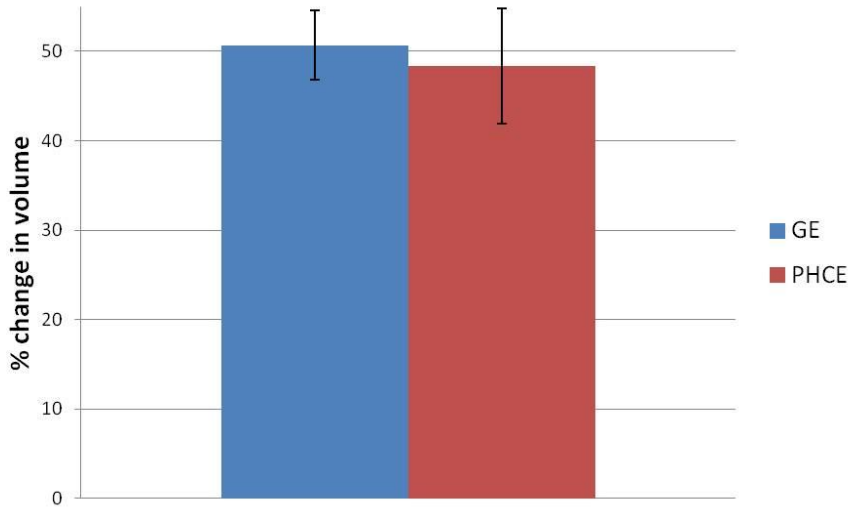

Figure 4.2 - Swelling percentage of GE and PHCE scaffolds upon hydration.

4.4.2. Scanning electron microscopy

Scanning electron microscopy (SEM) revealed surface characteristic differences between GE and PHCE scaffolds, as well as mineralized and non-mineralized scaffolds (Figure 4.3). GE scaffolds appear to have a smoother material surface with smaller pores while PHCE scaffolds contain a rougher surface with larger pores. Since GE scaffolds are only composed of gelatin, it is expected that they exhibit a more uniform surface composition. The addition of growth factors and nanofillers for PHCE scaffolds alter the scaffold characteristics by having a presence of the added molecules on the surface as well as a larger pore size. It is hypothesized that the small spheres and rougher surface visualized in Figure 4.3B is attributed to the incorporated nanofillers (HA and CW) present on or near the surface of the scaffold. After mineralization, GE-M scaffolds showed small clusters of mineral nucleation while PHCE-M scaffolds exhibited a more uniform

attraction. One of the aims of this dissertation is to evaluate differences between mineralized and non-mineralized scaffold protein release, mechanical properties, and cellular response to understand any added benefit to the nucleation of crystals to the scaffold surface.

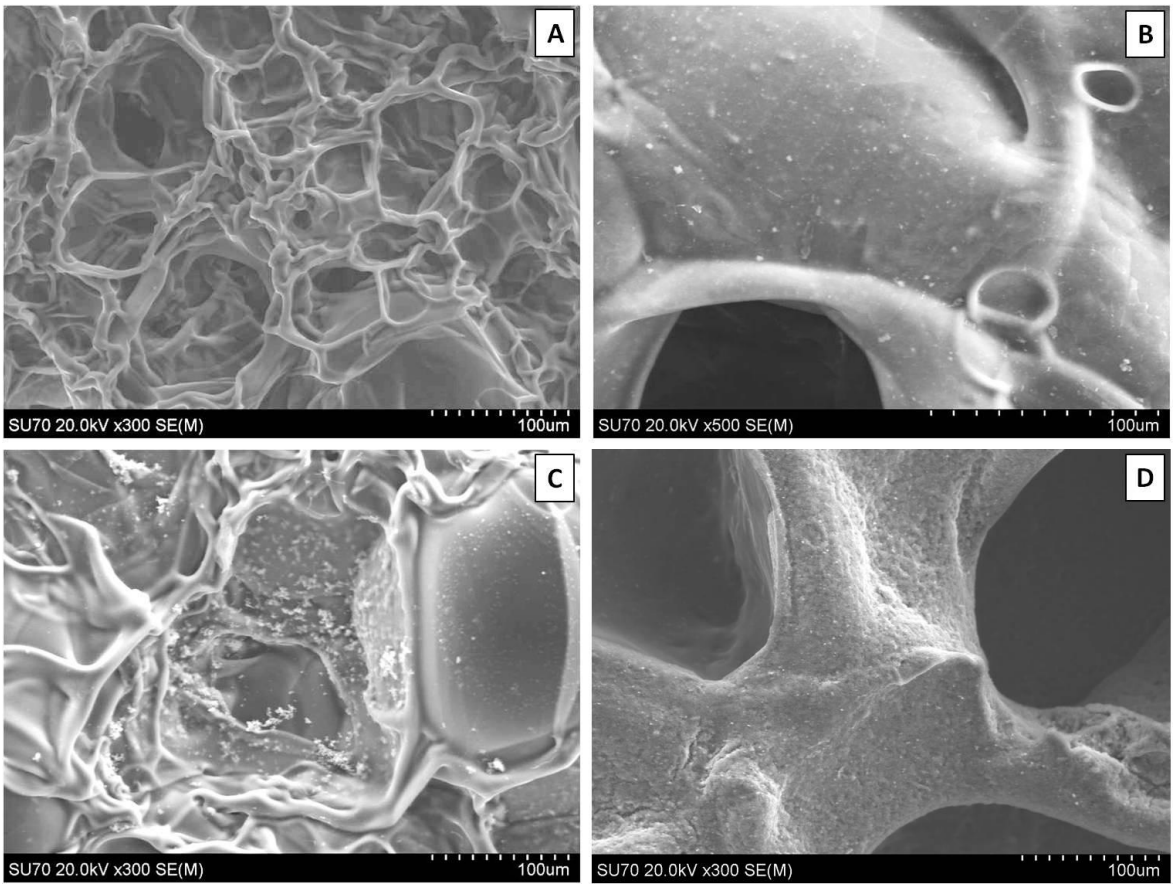

Figure 4.3 - SEM of (A) GE, (B) PHCE, (C) GE-M, and (D) PHCE-M scaffold surfaces. Scale bars at 100 µm.

4.4.3. Alizarin Red S staining

Alizarin Red S staining was performed on GE and PHCE scaffolds before and directly after mineralization (Day 0). ARS was also performed on all scaffold types after

21 days incubation in 1x PBS to asses any potential loss of mineral content as a result of scaffold degradation (Figure 4.4). Results indicate a significant increase ($p<0.05$) in mineral content between GE and PHCE scaffolds. This is expected since HA was incorporated into the PHCE scaffolds and not within GE scaffolds. The ARS assay was not sensitive enough to detect statistical differences between mineralized and non-mineralized scaffolds. There were no significant differences ($p<0.05$) in absorbance values between all scaffolds at day 21. In fact, all day 21 absorbance values (with the exception of GE-M) were significantly lower ($p<0.05$) than day 0 values for the same scaffold type. This suggests that some minerals are being released as the scaffold degrades. It is unclear as to why the GE scaffolds had lower values at day 21 when compared to day 0. It was noticed that ARS bound to GE scaffolds to some degree and is possible that this baseline affinity binding was decreased as the scaffold degraded.

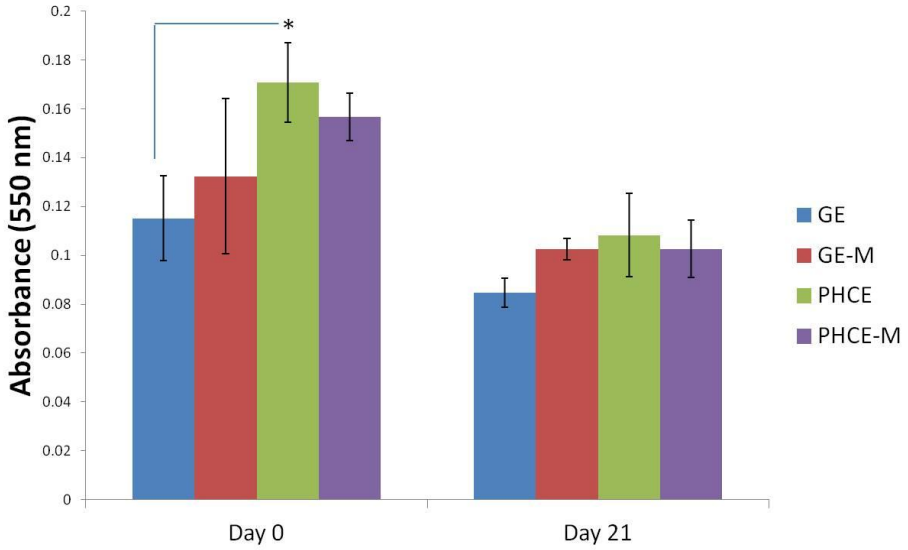

Figure 4.4 - ARS of GE and PHCE scaffolds directly before and after mineralization (Day 0) and of all scaffolds after 21 days incubation in 1x PBS.

4.4.4. Scaffold protein release

One of the main considerations to take into account when designing any tissue engineering scaffold is degradation. Scaffolds that degrade too quickly will fail early when implanted, while extremely slow degrading scaffolds do not allow a favorable environment for cells to remodel and replace the construct with new tissue. In this study, the Pierce BCA assay was used to quantify amounts of general protein released from the lyophilized composite gelatin sponges into solution. This data provides some insight into scaffold degradation in that as the scaffold degrades, it releases its protein contents.

In order to understand the degree to which the scaffold is breaking down, we first must know the original total protein content of the 6 mm discs. The original total protein of each disc was quantified by allowing non cross-linked gelatin (G) and gelatin+PRGF+HA+CW (PHC) scaffolds to fully degrade in PBS. There was no statistical difference ($p<0.05$) between the average original total protein content of the G (1022 µg) and PHC (1102 µg) scaffolds (Figure 4.5). It was expected that the PRGF containing scaffolds would record higher initial protein values since it was an additive to the existing gelatin solution. However, the small amounts of PRGF added (3.33 mg/mL) may not be enough protein to record detectable differences when compared to the majority component of gelatin (30 mg/mL). It is hypothesized that if a higher concentration of PRGF was added to the scaffolds, then a detectable increase in protein content would be observed.

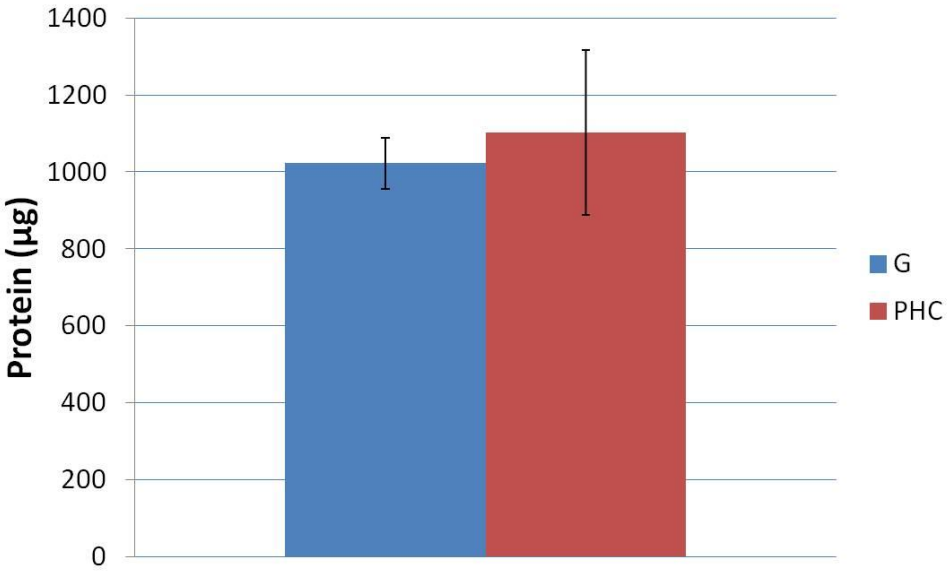

Figure 4.5 - Original total protein content of non cross-linked scaffolds.

Knowing that the G and PHC scaffolds contain the same amount of total protein, we can now directly compare GE, GE-M, PHCE, and PHCE-M release kinetics over 21 days without standardization. Figure 4.6A below graphically displays scaffold protein release quantification over 21 days such that a comparison can be made between which scaffolds released the most protein per time point. Interestingly, all scaffold types released similar amounts of protein (no significant difference, $p<0.05$) on days 1, 7, and 14. On the other hand, PHCE-M scaffolds released significantly more protein ($p<0.05$) on days 4 and 21 when compared to GE, GE-M, PHCE and GE, GE-M scaffolds, respectively. This data suggests that PHCE-M scaffolds are degrading and releasing its contents at a faster rate than all other scaffolds, particularly on days 4 and 21.

The same data presented in Figure 4.6A is graphed differently (Figure 4.6B) to examine the protein release kinetics of a given scaffold composition over 21 days

incubation in PBS. For GE scaffolds, there was a significant decrease ($p<0.05$) in release on day 21 when compared to days 1, 4, and 14. However, a significant increase ($p<0.05$) in release was observed between days 7 and 14. GE-M scaffolds exhibited a similar significant decrease ($p<0.05$) in release on day 21 when compared to days 1, 4, and 7. Day 14 release from GE-M was also significantly lower than day 1. This suggests that most of the release of GE-M scaffolds occurs within the first 7 days. For PHCE scaffolds, day 1 release was significantly higher ($p<0.05$) than all other time points. Day 4 PHCE release was also significantly higher ($p<0.05$) than day 21. This data supports that there is a bulk release of PHCE scaffolds on day 1, followed by sustained release of protein at lower doses. For PHCE-M scaffolds, protein release on day 4 was significantly higher ($p<0.05$) than on days 7, 14, and 21. These results suggest that for PHCE-M scaffolds, there is normal release on day 1, while day 4 releases more compared to the following time points. Overall, these results show that each scaffold has its own protein release profile which indicates that mineralization can alter the scaffold degradation.

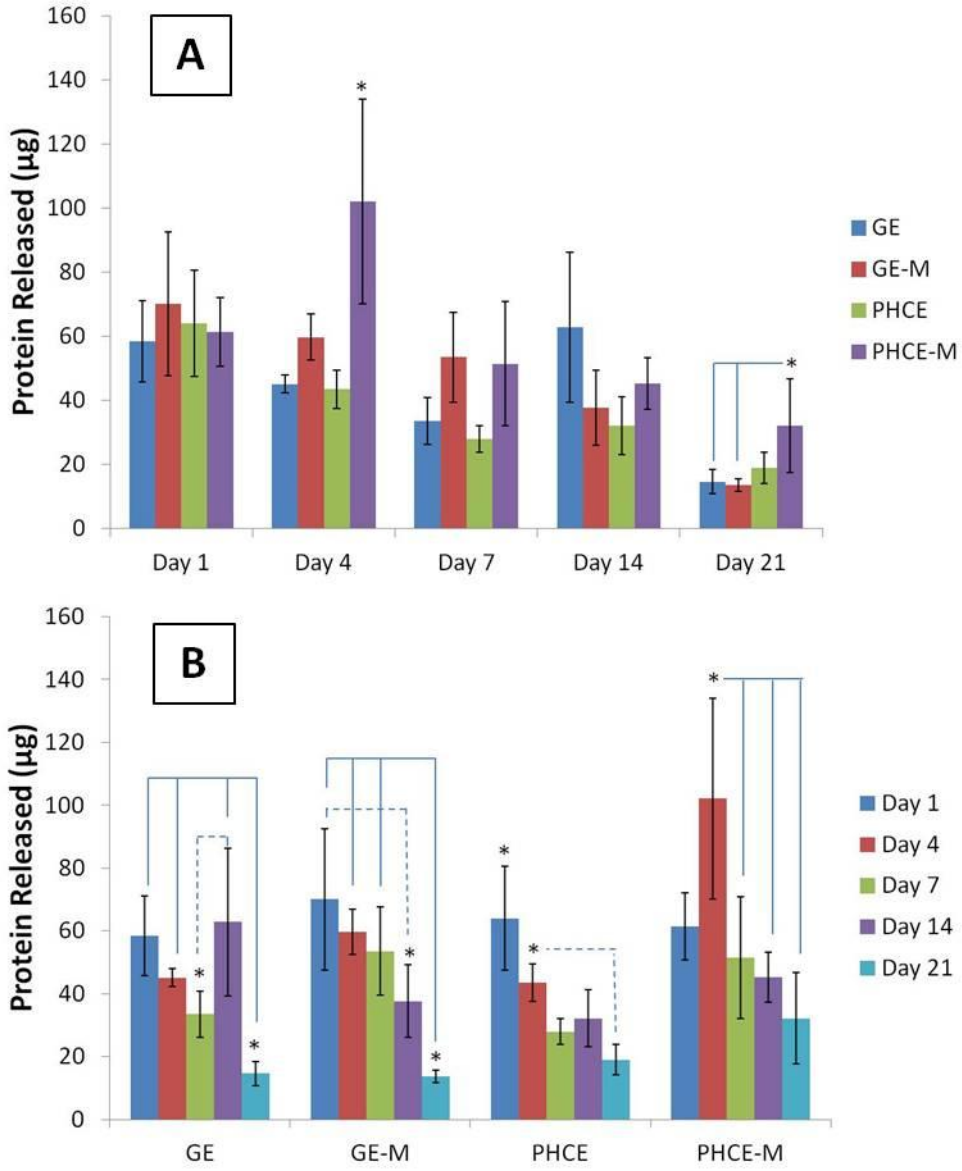

Figure 4.6 - Comparison of protein released A) by scaffolds at a given time point and B) over time, specific to each scaffold.

The protein release analysis presented up to this point focused on release kinetics of a particular scaffold at a specific time point. However, the overall cumulative protein release from each scaffold over the 21 days has yet to be discussed. Using the same data

presented above, the cumulative protein release as a concentration and percent of total protein released from each scaffold was summed and graphed (Figure 4.7). These graphs illustrate that starting on day 4, PHCE-M release more protein overall compared to all other scaffold types. Specifically looking at Figure 4.7B, we are able to demonstrate that PHCE-M scaffolds are releasing 5% of its total protein content between days 14 and 21 while all other scaffold types are only releasing approximately 1%. This suggests that PHCE-M scaffolds are capable of sustained release of high quantities of protein even at later time points.

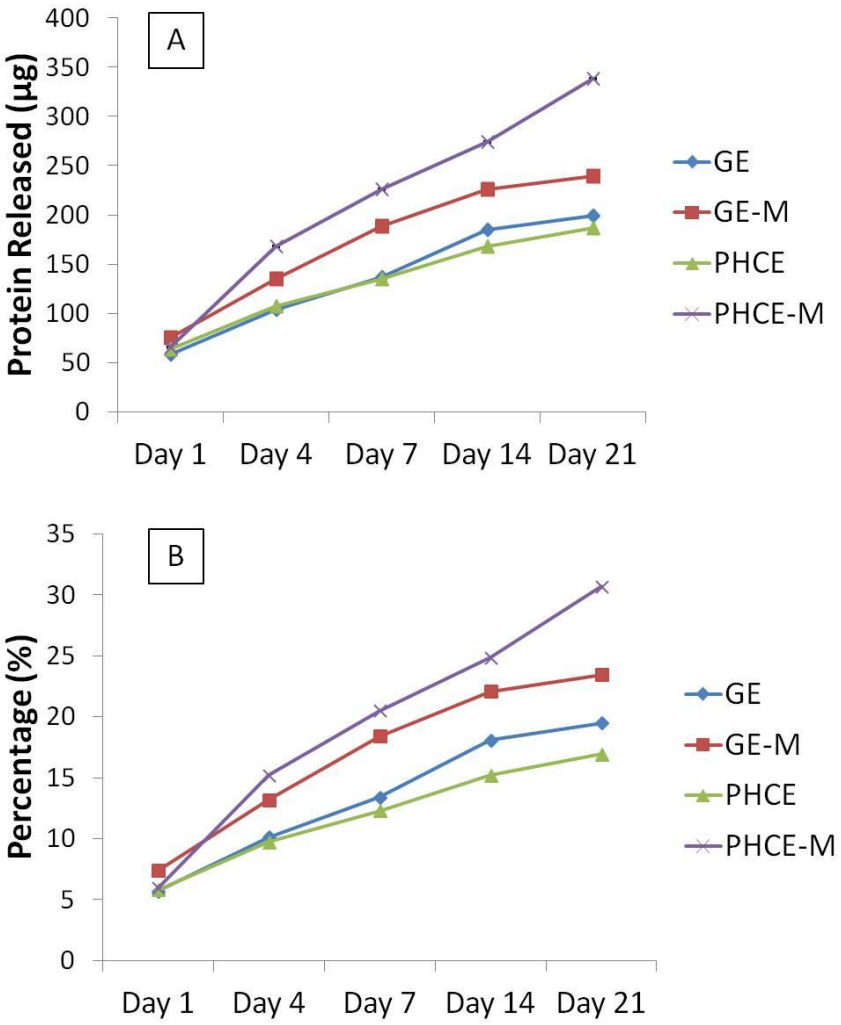

Figure 4.7 - Cumulative protein release measured as A) concentration and B) percent of total protein from scaffolds over 21 days.

In order to gain a relative understanding of protein quantity released by each scaffold, day 21 cumulative released amounts were compared to non cross-linked original total protein content to determine the percentage of protein released (Figure 4.8). GE, GE-M, PHCE, and PHCE-M released 19.5%, 21.4%, 16.9%, 30.7%, respectively. Cumulative protein release from PHCE-M scaffolds was significantly higher ($p<0.05$) than all other

scaffolds. GE-M cumulative release was also significantly higher ($p<0.05$) than only PHCE release. These results show that PHCE-M scaffolds are capable of 30.7% release of its incorporated protein within the first 21 days and that mineralization of PHCE scaffolds increases protein release. The increase in mineralized scaffold protein release could be attributed to the gaps that form during mineralization between the inorganic particles and the polymer matrix which can provide channels for the penetration of water [128]. Continuous elevated sustained release of protein is ideal for tissue engineering scaffolds, rendering PHCE-M scaffolds a viable candidate for tissue regeneration constructs.

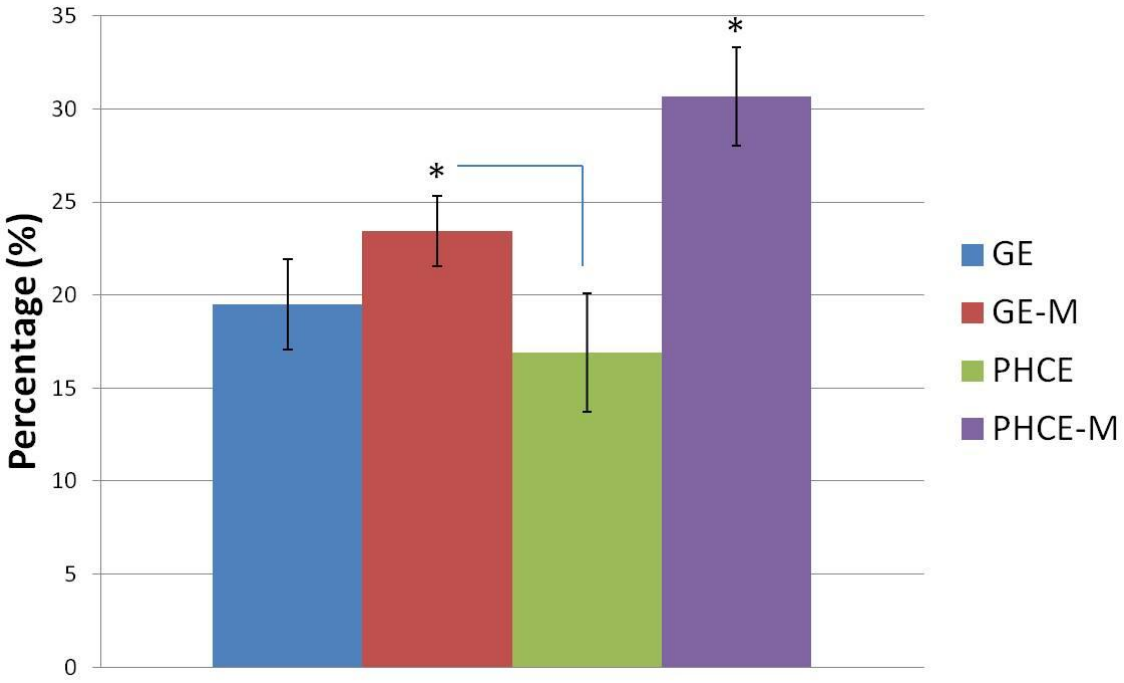

Figure 4.8 - Cumulative protein released (after 21 days) as a percentage of the original total protein content.

4.4.5. Growth factor analysis

Understanding which growth factors are present in liquid PRP and PRGF (lyophilized PRP) are important when analyzing cellular responses to scaffolds. Although PPP was not used in this study, a growth factor analysis of PPP was performed to understand the composition and difference between PRP and PPP. In this study, a PRGF, PRP, and PPP growth factor profile curve was obtained from dilutions of pure PRGF (100, 50, 10, 1, and 0.1 mg/mL), PRP (1:10 and 1:20), and PPP (1:10 and 1:20) in DI water. Although these profiles do not encompass all growth factors present in PRGF, PRP, and PPP, it does provide an analysis of the several key factors (Figure 4.9). Of the analytes used, only two growth factors (G-CSF and FGF-1) were not detected and therefore not present in PRGF, PRP, or PPP. The highest concentrations of growth factors detected in PRGF and PRP were HGF and VEGF-A. Lower amounts of EGF, FGF-2, and VEGF-C were also present. IL-8 and VEGF-D were detected at even lower concentrations. As expected, the dilutions of PRGF and PRP resulted in low recorded values for all growth factors. However, PRGF (100 and 50 mg/mL) and PRP (1:10 and 1:20) provide a strong profile of growth factors present. It was expected that PRGF and PRP report the same growth factor profile since PRGF is a lyophilized version of PRP. This demonstrates that of the factors analyzed, PRP lyophilization does not affect the growth factors present in PRGF. It was noticed that the concentrations for each growth factor within PRP (1:10 and 1:20) more closely resemble the PRGF values at 10 mg/mL dilution. Since PRP is a liquid, it is measured in volume when administered clinically and experimentally. Alternatively, PRGF is measured as a weight/volume concentration since it is a powdered substance. This

analysis suggests that the concentrations of growth factors present in a 1:10 and 1:20 dilution of PRP is comparable that found in 10 mg/mL of PRGF. Table 4.1 presents the mean value of all growth factor concentrations within PRGF, PRP, and PPP dilutions with PRP (1:10 and 1:20) and PRGF (10 mg/mL) highlighted to show the comparison of similar growth factor concentrations. As summarized in Chapter 2 and table 2.1, PRGF components have positive effects on angiogenesis and bone remodeling both *in vivo* and *in vitro*. PPP was not expected to contain high concentrations of growth factors since there are a low number of platelets. The analysis of PPP dilutions revealed the low presence of FGF-2, HGF, VEGF-A, VEGF-C, and VEGF-D. The growth factor profile of PPP (1:10) more closely resembles that of PRGF (1 and 0.1 mg/mL), both highly diluted solutions. The PPP growth factor analysis profile is also presented in Table 4.1.

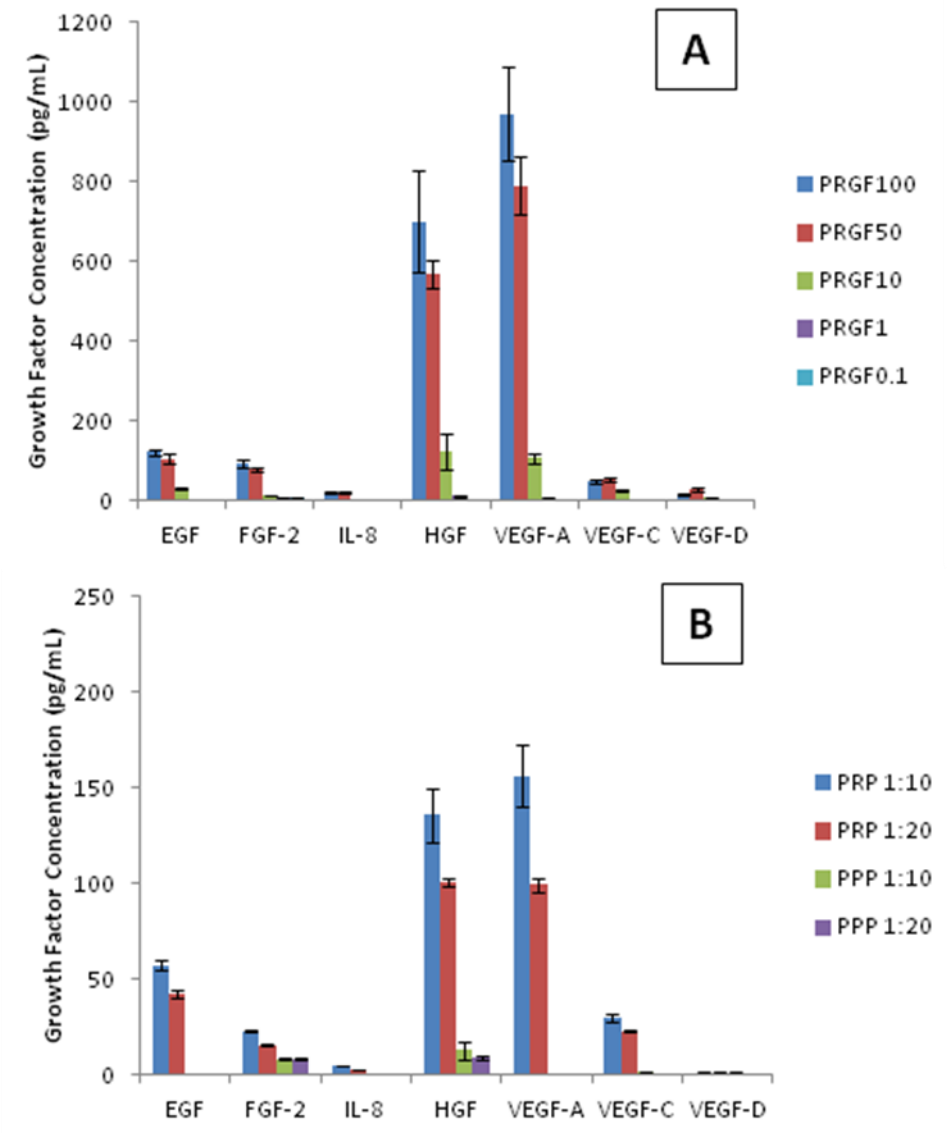

Figure 4.9 - Growth factor analysis of (A) PRGF, (B) PRP and PPP dilutions.

Table 4.1 - Average growth factor concentration (pg/mL) in PRGF, PRP, and PPP dilutions. The average of the lowest standard is presented as the minimum level of detection (Min Detection).

	EGF	FGF-2	IL-8	HGF	VEGF-A	VEGF-C	VEGF-D
PRGF100	121.0	93.6	20.5	700.2	970.8	48.1	13.8
PRGF50	105.3	78.0	19.3	569.2	789.8	51.9	25.6
PRGF10	28.9	12.6	3.9	124.3	105.6	25.6	7.2
PRGF1	0.0	9.0	0.2	12.2	4.4	1.2	0.0
PRGF0.1	0.0	9.0	0.0	1.1	0.0	0.0	0.0
PRP 1:10	57.3	22.8	4.9	135.8	156.4	30.1	1.0
PRP 1:20	42.4	15.7	3.2	100.4	99.3	22.7	0.9
PPP 1:10	0.0	8.3	0.0	12.7	0.0	1.5	0.8
PPP 1:20	0.0	8.1	0.0	8.9	0.8	0.4	0.1
PHC	13.9	10.1	0.0	4.3	9.4	2.4	0.2
Min Detection	2.7	13.7	1.4	27.2	13.7	6.8	6.9

Multiplexer analysis of the uncross-linked PHC scaffolds provides the growth factor profile of the original content of each scaffold. There were detectable amounts of all growth factors in PHC scaffolds with concentrations ranging between PRGF 10 mg/mL and PRGF 1 mg/mL (Table 4.1). The reported concentrations of growth factors are expected since 3.33 mg/mL PRGF was used to fabricate PHCE scaffolds. These results confirm that PRGF can successfully be incorporated within lyophilized gelatin sponges and the presence/concentrations of growth factors (specifically EGF) are maintained. Multiplexer analysis of PHCE and PHCE-M scaffold release over 21 days showed no quantifiable traces of the above growth factors. It was expected that some growth factors would be detectable as the scaffold degraded and released its contents. This absence of measurable growth factors from scaffold release could be a result of a highly diluted

sample since 6 mm discs were incubated in 1 mL of PBS to assess degradation. In this instance, growth factors released from the scaffold become diluted in the high volume of PBS which may result in no detection (as evident of the dilutions of pure PRGF in Figure 4.9). It is also possible that there was not enough PRGF originally incorporated within the PHCE scaffolds such that any release is in small amounts and therefore not detected by the multiplexer. On the other hand, it could be stated that there is no detectable growth factors in the release because PRGF is simply not being released. This non-release of PRGF can potentially be an added benefit in that the scaffold is able to maintain the incorporated growth factors and constantly provide a bioactive surface for cells to attach, proliferate, and remodel. Future studies will focus on which of these situations is occurring with lyophilized gelatin/PRGF sponges. This will be conducted by degrading the scaffold in less solution (to remove the possibility of severe dilution) and by incorporating higher initial concentrations of PRGF.

4.4.6. Uniaxial compression testing

Uniaxial compression testing using a platen system was used to record peak load (N) and Young's modulus (MPa) for compression of scaffolds incubated in media for up to 21 days. Day 4 of mechanical testing was not reported as the mechanical properties showed more significant changes weekly. Figure 4.10A reports and analyzes the peak loads of each scaffold type at a given time point. At days 1 and 14, GE-M scaffolds exhibited significantly higher ($p<0.05$) peak loads than all other scaffolds. On days 7 and 21, GE and GE-M had significantly higher ($p<0.05$) peak values than PHCE and PHCE-M

scaffolds. This data suggests that throughout 21 days, PHCE and PHCE-M scaffolds consistently report significantly lower ($p<0.05$) peak load values (0.1 – 1.0 N) when compared to GE and GE-M scaffolds (1.0 – 2.7 N).

The same data was graphed differently to compare peak values of a given scaffold throughout 21 days incubation (Figure 4.10B). For GE scaffolds, day 1 and day 14 produced the significantly lowest and highest ($p<0.05$) values, respectively. For GE-M scaffolds, incubation for 14 days in media produced the highest ($p<0.05$) peak load value compared to all other days. Day 1 for PHCE scaffolds was significantly lower ($p<0.05$) than all other days while PHCE-M scaffolds showed no significant changes ($p<0.05$) in peak load throughout 21 days. With the exception of PHCE-M scaffolds, this data shows that scaffolds have lower peak loads at earlier time points (days 1 and 7) when compared to later time points (day 14).

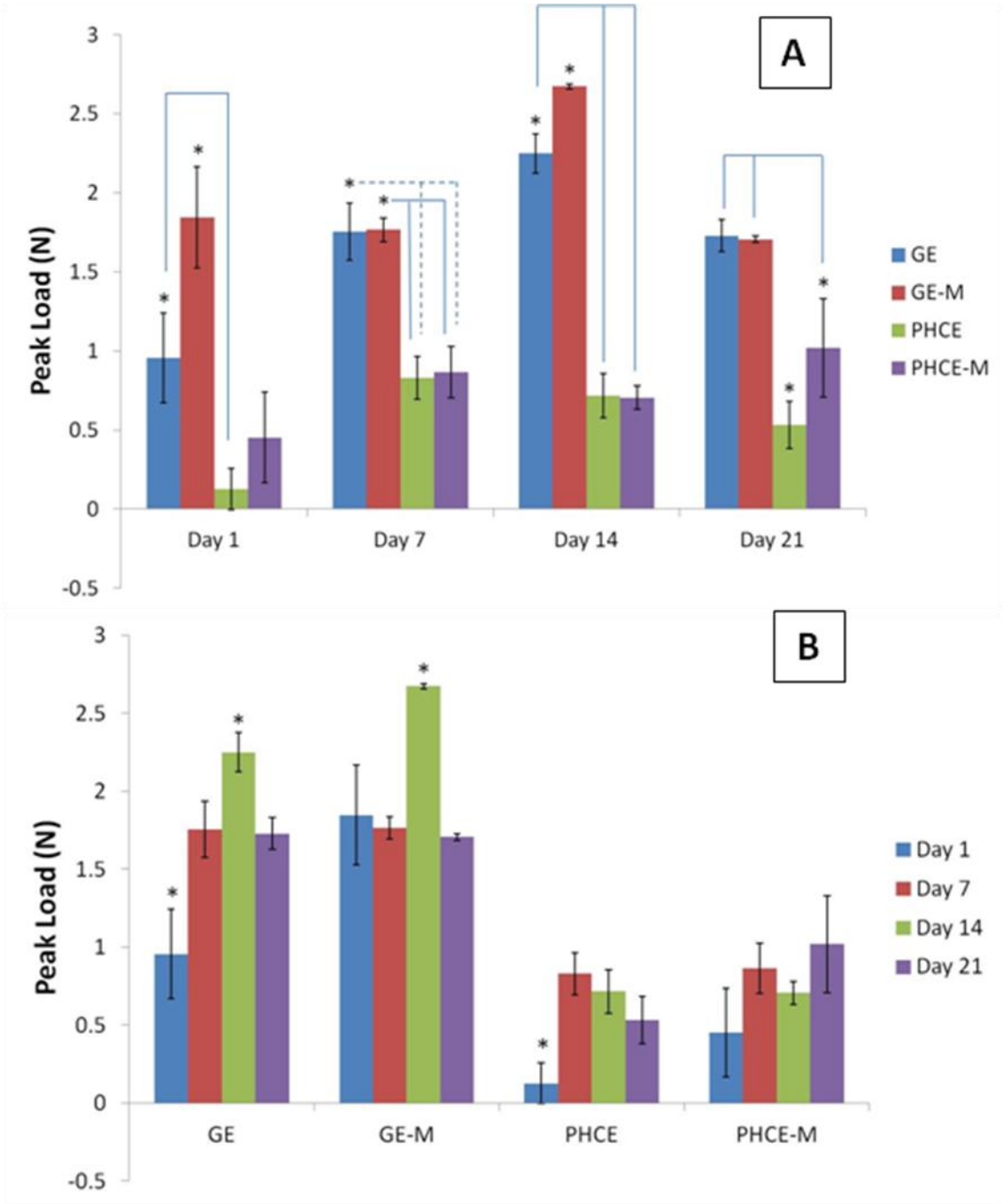

Figure 4.10 - Peak load of scaffolds A) at a given time point and B) over 21 days incubation in media.

Figure 4.11A reports and analyzes the compressive modulus of each scaffold type at a given time point. After 1 day incubation, PHCE-M scaffolds had a significantly lower ($p<0.05$) modulus than all other scaffold types. In fact, GE scaffolds had significantly higher ($p<0.05$) values than GE-M and PHCE-M. For day 7, GE scaffolds reported a significantly higher ($p<0.05$) modulus than both PHCE and PHCE-M scaffolds. After 14 days incubation, GE and GE-M scaffolds had significantly higher moduli when compared to PHCE-M scaffolds. Day 14 shows a higher modulus for GE-M scaffolds when compared to GE and PHCE-M scaffolds. Overall PHCE-M scaffolds report lower Young's modulus values (1.3 - 1.6 MPa) when compared to GE and GE-M scaffolds (1.6 - 3.2 MPa). One aim of this study is to create a scaffold with similar mechanical properties to that of native bone healing tissue. The first stages of bone healing involve granulation tissue and hyaline cartilage (soft tissue) formation before any mineralization occurs. The Young's modulus of cartilage in the literature is at similar low values of 0.5-0.8 MPa while mature bone and other materials are in the GPa range [129]. Zhang *et al.* report similar low compressive Young's modulus values (0.3 – 3.0 MPa) for gelatin-hyaluronic acid composite freeze-dried sponges intended for soft tissue engineering applications [127]. The low range of modulus values of these scaffolds provide a mechanical microenvironment similar to that found in the early stages of bone healing.

Evaluating statistical differences in Young's modulus of a given scaffold over 21 days will provide a different viewpoint on how each scaffold's properties change over time. To achieve this, the same modulus data was graphed with the legend and x-axis switched and statistics were performed (Figure 4.11B). The modulus for GE and PHCE

scaffolds significantly decreased ($p<0.05$) after 21 days incubation in media while their mineralized counterparts showed no significant changes ($p<0.05$) in modulus within the same time period. This suggests that mineralized scaffolds maintain their modulus throughout incubation while non-mineralized scaffolds show a decrease. It is also noticed from Figure 4.11A that the initial modulus (Day 1) of mineralized scaffolds is significantly lower ($p<0.05$) than non-mineralized scaffolds. This could attribute to the decrease in modulus as seen in non-mineralized scaffolds since they start off at higher values.

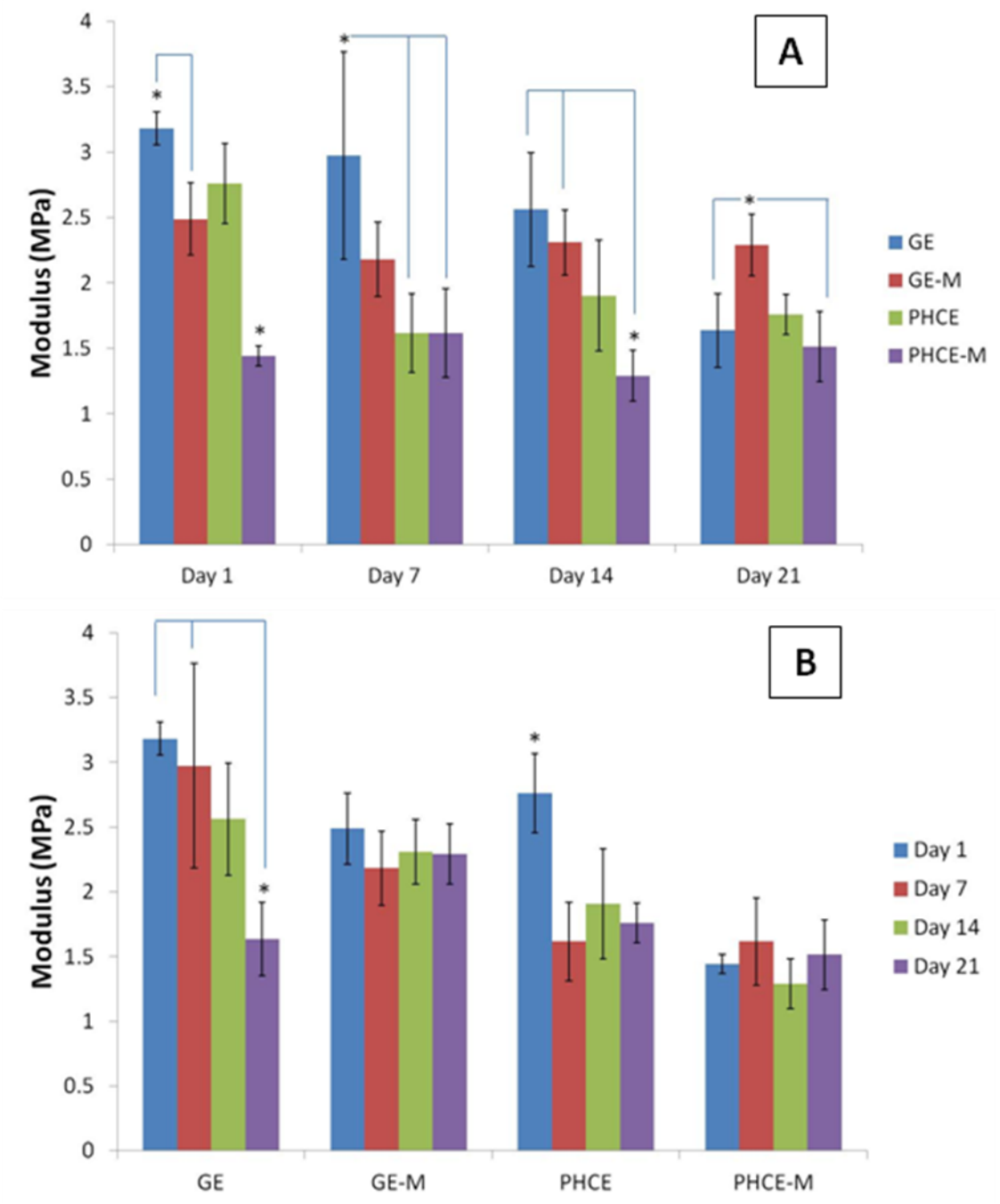

Figure 4.11 - Young's modulus for compression of A) scaffolds at a given time point and B) a given scaffold over 21 days incubation in media.

4.5. CONCLUSION

Lyophilized gelatin sponges were enhanced with PRGF, HA, and CW and cross-linked during gelation. Both control GE scaffolds and PHCE scaffolds swelled 50% their original size upon hydration. After fabrication, scaffolds were subsequently mineralized to create a bone-like surface. GE scaffolds nucleated minerals in more of a sparse aggregate manner while PHCE scaffolds showed more uniform mineralization across the surface. The highest concentrations of growth factors detected in PRGF and PRP were HGF and VEGF-A. As presented in Table 2.1, VEGF and HGF are known to increase angiogenesis, osteoblast proliferation, and endochondral ossification which are all vital to bone regeneration. The growth factor profile of PPP (1:10) more closely resembled that of PRGF (1 and 0.1 mg/mL), both highly diluted solutions. The BCA protein assay showed that PHCE-M scaffolds degraded faster and released 30% of its original protein content. Although PHCE-M scaffolds degraded the fastest, no PRGF growth factors were detectable after analyzing contents of released protein. However, multiplexer analysis did reveal the successful incorporation of PRGF within uncross-linked PHC sponges. The lower compression moduli values of PHCE and PCHE-M scaffolds are comparable to moduli values of tissues found in the early stages of bone healing. These findings suggest that PHCE and PHCE-M scaffolds have potential for use as early bone healing tissue scaffolds; however, *in vitro* cellularized studies are required to assess cellular responses to the various composite porous sponges.

5. *IN VITRO* RESPONSE OF MG-63 OSTEOBLAST-LIKE CELLS CULTURED ON LYOPHILIZED GEALTIN SPONGES ENHANCED WITH PRGF, HA, CW, AND A BONE-LIKE MINERAL SURFACE

5.1. ABSTRACT

The development of three-dimensional porous scaffolds with enhanced osteogenic and angiogenic factors are important characteristics to consider when fabricating scaffolds intended for bone tissue engineering, specifically early bone healing. The previous study demonstrated the advantages of PHCE and PHCE-M scaffolds which included: swelling potential, successful incorporation of growth factors, controlled release properties, and similar compression moduli as tissues present in early bone healing. In this study, GE, GE-M, PHCE, and PHCE-M scaffolds were dynamically seeded with MG-63 osteoblast like cells for 21 days and cellular responses to scaffolds as well as scaffolds response to cells were evaluated. Specifically, cell proliferation, attachment, infiltration, protein/cytokine secretion (osteocalcin, osteopontin, IL-6, IL-1β, TNF-α), and scaffold compressive mechanical properties (peak load and modulus) were evaluated. Scaffolds were cross-linked with EDC, a potentially cytotoxic carbodiimide. As such, a basic cytotoxicity experiment was performed to determine if uncross-linked EDC is harmful to the cells. Results indicated that uncross-linked EDC in media at any concentration (from 0.8 – 50 mM) is cytotoxic to MG-63 cells. Since cells on scaffolds were viable for up to 21 days in this study and up to 90 days in Chapter 3, it was concluded that there is no residual harmful uncross-linked EDC which will negatively affect cell response. Both DAPI staining and

MTS cell proliferation assay reported increased proliferation of cells on GE-M and PHCE scaffolds, and decreased proliferation on PHCE-M scaffolds. DAPI imaging showed a noticeable increase in initial cell attachment and infiltration of PHCE and PHCE-M scaffolds on day 1. GE-M scaffolds also attached more cells than the GE control. MTS results indicated that PHCE scaffolds increased cell proliferation after 4 and 7 days when compared to GE controls. It also showed that the addition of a mineral coating to GE scaffolds increases cell proliferation at day 4. Analysis of MG-63 protein/cytokine secretion suggests that the cells are responding in a bone regenerative fashion when seeded on all scaffolds, as evidence of osteocalcin secretion. Little to no secretion of osteopontin, IL-1β, and TNF-α demonstrates that scaffolds are not influencing cells to secrete factors associated with bone resorption. Cells also secreted small amounts of IL-6 when seeded on scaffolds for 1 day. IL-6 is a cytokine known to have both bone regenerating and resorbing effects. The compressive mechanical properties of cellularized scaffolds did not differ much from acellular scaffolds. There were a few exceptions where cells remodeled the scaffold such that increased peak load (PHCE, PHCE-M, GE-M day 14) and modulus (GE and PHCE day 21) were recorded. The combined results increased cellular attachment, infiltration, and bone regenerative protein/cytokine secretion by cells on GE-M scaffolds support the addition of a bone-like mineral surface to GE scaffolds. Cellularized PHCE and PHCE-M scaffolds report similar advantages as well as Young's modulus values in the range of native tissues present in the early stages of bone healing. These results suggested that the developed PHCE and PHCE-M scaffolds exhibit good cellular response and mechanical properties for early bone healing applications.

5.2. INTRODUCTION

As previously mentioned, designing scaffolds intended for bone tissue engineering must satisfy certain criteria such as: biocompatibility, degradability, porosity, mechanical integrity, osteoconductivity, and osteoinductivity. Chapter 3 illustrated that porous lyophilized gelatin sponges enhanced with PRGF, HA, and CW, allow the attachment (bioactivity), infiltration (porosity), and secretion of bone-like matrix (osteoconductivity) after static culture with MG-63 osteoblast-like cells. Chapter 4 further analyzed and reported positive results for protein release, mechanical integrity, and the ability to incorporate osteogenic factors within mineralized and non-mineralized PHCE scaffolds. The aim of this study is to analyze the cellular response of MG-63 cells dynamically seeded on GE, GE-M, PHCE, and PHCE-M scaffolds. The motive for dynamic cell seeding was to provide an environment where cells are not "forced" onto the scaffold (as seen in static cell seeding). In this seeding technique, the scaffolds were floating in a cell suspension in a rotary cell culture system (bioreactor) where they can come in contact with each other and if the scaffold is bioactive, it will promote cell attachment and infiltration. Since scaffolds are mineralized and/or incorporated with a variety of growth factors, it is hypothesized that cells will proliferate and secrete proteins/cytokines differently on various scaffolds. Osteocalcin and osteopontin are the main proteins secreted by osteoblasts indicative of bone regenerative and bone resorptive behavior, respectively. In addition to detecting osteocalcin and osteopontin, the secretion of other bone regenerating (IL-6) and resorbing factors (IL-6, IL-β, and TNF-α) were recorded. IL-6 is a controversial cytokine in that it is has been found to be associated with both bone resorption and regeneration

(Table 5.1). This study also compares acellular and cellular mechanical properties to determine what affect, if any, cells will have on the peak load and modulus of lyophilized sponges.

5.3. MATERIALS AND METHODS

5.3.1. Fabrication of gelatin composite sponges

Gelatin+EDC (GE) and PRGF+HA+CW+EDC (PHCE) lyophilized sponges were fabricated and subsequently mineralized (GE-M and PHCE-M) as previously outlined in Chapter 4, Sections 4.3.1 and 4.3.3. For all *in vitro* cell studies, MG-63 cells (human osteoblast-like cells derived from an osteosarcoma) were used. MG-63 cells behave similar to osteoblasts with their attachment, migration, proliferation, and bone matrix production.

5.3.2. Cytotoxicity of uncross-linked EDC

To determine the cytotoxic effect of potential residual uncross-linked EDC, a cell proliferation assay was performed and cells were exposed to various concentrations of uncross-linked EDC. Briefly, MG-63 cells were seeded subconfluently in a 96-well plate at 5,000 cells/well in 100 µL of control media (DMEM high glucose, 10% fetal bovine serum, 1% penicillin/streptomycin). Following the adhesion of cells to the well plate (approximately 1 hour), control media was removed and replaced with conditioned media (control media supplemented with 0, 0.8, 1.5, 3.1, 6.3, 12.5, 25, and 50 mM EDC). An MTS assay (Cell-Titer 96 Aqueous Non-Radioactive Cell Proliferation Assay, Promega, Madison,WI, USA) was performed on days 1, 4, and 7 (with media changes on days 1 and

4) to determine mean proliferative cell count. At the termination of each time point, conditioned media in each well was removed and replaced with 100 µL of control media and MTS was performed per manufacture's protocol.

5.3.3. Cell seeding on scaffolds

In Chapter 3, MG-63 cells were statically seeded on 6 mm-sized scaffold discs in a 96-well plate. Although the static method produced sufficient preliminary results, a more *in vivo*-mimicking method is appropriate for cell seeding. For this experiment, a dynamic (floating scaffold) cell seeding technique was used to not "force" the cells to attach to the scaffold. To accomplish this, a rotary cell culture system (Synthecon, Inc.) was used. Four bioreactors (60 mL volume capacity each) were autoclaved and attached to the rotary system in a sterile incubator for dynamic cell seeding. Twelve 6 mm discs of each scaffold type (GE, GE-M, PHCE, PHCE-M) were disinfected (30 mins ethanol followed by three 10 min washes in 1x PBS) and transferred to separate bioreactors. MG-63 osteoblast-like cells were suspended in control media at a concentration of 50,000 cells/mL. 60 mL of this cell solution was then added to each bioreactor containing disinfected scaffolds. Bioreactors with scaffolds floating in cell suspension were placed in an incubator with standard culture conditions (37°C and 5% CO_2) and turned on (42 rpm) to allow circulation of cell suspension solution and tumbling of floating scaffolds. After dynamic cell seeding for 6 hours, scaffolds were then transferred from the bioreactor to a 96-well plate containing 150 µL of culture media and statically cultured for 1, 4, 7, 14, 21 days with media changes every 3 days. Cellular scaffolds were characterized for attachment,

proliferation, infiltration, secretion of osteogenic factors, and compressive mechanical properties.

5.3.4. Scanning electron microscopy

After 1, 4, 7, 14, and 21 days in culture, cellularized scaffolds were fixed in 1 mL of 10% formalin and stored at 4°C until further analysis. Prior to imaging, cellularized scaffolds were removed from formalin, briefly rinsed in PBS and DI water, subjected to ethanol dehydration (10 minute soaks in 30, 50, 70, 90, and 100 % ethanol, subsequently), and air dried overnight. All dry samples were mounted on aluminum stubs, sputter coated in gold for 70 seconds, and examined using a JEOL JSM-5610LV scanning electron microscope (accelerating voltage at 20 kV).

5.3.5. Cell attachment and proliferation

After dynamic MG-63 cell seeding, GE, GE-M, PHCE, and PHCE-M scaffolds were cultured for 1, 4, and 7 days in a 96-well plate with 175 µL of control media with media changes on days 1 and 4. The MTS cell proliferation assay mentioned in Section 5.3.2 was also used to determine proliferative cell count on scaffolds. After each time period, scaffolds were transferred to a new well containing 100 µL of control media. 20 µL of MTS+PMS solution was then added to the well containing the media plus scaffold and incubated for 1 hour at 37°C. 100 µL of this solution was then transferred to a new 96-well plate and absorbance read at 490 nm.

5.3.6. DAPI staining

GE, GE-M, PHCE, and PHCE-M scaffolds were dynamically seeded with MG-63 cells as described in Section 5.3.3. After 1, 4, 7, 14, and 21 days in culture, cellularized scaffolds were fixed in 1 mL of 10% formalin and stored at 4°C until further analysis. Scaffolds were prepared for DAPI staining as mentioned in Chapter 3, Section 3.3.4. Briefly, scaffolds were removed from formalin, immersed in sucrose solution 48 hours at 4°C, suspended in frozen sectioning compound, and frozen at -70°C overnight. 60 µm slices were cryosectioned and transferred to microscope slides. Sample cross-sections were then stained with 4'-6-diamidino-2-phenylindole (DAPI) stain for 5 minutes and imaged using a UV fluorescent microscope to display the location of cell nuclei. As previously discovered, the ability to image cells via DAPI staining becomes increasingly difficult after weeks of culture. Therefore, only days 1 and 4 DAPI images are reported and serve as an indication to initial cell attachment and infiltration.

5.3.7. Multiplexer analysis of secreted osteoblast factors

GE, GE-M, PHCE, and PHCE-M scaffolds were dynamically seeded with MG-63 cells and statically cultured for 1, 4, 7, 14, and 21 days. At each time point, media from each well was collected and analyzed for osteoblast secretion of osteocalcin, osteopontin, interleukin -1 beta (IL-1β), IL-6, and tumor necrosis factor-alpha (TNF-α). This detection and quantification was accomplished by using a Luminex MagPix multiplexer (fluorescent imager) with the MILLIPLEX® MAP Human Bone Magnetic Bead panel (containing the

above mentioned analytes). This technology is the same as described in Chapter 4, Section 4.3.7.

5.3.8. Uniaxial compression testing

After 1, 4, 7, 14, and 21 days culture in media, cellularized scaffolds (6 mm diameter) of each scaffold type were subjected to compressive mechanical testing (as described Chapter 3, Section 3.3.5). Briefly, mechanical testing was conducted by using 2 flat metal platens and performed perpendicular to the scaffold surface without any circumferential constraints to allow for free lateral deformation. Scaffolds were removed from culture media, dabbed on a kimwipe to remove excess media/liquid, then placed on the flat metal surface (samples were still hydrated). Compression was performed as described in Chapter 4, Section 4.3.8. Peak load (N) and Young's modulus (MPa) were extracted and calculated using the graphical output from the MTS software TestWorks 4.0.

5.3.9. Statistical analysis

Statistical analysis was performed using JMP IN 9 statistical software (SAS Institute) to determine significant differences. Analysis of the data was based on a Kruskal-Wallis one-way analysis of variance on ranks and a Tukey-Kramer pairwise multiple comparison procedure. The results are presented in mean ± standard deviation (SD). Samples were run at least in triplicates (n=3) to ensure statistical significance ($p<0.05$).

5.4. RESULTS AND DISCUSSION

5.4.1. Cytotoxicity of uncross-linked EDC

EDC is a commonly used carbodiimide that has proven successful for cross-linking scaffolds while maintaining bioactivity [127, 130-132]. However, the MG-63 cellular response to potential exposure to any amount of uncross-linked EDC has not been determined. Figure 5.1 reports the MTS cell proliferation assay results of varying concentrations of EDC in media directly exposed to cells. It was determined that uncross-linked EDC in any concentration (from 0.8 – 50 mM) is cytotoxic to MG-63 cells. This is an important finding because any residual uncross-linked EDC present on or within the scaffold will cause the cells to die. As shown in Chapter 3 and later in this chapter, cells remain viable on all EDC cross-linked sponges for up to 90 days, suggesting there is no uncross-linked residual cytotoxic EDC that is harmful to the cells. For the control well (EDC 0 mM) there is a significant increase in cell proliferation from day 1 to 4 followed by a significant decrease in proliferation from days 4 to 7. Since MTS is commonly used as a cell viability assay, by quick glance of these results, one may conclude that cells began to die after 4 days of culture. However, by visual inspection of all the wells (conditioned and control), it was apparent that cells exposed to any concentration of EDC were in fact dying (cells balled up and floating). Cells in the control wells on day 4 and 7 were very confluent. The decrease in the MTS reading of 0 mM EDC on day 7 could be attributed to the decrease in the number of proliferating cells. As cells become confluent in the well plate (day 4), they stop proliferating and begin preparing to secrete factors conducive to

bone remodeling. Although both day 4 and 7 wells had a confluent layer of cells, day 7 recorded a lower number of proliferating cells suggesting cells are not dying, but rather progressing to the next stage of secreting factors for bone remodeling. Analysis of media for bone remodeling markers is one method to confirm this hypothesis.

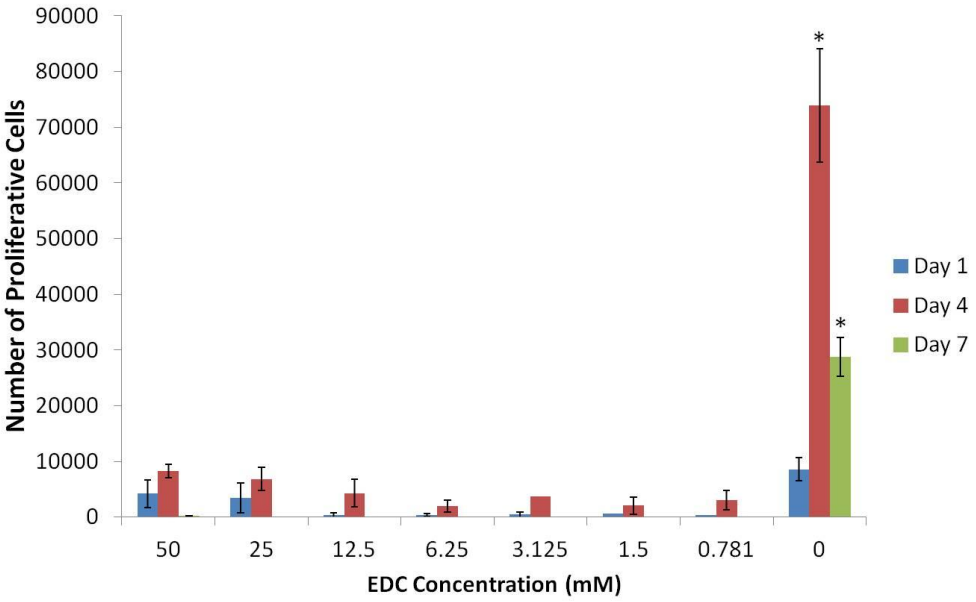

Figure 5.1 - MTS cell proliferation assay with varying concentrations of EDC in media.

5.4.2. Scanning electron microscopy

Scanning electron microscopy was performed on GE, GE-M, PHCE, and PHCE-M scaffolds after dynamic cell seeding and subsequent static culture for 1, 4, 7, 14, and 21 days (Figures 5.2 and 5.3). Scaffolds were subjected to ethanol dehydration in order to image cellularized scaffolds. Ethanol dehydration is a procedure commonly used to prepare cellular scaffolds for imaging. However, since these sponges are hygroscopic in nature,

dehydration caused the scaffolds to shrink upon preparation for imaging. Therefore, the images presented here and in Chapter 3 are not representative of a fully hydrated swollen scaffold that cells are in contact with. Although this is the case, basic observations can still be made. One noticeable difference with the images presented in this chapter is the visual appearance of no cells attached to any scaffolds at any time point. In Chapter 3, cells attached more as spheres and were easily visualized via SEM. Later in the chapter, DAPI staining confirms the presence of cells on and within GE, GE-M, PHCE, and PHCE-M scaffolds. It is plausible that the dynamic cell seeding technique caused the cells to attach to and integrate with the scaffold better than static cell seeding (where spheres of cells were visualized). It is also possible that there are more cells within the scaffold rather than on the surface, in which case will not be captured via SEM. Since mechanical stress is a factor for bone development, it has been shown that osteoblasts respond differently to mechanical stimuli when compared to a static environment [133, 134]. Future studies could focus on the degree of cell attachment and infiltration into the scaffold under dynamic and static culture conditions. For GE, GE-M, PHCE, and PHCE-M scaffolds, it was also observed that the scaffold became less porous over 21 days. This could be due to the remodeling of the scaffold by the cells, however, more in depth cell experiments analyzing the surface and entire cellular scaffold will need to be conducted for any conclusive results.

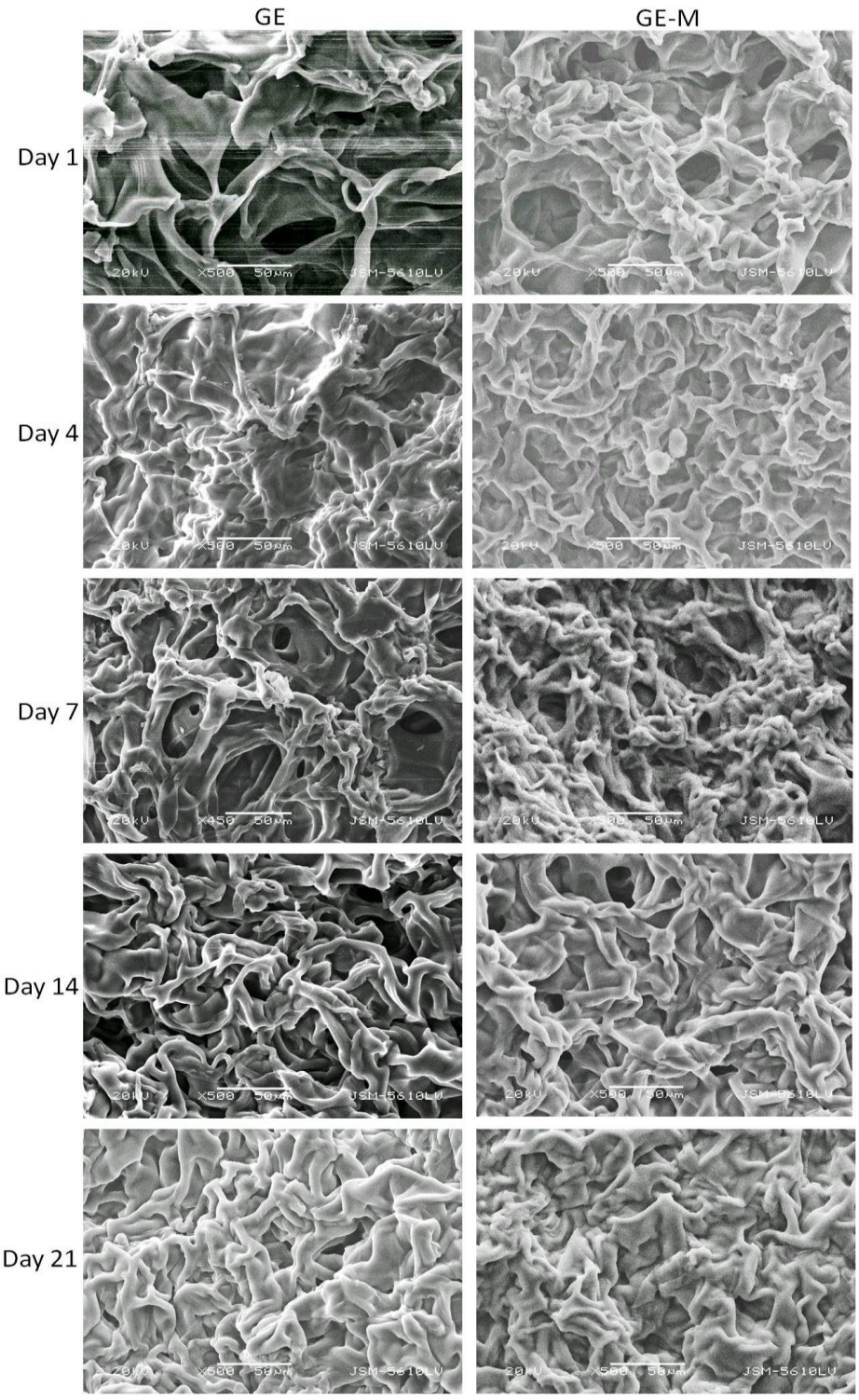

Figure 5.2 - SEM of cellularized GE and GE-M scaffolds. Scale bars at 50 µm.

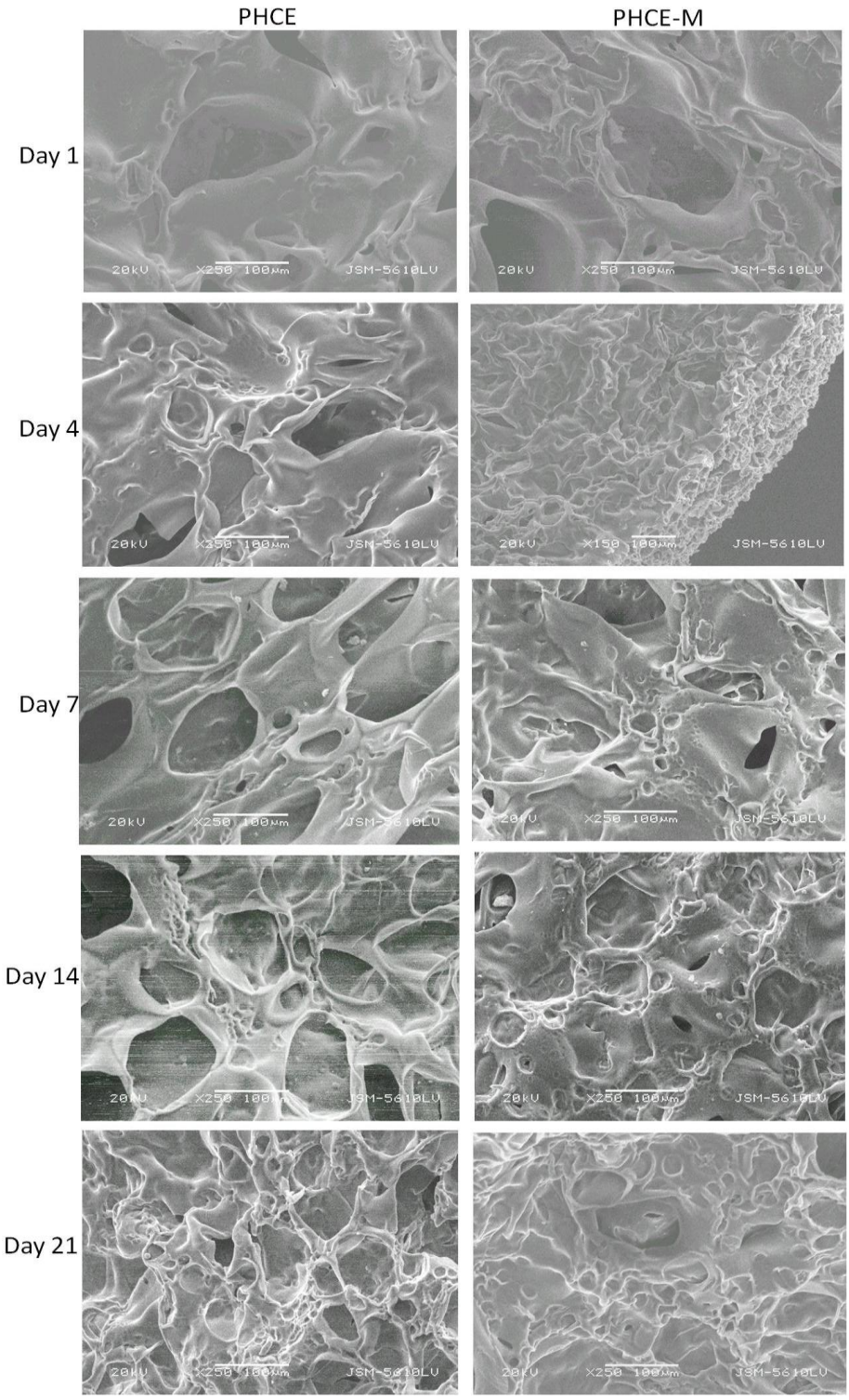

Figure 5.3 - SEM of cellularized PHCE and PHCE-M scaffolds. Scale bars at 100 µm.

5.4.3. Cell attachment and proliferation

The MTS assay was again used to determine the proliferative nature of cells dynamically seeded and subsequently statically cultured on scaffolds. MTS was also performed on acellular scaffolds of each type to determine any background or baseline values. As expected, MTS values for all acellular scaffolds ranged from 0 to 90 cells, indicating that there is no significant background or baseline value as a result of the MTS solution interacting with the acellular scaffold. Figure 5.4A reports the MTS values of cellularized scaffolds at a given time point. For day 1, there was no significant difference ($p<0.05$) in cell proliferation between all scaffold types. On day 4, both GE-M and PHCE scaffolds reported a significantly higher count of proliferative cells compared to GE and PHCE-M. Day 4 results offer contradicting effects of mineralization on GE and PHCE scaffolds. On day 4, a mineralized GE scaffold increases cellular proliferation when compared to a non-mineralized GE scaffold. The opposite effect is observed for PHCE scaffolds where a non-mineralized PHCE scaffold reports a higher cell proliferation count compared to its mineralized counterpart. By day 7, there was no detection of proliferating cells on PHCE-M scaffolds, while PHCE scaffolds showed increased proliferation when compared to the GE scaffolds. These results indicate that PHCE scaffolds increase cell proliferation after 4 and 7 days when compared to GE controls. It is also evident that the addition of a mineral coating to GE scaffolds increases cell proliferation on day 4.

The same MTS data was graphed differently to analyze the statistical differences of cell proliferation on a given scaffold over 7 days (Figure 5.4B). The only scaffold that recorded a significant difference (increase, $p<0.05$) in cell proliferation was PHCE after 4

and 7 days culture. An unexpected result evident in both graphs was the significantly low ($p<0.05$) cell proliferation count on PHCE-M scaffolds. As DAPI will confirm in the following section, cells are abundant and present throughout PHCE-M scaffolds. This interesting observation poses some unique questions for future studies, "Why doesn't the MTS assay register cells on PHCE-M scaffolds?", "Are cells not proliferating on PHCE-M scaffolds?", "Do cells on PHCE-M scaffolds quickly convert to a non-proliferative state?" When osteoblasts are present in an environment conducive to bone formation, the cells will stop proliferating and begin to secrete bone matrix. It is known that mature osteoblasts also have the ability to undergo apoptosis or become integrated within the mineral matrix to become osteocytes. It is a possibility that the PHCE-M scaffolds contain enough Ca-P such that osteoblasts are not scrambling to rebuild bone, but are rather content after attaching and begin integrating with the mineralized scaffold. This could also explain the non-proliferative state of osteoblasts and the low cell count reported by MTS.

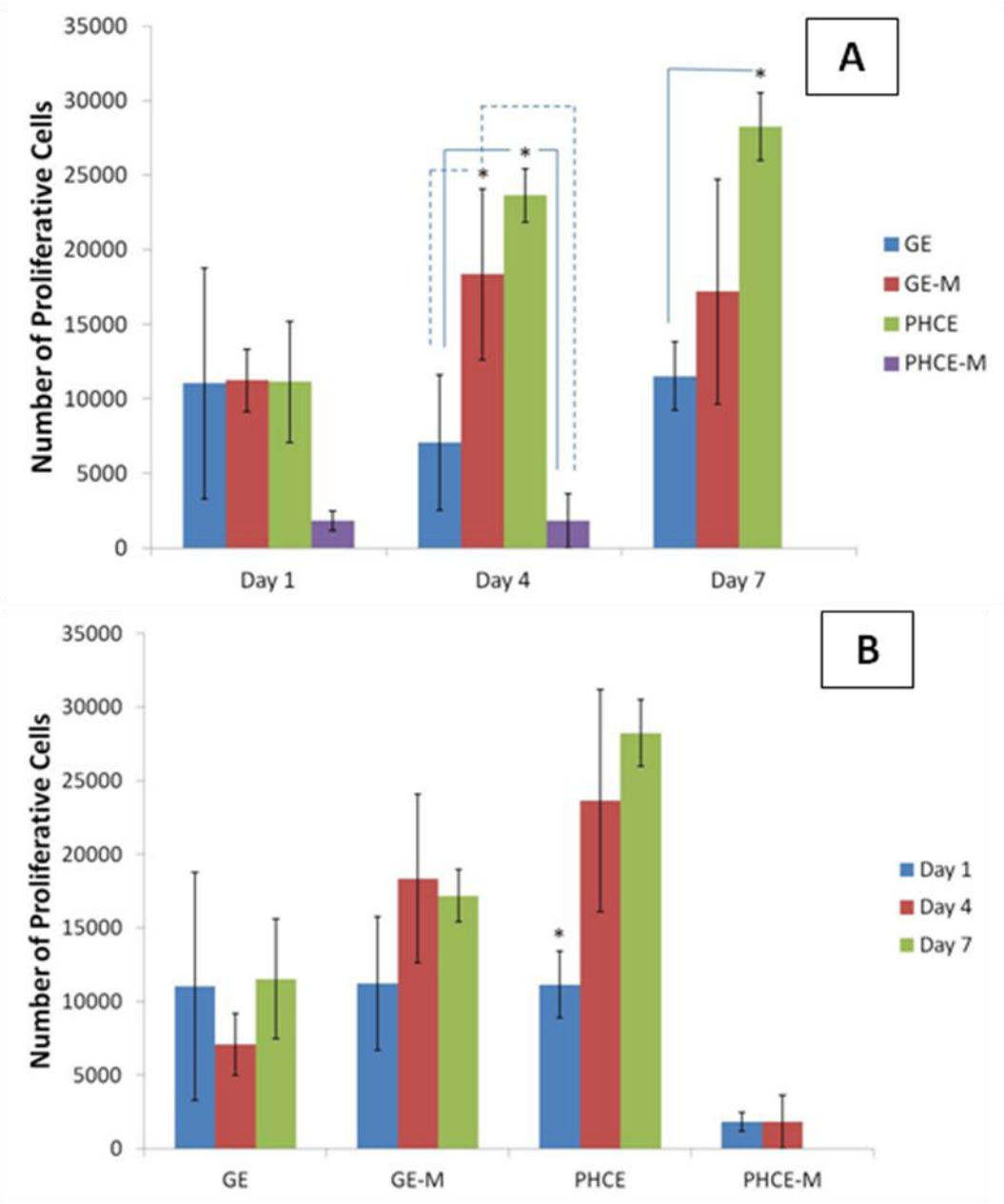

Figure 5.4 - MTS of cells cultured A) on each scaffold at a given time point and B) on a given scaffold for 7 days.

5.4.4. DAPI staining

Cell attachment and more importantly, infiltration into all scaffolds, was analyzed via DAPI staining after dynamic seeding followed by static culture for 1 and 4 days (Figure 5.5). The control GE scaffolds attached fewer cells than all other scaffold types, but did show appropriate cell infiltration after days 1 and 4. Cell infiltration into GE scaffolds is most likely attributed to the dynamic cell seeding method, since in Chapter 3, cells statically seeded on GE scaffolds primarily remained on the surface. A visual increase in cell attachment at the surface was observed for GE-M scaffolds suggesting that the minerals nucleated on the scaffold surface provide additional cell adhesion sites for osteoblasts. After 4 days in culture, cells were present throughout the entire scaffold indicating successful cell migration. Both PHCE and PHCE-M showed a large number of cells present throughout the scaffold on days 1 and 4. This increased cell attachment and infiltration was also reported for PHCE scaffolds in Chapter 3 using the static cell seeding method. This suggests that PHCE scaffolds increase initial cell attachment and infiltration independent of the cell seeding technique. Although there is no visual difference of cell attachment or infiltration between PHCE and PHCE-M scaffolds, there is a noticeable increase in initial cell attachment and infiltration when compared to GE and GE-M scaffolds on day 1. Even though cells on scaffolds are not clearly visible on the SEM images or detectable on PHCE-M scaffolds via MTS assay, DAPI results confirm the presence and viability of cells for up to 4 days.

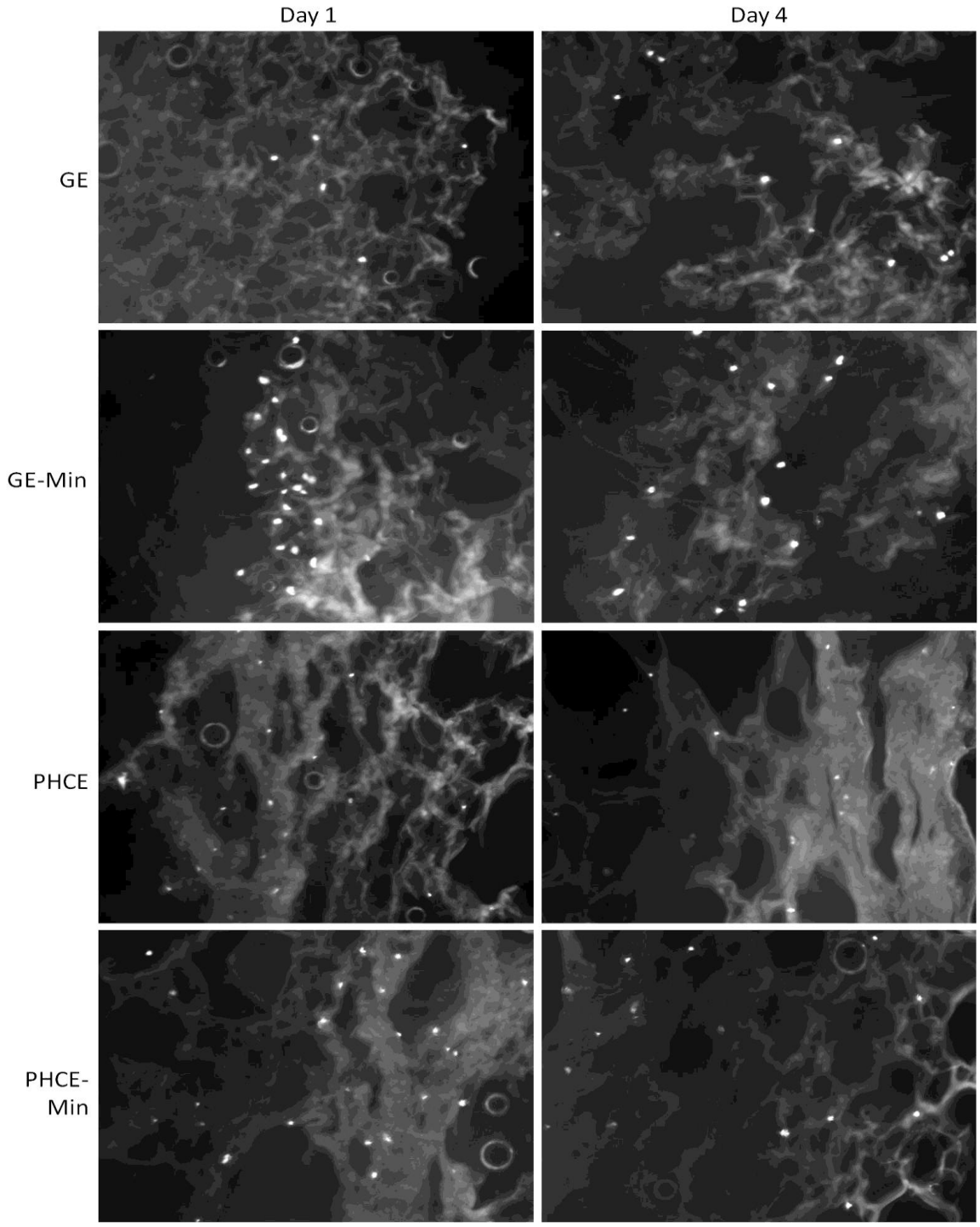

Figure 5.5 - DAPI staining of mineralized and non-mineralized GE and PHCE scaffolds after dynamic cell seeding and subsequent static culture for 1 and 4 days.

5.4.5. Multiplexer analysis of secreted osteoblast factors

After 1, 4, 7, 14, and 21 days of MG-63 cell culture on scaffolds, osteoblast secretion of osteocalcin, osteopontin, IL-1β, IL-6, and TNF-α were analyzed. At the tissue level, bone coupling (regeneration and resorption) is regulated through a large number of cytokines and proteins (some regenerative factors were presented in Table 2.1). These factors have a complex and overlapping effect such that bone regeneration and resorption can occur simultaneously depending on the need of the microenvironment. The exact roles of some factors, such as IL-6, are not clearly identified and have been found to have both resorbing and regenerating effects. TNF-α is primarily associated as a pro-inflammatory cytokine secreted by inflammatory cells. However, less commonly known, osteoblasts have the ability to synthesize and release TNF-α as a local regulator for osteoblast function [135]. The osteoblast secreted factors analyzed in this study are a mix of bone regenerating and bone resorbing markers which provide a comprehensive analysis of osteoblast response over 21 days culture on GE, GE-M, PHCE, and PHCE-M scaffolds. Table 5.1 briefly summarizes some known functions of each of these factors.

Table 5.1 - Role of multiplexer human bone panel analytes in bone remodeling.

	Function
osteocalcin	Marker for bone formation. Elevated secretion related to increase bone formation [136, 137]
Osteopontin	Bone resorption [138, 139]
IL-1β	Bone resorption [140, 141]
IL-6	Bone resorption [142-145] Osteoblast differentiation [146, 147]
TNF-α	Bone resorption [148, 149]

Multiplexer analysis revealed no traces (reported values below lowest standard) of osteopontin or IL-1β secretion by MG-63 cells cultured for 21 days on any scaffold type. These are positive results since both of these factors are associated with bone resorption. TNF-α secretion was detected in very small quantities (0.2 – 0.4 pg/mL), specifically on day 1 of GE, GE-M, and PHCE scaffolds (Figure 5.6). The lowest standard was 0.2 pg/mL, which suggests that the release of 0.2 – 0.4 pg/mL is at the lowest concentration detectable using the multiplexer. These results suggest that some cells that attached to GE, GE-M, and PHCE scaffolds secreted low amounts of TNF-α after 1 day culture on scaffolds. Although TNF-α is associated with bone resorption, the low concentrations detected on day 1 are not indicative of a bone resorbing response. In the body, bone resorption and regeneration occur simultaneously. It is possible that some cells attached in certain highly mineralized areas and began secreting TNF-α to initiate the resorption of that specific area on day 1. However, since low amounts of TNF-α were only detected on day 1, this suggests that this may be an initial response of some cells which is no longer the conditions from days 4 to 21. When comparing TNF-α secretion of all scaffolds on a given day, there were no significant differences ($p<0.05$) observed. This shows that on a given day, there was not a scaffold that induced significant secretion of TNF-α compared to the others.

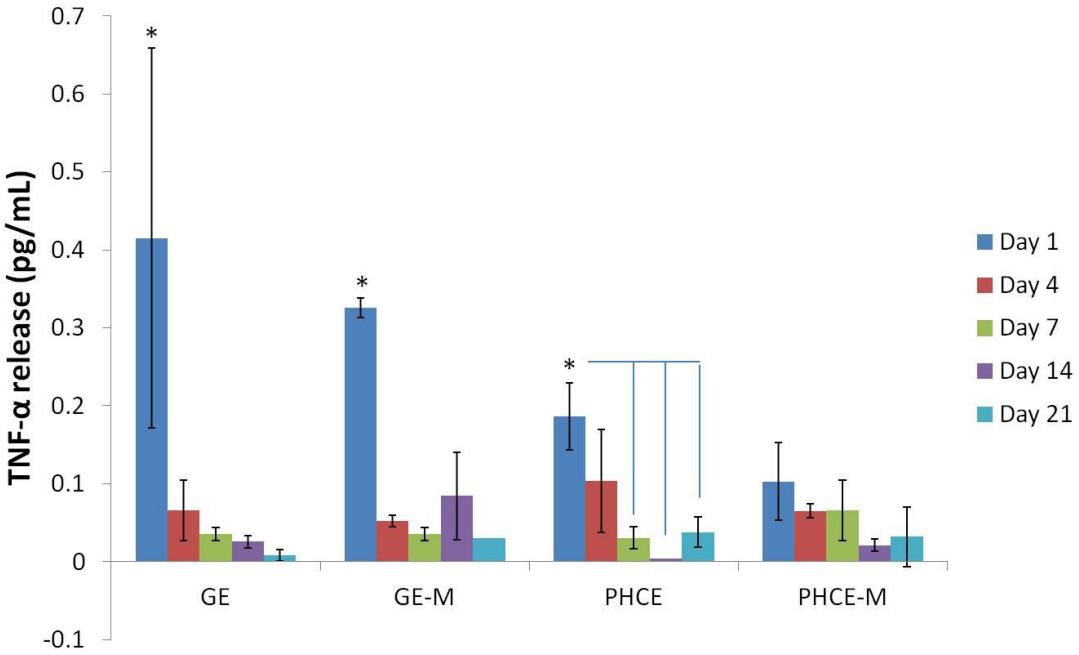

Figure 5.6 - Secretion of TNF-α by MG-63 cells cultured on each scaffold over 21 days.

Analysis of IL-6 cytokine secretion from cells showed some significant differences when comparing scaffold types as well as time points. After culture for 1 and 4 days, cells on GE-M scaffolds secreted significantly higher ($p<0.05$) amounts of IL-6 compared to all other scaffolds (Figure 5.7A). From days 7 to 21, all IL-6 release was below detectable and not significant ($p<0.05$) between scaffolds. Figure 5.7B graphs the secretion of IL-6 and statistically compares release over 21 days per scaffold type. These results show a common trend of significantly higher IL-6 secretion on day 1 for all scaffolds. As alluded to in Table 5.1, the effects of IL-6 within bone remodeling are not totally defined. The literature supports both theories of increased levels of IL-6 correlating to bone regeneration and resorption. This study did not investigate the bone remodeling effects of IL-6, but it clearly

demonstrated that cells seeded on GE-M scaffolds and cells seeded on any scaffold after 1 day secrete significantly higher levels of IL-6.

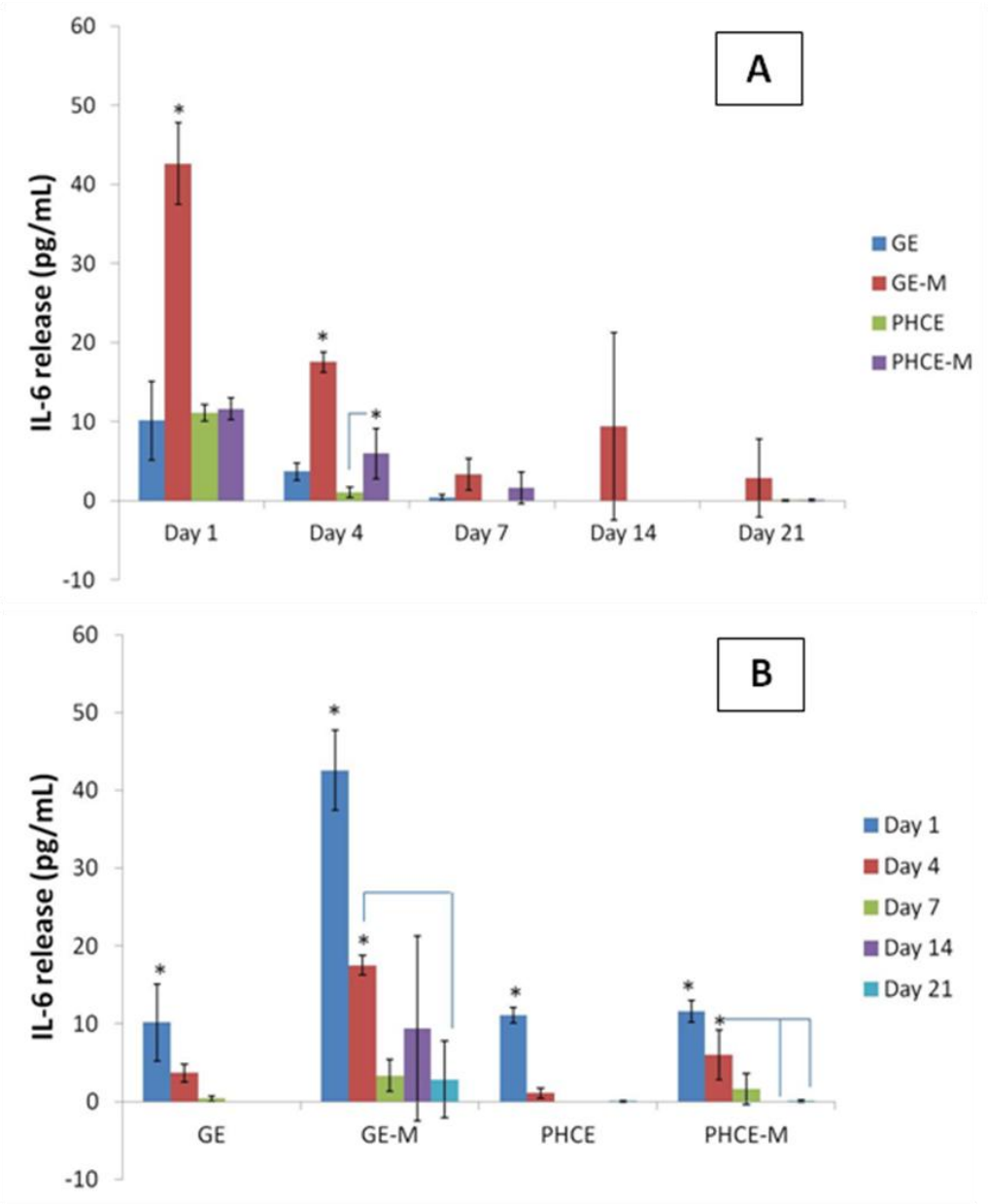

Figure 5.7 - IL-6 secretion by MG-63 cells comparing A) scaffold types at a given time point and B) each scaffold over 21 days.

Secretion of osteocalcin by MG-63 cells was detected for all scaffold types at all time points suggesting that the cultured cells are responding positively by promoting a bone regenerative environment. Figure 5.8A below shows the secretion of osteocalcin by cells on all scaffolds on a given day. There are several statistical differences which vary over 21 days. Briefly, the highest secretions of osteocalcin were recorded from cells on: GE & PHCE-M scaffolds on day 1; GE, GE-M, & PHCE-M scaffolds on days 4 and 7; GE-M scaffolds on day 14; and GE-M & PHCE on day 21. The most noticeable trend with this data is starting on day 4, cells on GE-M scaffolds consistently secreted high amounts of osteocalcin over 21 days. Osteocalcin secreted from cells cultured up to 21 days were also compared within each scaffold type (Figure 5.8B). For GE and PHCE-M scaffolds, osteocalcin secretion was highest on days 1, 4, and 7. Cells on GE-M scaffolds secreted lower amounts of osteocalcin on day 1 but then showed significant increases in secretion on days 4, 7, and 14. Constant levels of osteocalcin protein secretion were observed for PHCE scaffolds over 21 days. These results suggest that depending on the scaffold type, MG-63 cells will promote more bone regeneration at different time points within 21 days.

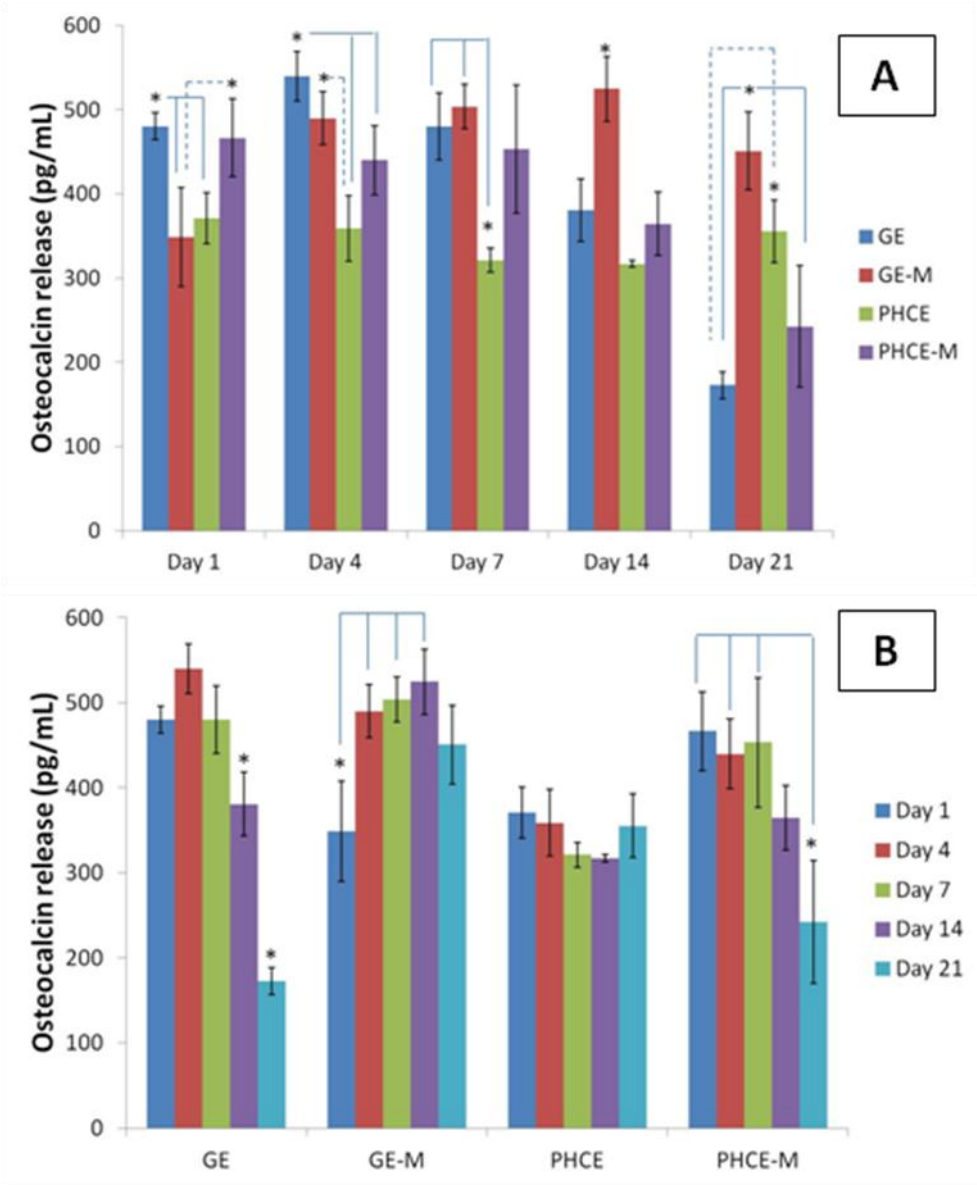

Figure 5.8 - Osteocalcin secretion by MG-63 cells comparing A) scaffold types at a given time point and B) each scaffold over 21 days.

Table 5.2 was constructed to summarize the secretion of all factors by MG-63 cells on all scaffolds on each day. This table compiles and identifies which scaffolds induced the highest secretion of all factors on each day. For osteopontin, IL-1β, and TNF-α, all

scaffolds on each day induced the same amount of secretion (little to none). This is a desired result since these factors are associated with bone resorption. For osteocalcin, GE-M scaffolds induced amongst the highest secretion from day 4 to 21, suggesting that these scaffolds would induce more bone regeneration within 21 days. For IL-6, GE-M scaffolds induced the highest secretion on day 1 and day 4 (along with PHCE-M). As previously mentioned, the role of IL-6 in bone remodeling is controversial. Therefore, in this study, it cannot be concluded if IL-6 relates to bone regeneration or resorption.

Table 5.2 - List of scaffolds that induced the highest secretion of factors at a given day.

	Day 1	**Day 4**	**Day 7**	**Day 14**	**Day 21**
osteocalcin	GE PHCE-M	GE GE-M	GE GE-M PHCE-M	GE-M	GE-M PHCE
osteopontin	-	-	-	-	-
IL-1β	-	-	-	-	-
IL-6	GE-M	GE-M PHCE-M	-	-	-
TNF-α	-	-	-	-	-

Table 5.3 was created to summarize the trends (increase or decrease) of osteoblasts factor secretion per scaffold over 21 days. All scaffolds showed decreases or low cell secretion of IL-6 and TNF-α at early time points (day 1 or 4). GE and PHCE-M scaffolds induced lower osteocalcin secretion after day 7 and 21, respectively. GE-M scaffolds induced increased levels of osteocalcin secretion after day 1, while cells on PHCE scaffolds secreted constant levels over 21 days.

Table 5.3 - Trend of secreted factors from MG-63 cells on scaffolds over 21 days.

	GE	GE-M	PHCE	PHCE-M
osteocalcin	↓ after day 7	↑ after day 1	constant	↓ on day 21
osteopontin	-	-	-	-
IL-1β	-	-	-	-
IL-6	↓ after day 1	↓ after day 1	↓ after day 1	↓ after day 1
TNF-α	↓ after day 1	↓ after day 1	↓ after day 4	constant

Overall, the analysis of secreted MG-63 cell factors suggests that the cells are responding in a bone regenerative fashion on all scaffolds, as evidence of osteocalcin secretion. Little to no secretion of osteopontin, IL-1β, and TNF-α proves that the scaffolds are not influencing the cells to respond in a resorptive manner. Again, the early secretion of IL-6 may be indicative of early bone regeneration or bone resorption response. In either instance, IL-6 secretion was only noticed at early time points and diminished after day 1. Since natural bone has the ability to regenerate and resorb simultaneously, the secretion of a combination of bone remodeling factors may be detected within the bone microenvironment. However, this study demonstrates the strong presence of MG-63 osteocalcin secretion (compared to other factors) that is consistent throughout 21 days of culture on all scaffolds.

5.4.6. Uniaxial compression testing

As previously mentioned in Chapter 4, day 4 of mechanical testing was not reported as the mechanical properties showed no differences between days 1 and 7 and significant changes weekly. To analyze compressive mechanical properties of cellularized

scaffolds, both peak load (N) and Young's modulus (MPa) for compression were recorded. Figure 5.9A below graphically displays the peak load of each cellularized scaffold type at a given time point. This allows us to determine which scaffolds have superior/inferior mechanical properties at each day. For day 1, GE-M scaffolds had significantly higher ($p<0.05$) peak loads to only PHCE scaffolds. By day 7, only GE scaffolds showed significantly higher ($p<0.05$) values than PHCE and PCHE-M scaffolds. On day 14 PHCE scaffolds showed the lowest ($p<0.05$) peak load values while on day 21 GE-M scaffold showed the highest ($p<0.05$) peak load values when compared to all scaffolds. These results do not show any predictable trends, but more of a variation with scaffold performance when compared to each day.

To better understand the peak load of each scaffold as it degraded, the same peak load data above was graphed differently and statistics performed (Figure 5.9B). For GE scaffolds seeded with cells, day 14 of culture produced significantly higher ($p<0.05$) peak load values than at all other time points while day 7 was only higher ($p<0.05$) than day 1 and 21. This suggests that for GE scaffolds, the cells strengthened the scaffold over 14 days. Since there was no detection of osteopontin, the cells are not resorbing the GE scaffolds which lead us to believe that the decrease in peak load at 21 days is not attributed to cell remodeling, but possibly the degradation of the scaffold. For GE-M scaffolds, only day 7 peak load values recorded different (significantly lower, $p<0.05$) than all other time points. There were no significant differences ($p<0.05$) in peak load values for PHCE scaffold over 21 days suggesting that the cells remodeling the scaffold were providing a balance of scaffold degradation and support. For PHCE-M scaffolds, only day 14 peak

values were significantly higher than day 21 values. Compared to acellular peak load values presented in chapter 4, there are fewer trends observed. This variation in peak load for cellular scaffolds is expected since the cells will continuously remodel each scaffold uniquely by attaching, applying their own mechanical forces, remodeling the scaffold, and producing matrix.

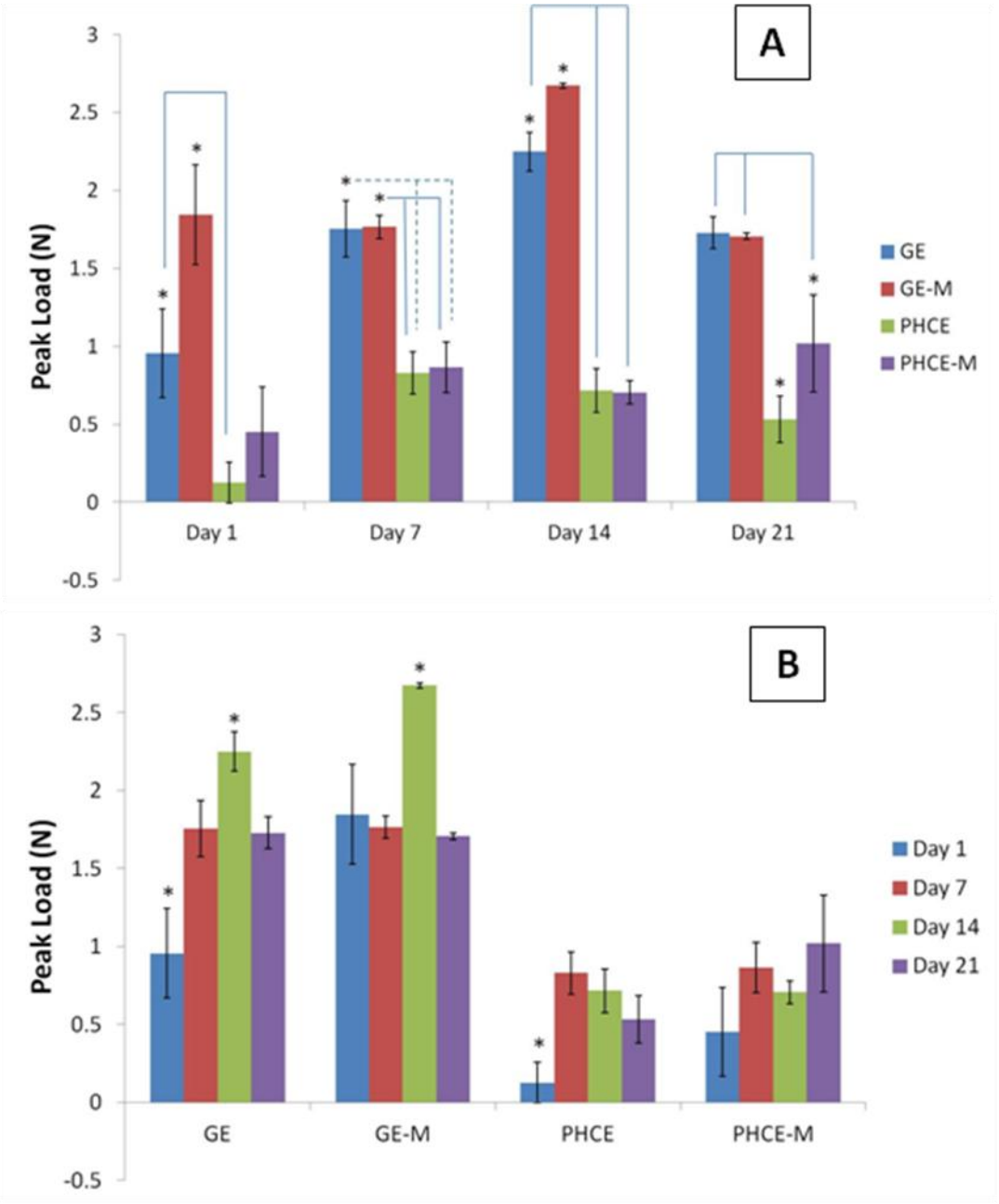

Figure 5.9 - Peak load of A) cellularized scaffolds at a given time point and B) of a given cellularized scaffold over 21 days in culture.

To compare acellular (Chapter 4) and cellular (Chapter 5) peak load results, data was combined, graphed, and statistically analyzed for significant differences (Figure 5.10). Statistics were only performed on data comparing acellular versus cellular scaffold properties on a given day. For GE scaffolds, only day 21 cellular scaffolds showed significantly lower ($p<0.05$) peak load values compared to acellular values. This suggests that for GE scaffolds, the addition of cells do not influence the compressive peak load properties until day 21. Comparing acellular and cellular GE-M scaffolds, day 1 reported no significant difference, day 7 cellular scaffolds had significantly lower ($p<0.05$) values, and both days 14 and 21 cellular scaffolds had significantly higher ($p<0.05$) values than their acellular counterparts. This suggests that for GE-M scaffolds, the addition of cells increases the peak load values after longer culture times (14 and 21 days). For both PHCE and PHCE-M scaffolds, only day 14 cellularized scaffolds reported a different (significantly higher, $p<0.05$) peak load when compared to acellular scaffolds at the same time point. With cells continuously remodeling the scaffolds, it is difficult to extract relationships. It does, however, appear that at one point (day 14) for PHCE and PHCE-M scaffolds, the cells are remodeling the scaffold in a fashion that increases the peak load compressive properties of the scaffold.

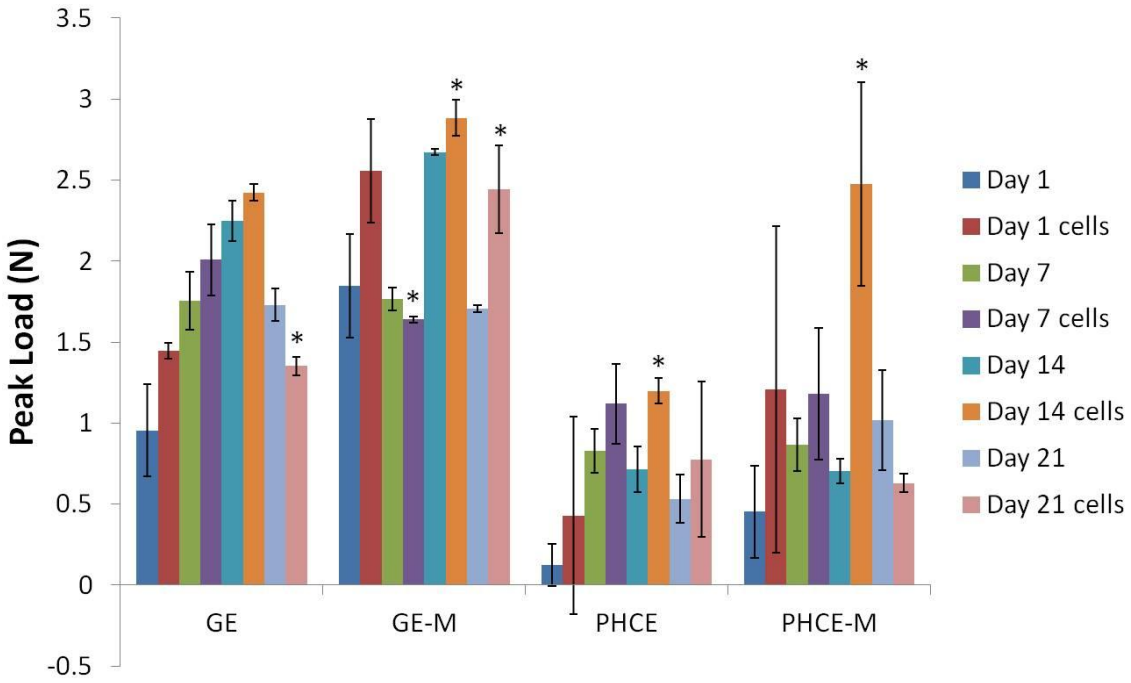

Figure 5.10 - Peak load comparison of acellular and cellularized scaffolds over 21 days.

The second mechanical property that was extracted from the testing data was Young's modulus for compression. Figure 5.11A displays the modulus of cellularized scaffolds at a given time point. It was determined that at each time point, there were no statistical differences ($p<0.05$) between the moduli of all scaffolds. This data reveals that independent of scaffold type, at a given time point all scaffolds exhibit similar Young's modulus for compression. The means of Young's modulus for all cellularized scaffolds throughout 21 days in culture ranged from 1.9 – 3.8 MPa. Figure 5.11B graphs the same Young's modulus data except in a form where statistics can compare the modulus of a given cellularized scaffold over the 21 days. Only cellularized GE scaffolds at day 21 had

significantly higher ($p<0.05$) moduli than day 7 scaffolds. All other scaffolds reported no significant changes ($p<0.05$) in moduli over the 21 days in culture.

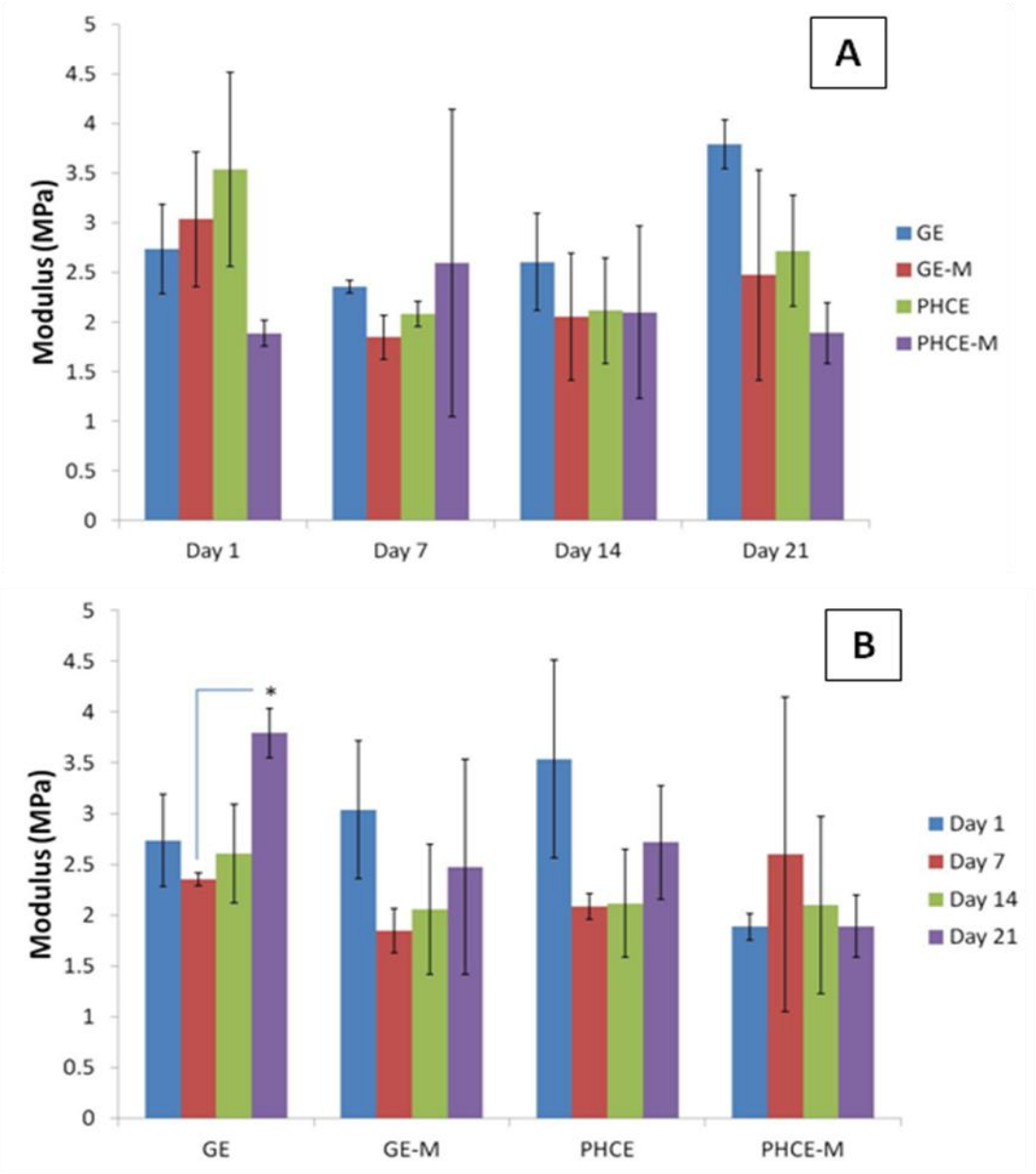

Figure 5.11 - Young's modulus for compression of A) cellularized scaffolds at a given time point and B) of a given cellularized scaffold over 21 days in culture.

To compare acellular (Chapter 4) and cellular (Chapter 5) Young's modulus results, data was combined, graphed, and statistically analyzed for significant differences (Figure 5.12). As mentioned for peak load combined results, statistics were only performed on data comparing acellular versus cellular scaffold properties on a given day. For non-mineralized cellular scaffolds (GE and PHCE), the only significant difference ($p<0.05$) was noticed on day 21 where cellular scaffolds reported higher modulus values that acellular scaffolds. This data suggests that after 21 days, the cells are remodeling non-mineralized scaffolds in a manner that ultimately increases the scaffold's stiffness. GE-M scaffolds showed no significant differences ($p<0.05$) while PHCE-M scaffolds only showed a significantly higher ($p<0.05$) modulus for day 1 cellular compared to acellular scaffolds. Overall, the Young's modulus for compression of mineralized scaffolds remained unaffected as a result of the addition of cells.

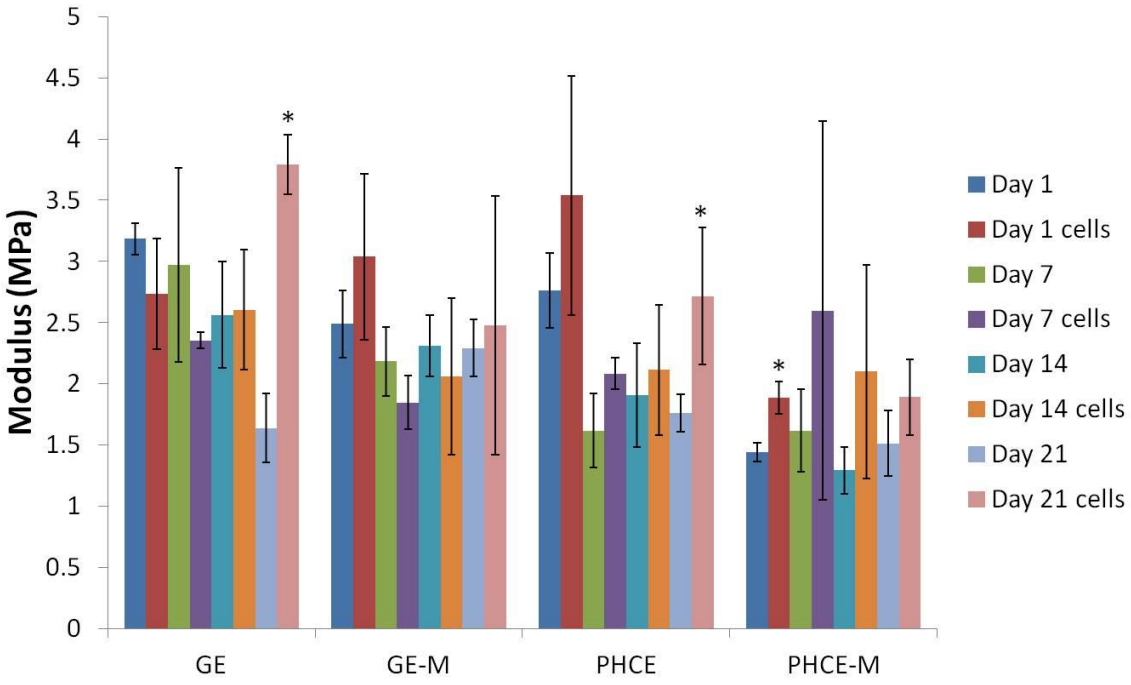

Figure 5.12 - Young's modulus for compression comparison of acellular and cellularized scaffolds over 21 days.

Although PHCE and PHCE-M had similar or lower peak load and modulus values compared to GE and GE-M scaffolds, the gross physical appearance of the mechanical integrity of the scaffolds were strikingly different once subjected to compressive mechanical loading. After subjection to compressive mechanical testing, the GE and GE-M scaffolds were demolished into pieces while the PHCE and PHCE-M scaffolds remained intact after complete compression (Figure 5.13). Although these images do not provide any quantifiable data, it does offer insight to future mechanical integrity studies that go beyond peak load and Young's modulus for compression. It is clear that the addition of PRGF, HA, and CW to gelatin sponges allowed the scaffold to remain intact after maximum

compression, however, the degree to which each individual component contributed is a direction of future research.

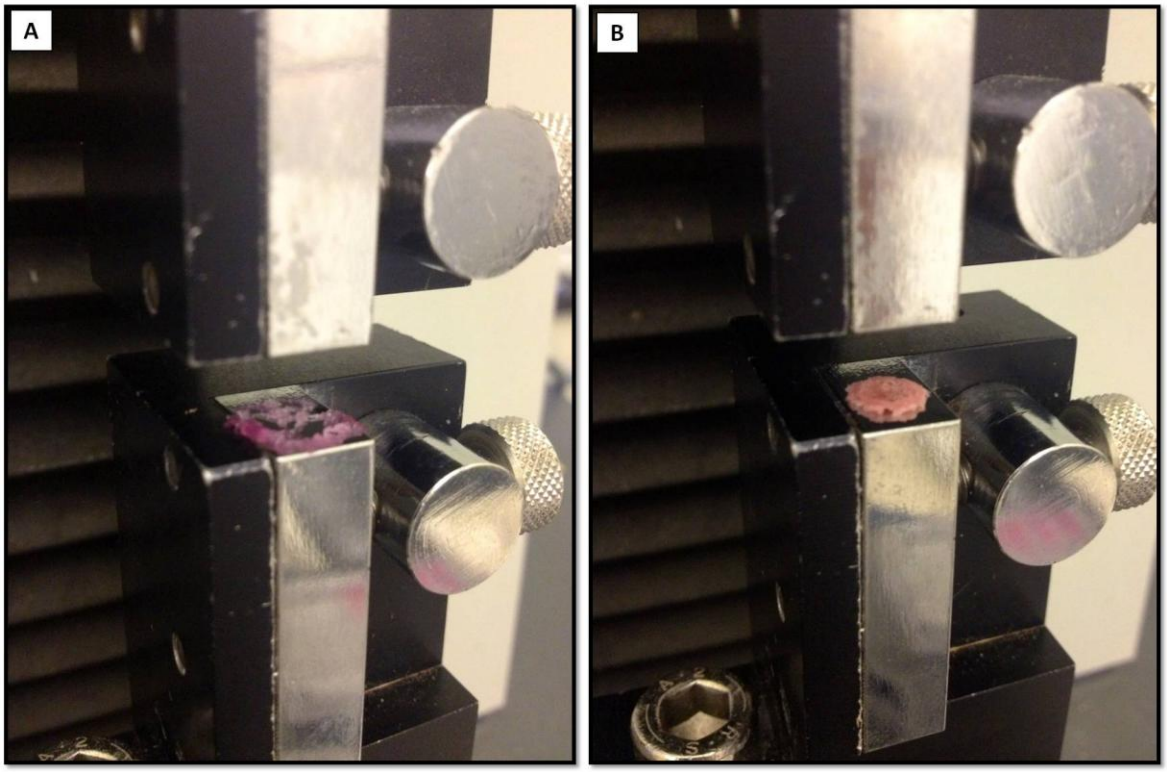

Figure 5.13 - Example of 21 day cellularized (A) GE and (B) PHCE scaffolds after complete compression post mechanical testing. GE-M and PHCE-M are not pictured as their gross appearances were similar to their non-mineralized counterparts.

5.5. CONCLUSION

Lyophilized gelatin sponges were enhanced with PRGF, HA, and CW, cross-linked during gelation, and subsequently mineralized to create a bone-like surface. This study presents several analyses of MG-63 cell response to scaffolds and scaffold response to cells. Chapter 3 concluded that MG-63 cells were viable on scaffolds for up to 90 days.

Since Chapter 4 determined that PHCE-M scaffolds release about 30% of their original protein, a basic EDC cytotoxicity assay was performed. It was determined that uncross-linked EDC in any concentration (from 0.8 – 50 mM) is cytotoxic to MG-63 cells. Therefore, since cells on scaffolds survived for up to 21 days in this study, it can be concluded that there is no residual harmful uncross-linked EDC which will affect cell response. Upon SEM examination of cells on scaffolds, it is believed that the dynamic cell seeding technique enhances cell infiltration and potentially cell integration with the scaffolds since individual cells were not discernible on the scaffold surface. Both DAPI and MTS confirmed the presence and viability of cells cultured on scaffolds. DAPI imaging showed a noticeable increase in initial cell attachment and infiltration of PHCE and PHCE-M scaffolds when compared to GE and GE-M scaffolds on day 1. GE-M scaffolds also attached more cells than the GE control providing mineralized GE scaffolds with an advantage. MTS cell proliferation results indicated that PHCE scaffolds increased cell proliferation after 4 and 7 days when compared to GE controls. It is also evident that the addition of a mineral coating to GE scaffolds increases cell proliferation at day 4. Analysis of MG-63 protein/cytokine secretion suggests that the cells are responding in a bone regenerative fashion on all scaffolds, as evidence of osteocalcin secretion. Little to no secretion of osteopontin, IL-1β, and TNF-α proves that the scaffolds are not influencing the cells to respond in a resorptive manner. For compressive mechanical testing, cells continuously remodeled the scaffolds making it is difficult to extract relationships. Some key observations for peak load included at one point (day 14) for PHCE and PHCE-M scaffolds, cells remodeled the scaffold which increased peak load. Also the GE-M

cellularized scaffolds recorded higher peak load values on days 14 and 21. Analysis of compressive modulus suggests that for non-mineralized cellular scaffolds (GE and PHCE), only significant increases were recorded on day 21. This data suggests that after 21 days, the cells are remodeling non-mineralized scaffolds in a manner that ultimately increases the scaffold's stiffness. Generally, the Young's modulus for compression of mineralized scaffolds remained unaffected as a result of the addition of cells. The comprehensive results from this study support the notion of mineralizing GE scaffolds to increase cellular attachment, infiltration, and bone regenerative protein/cytokine secretion. Cellularized PHCE and PHCE-M scaffolds also report similar advantages as GE-M scaffolds, but also have compressive mechanical modulus values in the range of native tissues present in the early stages of bone healing. Visually, after complete mechanical compression, cellularized PHCE and PHCE-M scaffolds performed superior as they remained intact suggesting their ability to withstand increased mechanical stress.

6. CONCLUSION AND FUTURE STUDIES

To certain extents, the human body has the unique ability to repair itself following injury. However, if the injuries exceed a critical size or level of damage, then surgical intervention is required to enhance the body's own reparative process. The field of tissue engineering focuses on developing viable substitutes that are able to repair and regenerate the functions of damaged tissue. Specifically, bone tissue engineering can provide improved bone grafting materials such as a porous, biocompatible, and biodegradable scaffold capable of sustained release of growth factors and cytokines to promote osteogenesis. Scaffolds such as these can improve the quality of life in patients by eliminating common drawbacks of current bone grafting procedures and materials such as the need for a secondary surgery for an autograft and the lack of biodegradability with ceramic/metal implants.

Lyophilizing a frozen gelatin solution is one fabrication method that has been used to create bone graft analogues, as it consistently produces hygroscopic porous scaffolds of any size with the ability to swell and fill any void space or defect. These freeze-dried scaffolds also have tailorable degradation rates and the ability to incorporate several factors (proteins, growth factors, nanofillers, etc.). HA is a popular biocompatible nanofiller which is incorporated within lyophilized sponges and several other bone tissue engineering scaffolds. This study investigates the very first attempts of incorporating PRGF and/or CW within lyophilized sponges. The present study was dedicated to developing a scaffold intended for bone repair. This biodegradable scaffold was specifically designed to mimic

the biological, biochemical, and mechanical microenvironment of the early stages of bone healing. In the present study, the first goal was to fabricate a cross-linked three-dimensional porous lyophilized gelatin sponge enhanced with PRGF, HA, and/or CW. We then investigated the different ways in which these enhancements altered the biological, mechanical, and regenerative characteristics with the intention of creating a bioresorbable graft that would have the ability to become completely remodeled into functioning new bone. Scaffolds were preliminarily evaluated to determine the advantages of various compositions and cross-linking methods of composite lyophilized gelatin sponges. This study illustrated that a lyophilized gelatin sponge, incorporated with PRGF, HA, and CW, demonstrated osteogenic potential when cultured with an MG-63 osteoblast-like cell line. These scaffolds, further modified through EDC cross-linking during gelation, exhibited controlled protein release (degradation), increased cellular attachment/infiltration, remained intact after 90 days in culture, and promoted the secretion of cell-created bone matrix. This tailorable rate of degradation is critical in a bone repair scaffold, where scaffold breakdown needs to match the ingrowth of vasculature and new bony matrix to prevent catastrophic failure. While the overall comparison of scaffolds did not clearly predict which combinations of PRGF, HA, and CW would induce optimal bone regeneration, it does give some insight to the advantages of the addition of growth factors and nanofillers to lyophilized gelatin sponges. The lyophilized sponges containing PRGF, HA, CW, and cross-linked during gelation (PHCE) performed well in the preliminary evaluations and were further investigated.

In an effort to further enhance the bioactivity and biocompatibility of cross-linked during gelation gelatin (GE) and PHCE scaffolds, SBF treatment was used to create a bone-like mineral surface on the scaffolds. For PHCE scaffolds, this is similar to the dual mineralization strategy used in our lab where a scaffold is fabricated with HA and subsequently mineralized with SBF. GE scaffolds nucleated minerals in more of a sparse aggregate manner while PHCE scaffolds showed more uniform biomimetic mineralization across the surface. GE and PHCE scaffolds were also evaluated for the ability to swell and both demonstrated the ability to swell 50% of their original volume upon hydration. In addition to analyzing scaffold characteristics, a growth factor profile of PRGF, PRP, and PPP was obtained to identify which factors were present and at what concentrations. The highest concentrations of growth factors detected in PRGF and PRP were HGF and VEGF-A. The growth factor profile of PPP (1:10) more closely resembled that of PRGF (1 and 0.1 mg/mL), both highly diluted solutions. These factors all have been shown to increase the formation of bone either through increased vascularization or bone mineral density and support their incorporation within scaffolds. This study also showed that PHCE-M scaffolds degraded faster and released 30% of its original protein content over 21 days. Although PHCE-M scaffolds degraded the fastest, no PRGF growth factors were detectable after analyzing scaffold release contents. However, multiplexer analysis did reveal the successful incorporation of PRGF within uncross-linked PHC sponges. As previously mentioned, an important parameter for tissue engineering scaffolding is the comparable mechanical properties of the scaffold and the native tissue being regenerated. The lower compression moduli values of PHCE and PCHE-M scaffolds are comparable to

moduli values of tissues found in the early stages of bone healing. The creation of these enhanced lyophilized sponges proved to have sustainable release, osteoinductive, and mechanical properties that could be conducive for bone graft applications; however, the bioactivity and cellular response of these materials were not investigated in this study. These findings suggest that PHCE and PHCE-M scaffolds have potential for use as early bone healing tissue scaffolds and support future *in vitro* cellularized studies to assess cellular responses to the various composite porous sponges.

Finally, the MG-63 cell response to scaffolds and scaffold response to cells was explored. A basic EDC cytotoxicity assay was performed and determined that uncross-linked EDC in any concentration (from 0.8 – 50 mM) is cytotoxic to MG-63 cells. Therefore, since cells on scaffolds survived for up to 90 days (Chapter 3) and 21 days (Chapter 5), it can be concluded that there is no residual uncross-linked EDC that will negatively affect cell response. In this study, cells were dynamically seeded on floating scaffolds in a bioreactor to more appropriately simulate cell recruitment and attachment to scaffolds compared to the static cell seeding method. Since individual cells were not discernible on the scaffold surface upon SEM examination, it is believed that the dynamic cell seeding technique enhanced cell infiltration and potentially cell integration with the scaffolds. Both DAPI staining and MTS cell proliferation assay confirmed the presence and viability of cells cultured on scaffolds. DAPI imaging showed a noticeable increase in initial cell attachment and infiltration of GE-M, PHCE, and PHCE-M scaffolds when compared to GE controls. This data supports the mineralization of GE sponges and the incorporation of PRGF, HA, and CW within GE scaffolds. The ability to attach cells

throughout the entire scaffold at early time points is an attractive quality when considering scaffolds for any tissue engineering applications where the cells are able to remodel the scaffold as a unit rather than portions at a time. Cell proliferation results indicated that GE-M and PHCE scaffolds increased cell proliferation after day 1 when compared to GE. For PHCE-M scaffolds, cell proliferation results showed a significant decrease in cell number. This was a surprising result since DAPI staining confirmed the presence of many cells on PHCE-M scaffolds at days 1 and 4. Since MTS measures the mitochondrial activity of proliferating cells, it is possible that the cells attached to PHCE-M are no longer in a proliferative state. These results propose interesting questions to be answered in future studies in which alternative methods for cell counting (such as trypan blue) can be explored. Analysis of MG-63 protein/cytokine secretion suggests that the cells are responding in a bone regenerative fashion on all scaffolds, as evidence of osteocalcin secretion. At early time points (day 1), small amounts of IL-6 secretion was detected. IL-6 is debated in the literature and appears to have effects both on bone regeneration and resorption. Multiplexer analysis also reported little to no secretion of osteopontin, IL-1β, and TNF-α, which demonstrates that the scaffolds are not influencing the cells to respond in a resorptive manner. Analysis of compressive modulus suggests that after 21 days, the cells are remodeling non-mineralized scaffolds in a manner that ultimately increases the scaffold's stiffness. Generally, the Young's modulus for compression of mineralized scaffolds remained unaffected as a result of the addition of cells. The moduli values for cellularized scaffolds remained in the low MPa range as found in native tissue involved in early bone healing. Upon examination after complete mechanical compression, the gross

appearance of cellularized PHCE and PHCE-M scaffolds performed superior as they remained intact, suggesting their ability to withstand increased mechanical stress.

The comprehensive results from this study support the notion of mineralizing GE scaffolds to increase cellular attachment, infiltration, and bone regenerative protein/cytokine secretion. Cellularized PHCE and PHCE-M scaffolds also report similar advantages as GE-M scaffolds, but also have compressive mechanical modulus values in the range of native tissues present in the early stages of bone healing. Lyophilized PHCE and PHCE-M are bioactive, biocompatible, porous, degradable, osteogenic, and mechanically similar to tissues found in early bone healing. These scaffolds satisfy the requirements of a bone tissue engineering scaffold and the presented comprehensive results support future inflammatory bone healing response and eventually *in vivo* studies.

6.1. Future research

A couple areas of interest for future direction are analysis of nanofiller particle dispersion throughout the scaffold and chemical analysis of the scaffold surface. Transmission electron microscopy can be performed on various cross sections of each scaffold to visually determine the location and dispersal of the nanofillers (HA and CW) within the scaffolds. Ideally, sonication of these particles prior to gelation achieves a homogeneous dispersal of HA and CW throughout the scaffold. Very preliminary experiments have been performed to analyze the chemical composition of the scaffold surface. Energy dispersive x-ray spectroscopy (EDS) was performed on the original GE and PHCE scaffolds to determine if the incorporation of the nanofillers (particularly HA)

are detected on the surface. Figure 6.1 illustrates the SEM image and corresponding EDS analysis for both GE and PHCE scaffolds. EDS was performed in two different areas within the sample to ensure homogeneity (only one is reported below). Defined peaks of carbon and oxygen were recorded for both scaffolds. This could be attributed to the carbon coating used to prepare the samples and the fact that the primary material of these scaffolds is gelatin (chemical structure of carbon, hydrogen, oxygen, and nitrogen). For the GE EDS spectrum, chlorine and sulfur were also detected. This is thought to be the result of the presence of residual ions left behind by the DI water (which when filtered, did not entirely remove ions present in the standard tap water). The more defined chlorine peak is more likely a result from the detection of EDC cross-linking. EDC has a chemical composition of carbon, hydrogen, nitrogen, and chlorine elements. In either instance, the GE EDS spectrum was used as a control. Upon PHCE EDS analysis, elemental peaks of calcium, phosphate, and sodium (smaller peak) are detected. This suggests that HA is successfully incorporated within the scaffold and present to some degree on its surface. EDS was also performed on mineralized samples, however the results were not consistent enough to draw any conclusions. The chemical analysis of a mineralized scaffold is of interest for future studies.

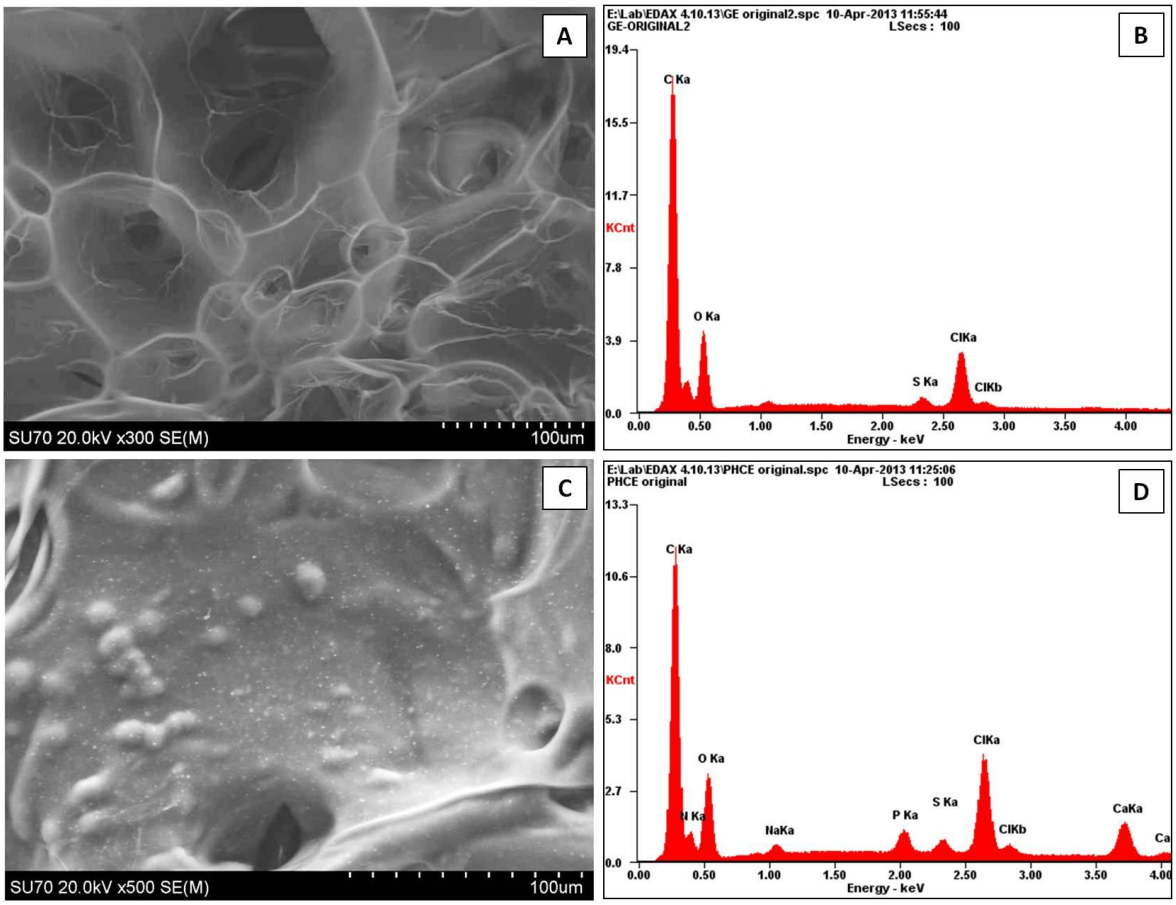

Figure 6.1 - SEM and EDS analysis of GE (A and B) and PHCE (C and D) scaffolds.

In addition to surface characterization, degradation will be more appropriately assessed through a variety of experiments analyzing specific components. First the release of gelatin, PRGF, and Ca-P, will be studied individually to determine how the scaffold is degrading and which contents are being released. The presence of calcium on the scaffold surface can be quantified over time which will provide insight to the scaffold mineral content as components are being released. The combination of these experiments provides a more comprehensive analysis of scaffold degradation. Other future experiments include analysis of porosity, detection of RANKL for a more general understanding of osteoblast

bone remodeling signals, and the potential application of these scaffolds for cartilage tissue engineering (since mechanical properties are within the range of native cartilage).

To more appropriately assess each scaffold's ability to promote bone healing, the response of inflammatory (monocytes/macrophages) and primary (osteoprogenitor) cells will need to be explored. As previously mentioned, bone healing consists of three main stages: inflammatory, repair, and remodeling. One of the main interests of this study is to determine the scaffold's ability to influence inflammatory cell behavior (cells present in the first stages of bone healing). This includes the attraction and differentiation of monocytes into macrophages, the subsequent polarization of macrophages to a pro-inflammatory (M1) or pro-regenerative (M2) state, the characterization of growth factors released by macrophages, and the osteoinductive capability of these growth factors with respect to MSC differentiation into osteoblasts. It is known that macrophages must transition to the M2 phenotype to facilitate proper tissue remodeling after disinfecting and debriding a site of injury [150]. Clinically, scaffolds can be fabricated with a quick turnaround from a patient's PRP blood draw to fabrication of the sponges. The hypothesis of this future study is that the PHCE sponge will serve as a bioactive structure to facilitate sustained delivery and presence of PRGF, differentiation of monocytes into pro-regenerative (M2) macrophages, and macrophage secretion of osteoinductive growth factors which will result in the differentiation of osteoprogenitor cells (such as mesenchymal stem cells) into osteoblasts. The end goal of this future work will be to create an implantable bone healing microenvironment mimicking analogue containing the necessary cues to integrate properly with a patient's own bone which has been injured.

Literature Cited

1. Greenwald, A.S., Boden, S.D., Barrack, R.L., Bostrom, M.P.G., Goldberg, V.M., Yaszemski, M.J., and Heim, C.S., *The evolving role of bone-graft substitutes.* American Academy of Orthopaedic Surgeons, 2010.
2. Glassman, S.D., Carreon, L.Y., Campbell, M.J., Johnson, J.R., Puno, R.M., Djurasovic, M., and Dimar, J.R., *The perioperative cost of Infuse bone graft in posterolateral lumbar spine fusion.* Spine J, 2008. **8**(3): p. 443-8.
3. Logeart-Avramoglou, D., Anagnostou, F., Bizios, R., and Petite, H., *Engineering bone: challenges and obstacles.* J Cell Mol Med, 2005. **9**(1): p. 72-84.
4. Finkemeier, C.G., *Bone-grafting and bone-graft substitutes.* J Bone Joint Surg Am, 2002. **84-A**(3): p. 454-64.
5. Kim, S.S., Sun Park, M., Jeon, O., Yong Choi, C., and Kim, B.S., *Poly(lactide-co-glycolide)/hydroxyapatite composite scaffolds for bone tissue engineering.* Biomaterials, 2006. **27**(8): p. 1399-409.
6. Al-Munajjed, A.A., Plunkett, N.A., Gleeson, J.P., Weber, T., Jungreuthmayer, C., Levingstone, T., Hammer, J., and O'Brien, F.J., *Development of a biomimetic collagen-hydroxyapatite scaffold for bone tissue engineering using a SBF immersion technique.* J Biomed Mater Res B Appl Biomater, 2009. **90**(2): p. 584-91.

7. Kim, S.S., Ahn, K.M., Park, M.S., Lee, J.H., Choi, C.Y., and Kim, B.S., *A poly(lactide-co-glycolide)/hydroxyapatite composite scaffold with enhanced osteoconductivity.* J Biomed Mater Res A, 2007. **80**(1): p. 206-15.

8. Venugopal, J.R., Low, S., Choon, A.T., Kumar, A.B., and Ramakrishna, S., *Nanobioengineered electrospun composite nanofibers and osteoblasts for bone regeneration.* Artif Organs, 2008. **32**(5): p. 388-97.

9. Kim, S.S., Park, M.S., Gwak, S.J., Choi, C.Y., and Kim, B.S., *Accelerated bonelike apatite growth on porous polymer/ceramic composite scaffolds in vitro.* Tissue Eng, 2006. **12**(10): p. 2997-3006.

10. Fischer, C.R., Cassilly, R., Cantor, W., Edusei, E., Hammouri, Q., and Errico, T., *A systematic review of comparative studies on bone graft alternatives for common spine fusion procedures.* Eur Spine J, 2013.

11. So, L.L. and Lui, W.W., *Alternative donor site for alveolar bone grafting in adults with cleft lip and palate.* Angle Orthod, 1996. **66**(1): p. 9-16.

12. Nadal, E., Sabas, M., Dogliotti, P., and Esposito, R., *Secondary alveolar bone grafting: our experience with olecranon bone graft.* J Craniofac Surg, 2010.

13. Boyce, T., Edwards, J., and Scarborough, N., *Allograft bone. The influence of processing on safety and performance.* Orthop Clin North Am, 1999. **30**(4): p. 571-81.

14. Kao, S.T. and Scott, D.D., *A review of bone substitutes.* Oral Maxillofac Surg Clin North Am, 2007. **19**(4): p. 513-21, vi.

15. Hoexter, D.L., *Bone regeneration graft materials.* J Oral Implantol, 2002. **28**(6): p. 290-4.

16. Trice, M.E., *Xenograft risks: What you and your patients need to know.* AAOS Now, 2009(June).

17. Moreau, J.L., Caccamese, J.F., Coletti, D.P., Sauk, J.J., and Fisher, J.P., *Tissue engineering solutions for cleft palates.* J Oral Maxillofac Surg, 2007. **65**(12): p. 2503-11.

18. Ciardelli, G., Gentile, P., Chiono, V., Mattioli-Belmonte, M., Vozzi, G., Barbani, N., and Giusti, P., *Enzymatically crosslinked porous composite matrices for bone tissue regeneration.* J Biomed Mater Res A, 2010. **92**(1): p. 137-51.

19. Weiner, S. and Traub, W., *Bone structure: from angstroms to microns.* Faseb J, 1992. **6**(3): p. 879-85.

20. Salo, J., *Bone resorbing osteoclasts reveal two basal plasma membrane domains and transcytosis of degraded matrix material.* Anatomy and Cell Biology, 2002.

21. Jang, J.H., Castano, O., and Kim, H.W., *Electrospun materials as potential platforms for bone tissue engineering.* Adv Drug Deliv Rev, 2009. **61**(12): p. 1065-83.

22. Hutmacher, D.W., Schantz, J.T., Lam, C.X., Tan, K.C., and Lim, T.C., *State of the art and future directions of scaffold-based bone engineering from a biomaterials perspective.* J Tissue Eng Regen Med, 2007. **1**(4): p. 245-60.

23. LaStayo, P.C., Winters, K.M., and Hardy, M., *Fracture healing: bone healing, fracture management, and current concepts related to the hand.* J Hand Ther, 2003. **16**(2): p. 81-93.

24. Hughes, F.J., Turner, W., Belibasakis, G., and Martuscelli, G., *Effects of growth factors and cytokines on osteoblast differentiation.* Periodontol 2000, 2006. **41**: p. 48-72.

25. Sanchez-Fernandez, M.A., Gallois, A., Riedl, T., Jurdic, P., and Hoflack, B., *Osteoclasts control osteoblast chemotaxis via PDGF-BB/PDGF receptor beta signaling.* PLoS One, 2008. **3**(10): p. e3537.

26. Pettit, A.R., Chang, M.K., Hume, D.A., and Raggatt, L.J., *Osteal macrophages: a new twist on coupling during bone dynamics.* Bone, 2008. **43**(6): p. 976-82.

27. Chang, M.K., Raggatt, L.J., Alexander, K.A., Kuliwaba, J.S., Fazzalari, N.L., Schroder, K., Maylin, E.R., Ripoll, V.M., Hume, D.A., and Pettit, A.R., *Osteal tissue macrophages are intercalated throughout human and mouse bone lining tissues and regulate osteoblast function in vitro and in vivo.* J Immunol, 2008. **181**(2): p. 1232-44.

28. Alexander, K.A., Chang, M.K., Maylin, E.R., Kohler, T., Muller, R., Wu, A.C., Van Rooijen, N., Sweet, M.J., Hume, D.A., Raggatt, L.J., et al., *Osteal macrophages promote in vivo intramembranous bone healing in a mouse tibial injury model.* J Bone Miner Res, 2008. **26**(7): p. 1517-32.

29. Glimcher, M.J., *Mechanism of calcification: role of collagen fibrils and collagen-phosphoprotein complexes in vitro and in vivo.* Anat Rec, 1989. **224**(2): p. 139-53.

30. Shin, K., Jayasuriya, A.C., and Kohn, D.H., *Effect of ionic activity products on the structure and composition of mineral self assembled on three-dimensional poly(lactide-co-glycolide) scaffolds.* J Biomed Mater Res A, 2007. **83**(4): p. 1076-86.

31. Kalfas, I.H., *Principles of bone healing.* Neurosurg Focus, 2001. **10**(4): p. E1.

32. Jahagirdar, R. and Scammell, B.E., *Principles of fracture healing and disorders of bone union.* Surgery (Oxford), 2009. **27**(2): p. 63-69.

33. Leong, P.L. and Morgan, E.F., *Correlations between indentation modulus and mineral density in bone-fracture calluses.* Integr Comp Biol, 2009. **49**(1): p. 59-68.

34. Langer, R. and Vacanti, J.P., *Tissue engineering.* Science, 1993. **260**(5110): p. 920-6.

35. Murugan, R. and Ramakrishna, S., *Nano-featured scaffolds for tissue engineering: a review of spinning methodologies.* Tissue Eng, 2006. **12**(3): p. 435-47.

36. Liao, S., Murugan, R., Chan, C.K., and Ramakrishna, S., *Processing nanoengineered scaffolds through electrospinning and mineralization suitable for biomimetic bone tissue engineering.* J Mech Behav Biomed Mater, 2008. **1**(3): p. 252-60.

37. Murphy, W.L., Kohn, D.H., and Mooney, D.J., *Growth of continuous bonelike mineral within porous poly(lactide-co-glycolide) scaffolds in vitro.* J Biomed Mater Res, 2000. **50**(1): p. 50-8.

38. Oyane, A., Uchida, M., Yokoyama, Y., Choong, C., Triffitt, J., and Ito, A., *Simple surface modification of poly(epsilon-caprolactone) to induce its apatite-forming ability.* J Biomed Mater Res A, 2005. **75**(1): p. 138-45.

39. Jayasuriya, A.C., Shah, C., Ebraheim, N.A., and Jayatissa, A.H., *Acceleration of biomimetic mineralization to apply in bone regeneration.* Biomed Mater, 2008. **3**(1): p. 015003.

40. Zhang, R. and Ma, P.X., *Biomimetic polymer/apatite composite scaffolds for mineralized tissue engineering.* Macromol Biosci, 2004. **4**(2): p. 100-11.

41. Zhang, D., Chang, J., and Zeng, Y., *Fabrication of fibrous poly(butylene succinate)/wollastonite/apatite composite scaffolds by electrospinning and biomimetic process.* J Mater Sci Mater Med, 2008. **19**(1): p. 443-9.

42. Prabhakaran, M.P., Venugopal, J., and Ramakrishna, S., *Electrospun nanostructured scaffolds for bone tissue engineering.* Acta Biomater, 2009. **5**(8): p. 2884-93.

43. Chen, J., Chu, B., and Hsiao, B.S., *Mineralization of hydroxyapatite in electrospun nanofibrous poly(L-lactic acid) scaffolds.* J Biomed Mater Res A, 2006. **79**(2): p. 307-17.

44. Zhang, Y.Z., Su, B., Venugopal, J., Ramakrishna, S., and Lim, C.T., *Biomimetic and bioactive nanofibrous scaffolds from electrospun composite nanofibers.* Int J Nanomedicine, 2007. **2**(4): p. 623-38.

45. Li, X., Xie, J., Yuan, X., and Xia, Y., *Coating electrospun poly(epsilon-caprolactone) fibers with gelatin and calcium phosphate and their use as biomimetic scaffolds for bone tissue engineering.* Langmuir, 2008. **24**(24): p. 14145-50.

46. Yu, H.S., Jang, J.H., Kim, T.I., Lee, H.H., and Kim, H.W., *Apatite-mineralized polycaprolactone nanofibrous web as a bone tissue regeneration substrate.* J Biomed Mater Res A, 2009. **88**(3): p. 747-54.

47. Carlisle, C.R., Coulais, C., Namboothiry, M., Carroll, D.L., Hantgan, R.R., and Guthold, M., *The mechanical properties of individual, electrospun fibrinogen fibers.* Biomaterials, 2009. **30**(6): p. 1205-13.

48. Amini, A.R., Adams, D.J., Laurencin, C.T., and Nukavarapu, S.P., *Optimally porous and biomechanically compatible scaffolds for large-area bone regeneration.* Tissue Eng Part A, 2012. **18**(13-14): p. 1376-88.

49. Kuhne, J.H., Bartl, R., Frisch, B., Hammer, C., Jansson, V., and Zimmer, M., *Bone formation in coralline hydroxyapatite. Effects of pore size studied in rabbits.* Acta Orthop Scand, 1994. **65**(3): p. 246-52.

50. Volkmer, E., Drosse, I., Otto, S., Stangelmayer, A., Stengele, M., Kallukalam, B.C., Mutschler, W., and Schieker, M., *Hypoxia in static and dynamic 3D culture systems for tissue engineering of bone.* Tissue Eng Part A, 2008. **14**(8): p. 1331-40.

51. Holtorf, H.L., Datta, N., Jansen, J.A., and Mikos, A.G., *Scaffold mesh size affects the osteoblastic differentiation of seeded marrow stromal cells cultured in a flow perfusion bioreactor.* J Biomed Mater Res A, 2005. **74**(2): p. 171-80.

52. Hubbell, J.A., *Biomaterials in tissue engineering.* Biotechnology (N Y), 1995. **13**(6): p. 565-76.

53. Laurencin, C.T., Ambrosio, A.M., Borden, M.D., and Cooper, J.A., Jr., *Tissue engineering: orthopedic applications.* Annu Rev Biomed Eng, 1999. **1**: p. 19-46.

54. Bigi, A., Boanini, E., Panzavolta, S., Roveri, N., and Rubini, K., *Bonelike apatite growth on hydroxyapatite-gelatin sponges from simulated body fluid.* J Biomed Mater Res, 2002. **59**(4): p. 709-15.

55. Ohgushi, H. and Caplan, A.I., *Stem cell technology and bioceramics: from cell to gene engineering.* J Biomed Mater Res, 1999. **48**(6): p. 913-27.

56. Stupp, S.I. and Ciegler, G.W., *Organoapatites: materials for artificial bone. I. Synthesis and microstructure.* J Biomed Mater Res, 1992. **26**(2): p. 169-83.

57. Kane, R.J. and Roeder, R.K., *Effects of hydroxyapatite reinforcement on the architecture and mechanical properties of freeze-dried collagen scaffolds.* J Mech Behav Biomed Mater, 2012. **7**: p. 41-9.

58. Prosecka, E., Rampichova, M., Vojtova, L., Tvrdik, D., Melcakova, S., Juhasova, J., Plencner, M., Jakubova, R., Jancar, J., Necas, A., et al., *Optimized conditions for mesenchymal stem cells to differentiate into osteoblasts on a collagen/hydroxyapatite matrix.* J Biomed Mater Res A, 2011. **99**(2): p. 307-15.

59. Wang, G., Babadagli, M.E., and Uludag, H., *Bisphosphonate-derivatized liposomes to control drug release from collagen/hydroxyapatite scaffolds.* Mol Pharm, 2011. **8**(4): p. 1025-34.

60. Gleeson, J.P., Plunkett, N.A., and O'Brien, F.J., *Addition of hydroxyapatite improves stiffness, interconnectivity and osteogenic potential of a highly porous collagen-based scaffold for bone tissue regeneration.* Eur Cell Mater, 2010. **20**: p. 218-30.

61. Neffe, A.T., Loebus, A., Zaupa, A., Stoetzel, C., Muller, F.A., and Lendlein, A., *Gelatin functionalization with tyrosine derived moieties to increase the interaction with hydroxyapatite fillers.* Acta Biomater, 2011. **7**(4): p. 1693-701.

62. Perez, R.A., Kim, H.W., and Ginebra, M.P., *Polymeric additives to enhance the functional properties of calcium phosphate cements.* J Tissue Eng, 2012. **3**(1): p. 2041731412439555.

63. Azami, M., Samadikuchaksaraei, A., and Poursamar, S.A., *Synthesis and characterization of a laminated hydroxyapatite/gelatin nanocomposite scaffold with controlled pore structure for bone tissue engineering.* Int J Artif Organs, 2010. **33**(2): p. 86-95.

64. Kim, H.W., Knowles, J.C., and Kim, H.E., *Porous scaffolds of gelatin-hydroxyapatite nanocomposites obtained by biomimetic approach: characterization and antibiotic drug release.* J Biomed Mater Res B Appl Biomater, 2005. **74**(2): p. 686-98.

65. Kim, H.W., Kim, H.E., and Salih, V., *Stimulation of osteoblast responses to biomimetic nanocomposites of gelatin-hydroxyapatite for tissue engineering scaffolds.* Biomaterials, 2005. **26**(25): p. 5221-30.

66. Woo, K.M., Seo, J., Zhang, R., and Ma, P.X., *Suppression of apoptosis by enhanced protein adsorption on polymer/hydroxyapatite composite scaffolds.* Biomaterials, 2007. **28**(16): p. 2622-30.

67. Rohanizadeh, R., Swain, M.V., and Mason, R.S., *Gelatin sponges (Gelfoam) as a scaffold for osteoblasts.* J Mater Sci Mater Med, 2008. **19**(3): p. 1173-82.

68. Barbani, N., Guerra, G.D., Cristallini, C., Urciuoli, P., Avvisati, R., Sala, A., and Rosellini, E., *Hydroxyapatite/gelatin/gellan sponges as nanocomposite scaffolds for bone reconstruction.* J Mater Sci Mater Med, 2012. **23**(1): p. 51-61.

69. Kohara, H. and Tabata, Y., *Enhancement of ectopic osteoid formation following the dual release of bone morphogenetic protein 2 and Wnt1 inducible signaling pathway protein 1 from gelatin sponges.* Biomaterials, 2011. **32**(24): p. 5726-32.

70. Zeng, J.B., He, Y.S., Li, S.L., and Wang, Y.Z., *Chitin whiskers: an overview.* Biomacromolecules, 2012. **13**(1): p. 1-11.

71. Lopez-Lopez, J., Chimenos-Kustner, E., Manzanares-Cespedes, C., Munoz-Sanchez, J., Castaneda-Vega, P., Jane-Salas, E., Alvarez-Lopez, J.M., and Gimeno-Sanding, A., *Histomorphological study of the bone regeneration capacity of platelet-rich plasma, bone marrow and tricalcium phosphate: Experimental study on pigs.* Med Oral Patol Oral Cir Bucal, 2009. **14**(12): p. e620-7.

72. Messora, M.R., Nagata, M.J., Fucini, S.E., Pola, N.M., Campos, N., Oliveira, G.C., Bosco, A.F., Garcia, V.G., and Furlaneto, F.A., *Effect of platelet-rich plasma on the healing of mandibular defects treated with bone allograft. A radiographic study in dogs.* J Oral Implantol, 2012.

73. Sriupayo, J., Supaphol, P., Blackwell, J., and Rujiravanit, R., *Preparation and characterization of α-chitin whisker-reinforced poly(vinyl alcohol) nanocomposite films with or without heat treatment.* Polymer, 2005. **46**(15): p. 5637–5644.

74. Ji, Y.-L., Wolfe, P.S., Rodriguez, I.A., and Bowlin, G.L., *Preparation of chitin nanofibril/polycaprolactone nanocomposite from a nonaqueous medium suspension.* Carbohydrate Polymers, 2012. **87**: p. 2313-2319.

75. Junkasem, J., Rujiravanit, R., and Supaphol, P., *Fabrication of α-chitin whisker-reinforced poly(vinyl alcohol) nanocomposite nanofibres by electrospinning.* 2006. **17**: p. 4519–4528.

76. Wongpanit, P., Sanchavanakit, N., Pavasant, P., Bunaprasert, T., Tabata, Y., and Rujiravanit, R., *Preparation and characterization of chitin whisker-reinforced silk fibroin nanocomposite sponges.* European Polymer Journal, 2007. **43**(10): p. 4123–4135.

77. Hariraksapitak, P. and Supaphol, P., *Preparation and properties of a-chitin-whisker-reinforced hyaluronan-gelatin nanocomposite scaffolds.* Journal of Applied Polymer Science, 2010. **117**(6): p. 3406-3418.

78. Han, T., Wang, H., and Zhang, Y.Q., *Combining platelet-rich plasma and tissue-engineered skin in the treatment of large skin wound.* J Craniofac Surg, 2012. **23**(2): p. 439-47.

79. Kushida, S., Kakudo, N., Suzuki, K., and Kusumoto, K., *Effects of platelet-rich plasma on proliferation and myofibroblastic differentiation in human dermal fibroblasts.* Ann Plast Surg, 2012.

80. Taylor, D.W., Petrera, M., Hendry, M., and Theodoropoulos, J.S., *A systematic review of the use of platelet-rich plasma in sports medicine as a new treatment for tendon and ligament injuries.* Clin J Sport Med, 2011. **21**(4): p. 344-52.

81. Xie, X., Wang, Y., Zhao, C., Guo, S., Liu, S., Jia, W., Tuan, R.S., and Zhang, C., *Comparative evaluation of MSCs from bone marrow and adipose tissue seeded in PRP-derived scaffold for cartilage regeneration.* Biomaterials, 2012. **33**(29): p. 7008-18.

82. Gentile, P., Di Pasquali, C., Bocchini, I., Floris, M., Eleonora, T., Fiaschetti, V., Floris, R., and Cervelli, V., *Breast reconstruction with autologous fat graft mixed with platelet-rich plasma.* Surg Innov, 2012.

83. Jo, C.H., Kim, J.E., Yoon, K.S., and Shin, S., *Platelet-rich plasma stimulates cell proliferation and enhances matrix gene expression and synthesis in tenocytes from human rotator cuff tendons with degenerative tears.* Am J Sports Med, 2012. **40**(5): p. 1035-45.

84. Li, N.Y., Yuan, R.T., Chen, T., Chen, L.Q., and Jin, X.M., *Effect of platelet-rich plasma and latissimus dorsi muscle flap on osteogenesis and vascularization of tissue-engineered bone in dogs.* J Oral Maxillofac Surg, 2009. **67**(9): p. 1850-8.

85. Rai, B., Oest, M.E., Dupont, K.M., Ho, K.H., Teoh, S.H., and Guldberg, R.E., *Combination of platelet-rich plasma with polycaprolactone-tricalcium phosphate scaffolds for segmental bone defect repair.* J Biomed Mater Res A, 2007. **81**(4): p. 888-99.

86. Huang, S., Jia, S., Liu, G., Fang, D., and Zhang, D., *Osteogenic differentiation of muscle satellite cells induced by platelet-rich plasma encapsulated in three-dimensional alginate scaffold.* Oral Surg Oral Med Oral Pathol Oral Radiol Endod, 2012.

87. Sell, S.A., Wolfe, P.S., Ericksen, J.J., Simpson, D.G., and Bowlin, G.L., *Incorporating platelet-rich plasma into electrospun scaffolds for tissue engineering applications.* Tissue Eng Part A, 2011. **17**(21-22): p. 2723-37.

88. Wolfe, P.S., Sell, S.A., Ericksen, J.J., Simpson, D.G., and Bowlin, G.L., *The creation of electrospun nanofibers from platelet rich plasma.* J Tissue Sci Eng, 2011. **2**(2).

89. Sell, S.A., Wolfe, P.S., Spence, A.J., Rodriguez, I.A., McCool, J.M., Garg, K., Ericksen, J.J., and Bowlin, G.L., *A preliminary study on the potential of manuka honey and platelet-rich plasma in wound healing.* International Journal of Biomaterials, 2012. **2012**: p. 313781.

90. Anitua, E., Orive, G., and Andia, I., *Use of PRGF to accelerate bone and soft tissue regeneration in postextraction sites.* Implant Dialogue, 2009: p. 3-14.

91. Lu, H.H., Vo, J.M., Chin, H.S., Lin, J., Cozin, M., Tsay, R., Eisig, S., and Landesberg, R., *Controlled delivery of platelet-rich plasma-derived growth factors for bone formation.* J Biomed Mater Res A, 2008. **86**(4): p. 1128-36.

92. Arvidson, K., Abdallah, B.M., Applegate, L.A., Baldini, N., Cenni, E., Gomez-Barrena, E., Granchi, D., Kassem, M., Konttinen, Y.T., Mustafa, K., et al., *Bone regeneration and stem cells.* J Cell Mol Med, 2011. **15**(4): p. 718-46.

93. Anitua, E., Orive, G., and Andia, I., *The therapeutic potential of PRGF in dentistry and oral implantology.* Implant and Regenerative Therapy in Dentistry: A Guide to Decision Making, 2009: p. 113-121.

94. Marquez, L., de Abreu, F.A., Ferreira, C.L., Alves, G.D., Miziara, M.N., and Alves, J.B., *Enhanced bone healing of rat tooth sockets after administration of epidermal growth factor (EGF) carried by liposome.* Injury, 2013. **44**(4): p. 558-64.

95. Mendoza-Barrera, C., Meléndez-Lira, M., Altuzar, V., and Tomás, S.A., *Ricinus communis-based biopolymer and epidermal growth factor regulations on bone defect repair: A rat tibia model.* 2003. **74**: p. 390.

96. Cuevas, P., de Paz, V., Cuevas, B., Marin-Martinez, J., Picon-Molina, M., Fernandez-Pereira, A., and Gimenez-Gallego, G., *Osteopromotion for cranioplasty: an experimental study in rats using acidic fibroblast growth factor.* Surg Neurol, 1997. **47**(3): p. 242-6.

97. Kelpke, S.S., Zinn, K.R., Rue, L.W., and Thompson, J.A., *Site-specific delivery of acidic fibroblast growth factor stimulates angiogenic and osteogenic responses in vivo.* J Biomed Mater Res A, 2004. **71**(2): p. 316-25.

98. Lisignoli, G., Zini, N., Remiddi, G., Piacentini, A., Puggioli, A., Trimarchi, C., Fini, M., Maraldi, N.M., and Facchini, A., *Basic fibroblast growth factor enhances in vitro mineralization of rat bone marrow stromal cells grown on non-woven hyaluronic acid based polymer scaffold.* Biomaterials, 2001. **22**(15): p. 2095-105.

99. Chen, J.N., Tu, C.Q., and Gong, Q., *[Experimental study on stimulation of guided bone regeneration by acid fibroblast growth factor].* Zhongguo Xiu Fu Chong Jian Wai Ke Za Zhi, 1999. **13**(5): p. 309-14.

100. Jeong, I., Yu, H.S., Kim, M.K., Jang, J.H., and Kim, H.W., *FGF2-adsorbed macroporous hydroxyapatite bone granules stimulate in vitro osteoblastic gene expression and differentiation.* J Mater Sci Mater Med, 2010. **21**(4): p. 1335-42.

101. Hong, K.S., Kim, E.C., Bang, S.H., Chung, C.H., Lee, Y.I., Hyun, J.K., Lee, H.H., Jang, J.H., Kim, T.I., and Kim, H.W., *Bone regeneration by bioactive hybrid membrane containing FGF2 within rat calvarium.* J Biomed Mater Res A, 2010. **94**(4): p. 1187-94.

102. Matsubara, H., Tsuchiya, H., Watanabe, K., Takeuchi, A., and Tomita, K., *Percutaneous nonviral delivery of hepatocyte growth factor in an osteotomy gap promotes bone repair in rabbits: a preliminary study.* Clin Orthop Relat Res, 2008. **466**(12): p. 2962-72.

103. Bussolino, F., Di Renzo, M.F., Ziche, M., Bocchietto, E., Olivero, M., Naldini, L., Gaudino, G., Tamagnone, L., Coffer, A., and Comoglio, P.M., *Hepatocyte growth factor is a potent angiogenic factor which stimulates endothelial cell motility and growth.* J Cell Biol, 1992. **119**(3): p. 629-41.

104. Tsai, S.Y., Huang, Y.L., Yang, W.H., and Tang, C.H., *Hepatocyte growth factor-induced BMP-2 expression is mediated by c-Met receptor, FAK, JNK, Runx2, and p300 pathways in human osteoblasts.* Int Immunopharmacol, 2012. **13**(2): p. 156-62.

105. Zhang, Y. and Zhang, M., *Calcium phosphate/chitosan composite scaffolds for controlled in vitro antibiotic drug release.* J Biomed Mater Res, 2002. **62**(3): p. 378-86.

106. Zhang, Y. and Zhang, M., *Cell growth and function on calcium phosphate reinforced chitosan scaffolds.* J Mater Sci Mater Med, 2004. **15**(3): p. 255-60.

107. Gentile, P., Mattioli-Belmonte, M., Chiono, V., Ferretti, C., Baino, F., Tonda-Turo, C., Vitale-Brovarone, C., Pashkuleva, I., Reis, R.L., and Ciardelli, G., *Bioactive glass/polymer composite scaffolds mimicking bone tissue.* J Biomed Mater Res A, 2012. **100**(10): p. 2654-67.

108. Sagar, N., Soni, V.P., and Bellare, J.R., *Influence of carboxymethyl chitin on stability and biocompatibility of 3D nanohydroxyapatite/gelatin/carboxymethyl chitin composite for bone tissue engineering.* J Biomed Mater Res B Appl Biomater, 2012. **100**(3): p. 624-36.

109. Palazzo, B., Gallo, A., Casillo, A., Nitti, P., Ambrosio, L., and Piconi, C., *Fabrication, characterization and cell cultures on a novel composite chitosan-nano-hydroxyapatite scaffold.* Int J Immunopathol Pharmacol, 2011. **24**(1 Suppl 2): p. 73-8.

110. Kokubo, T., Kushitani, H., Sakka, S., Kitsugi, T., and Yamamuro, T., *Solutions able to reproduce in vivo surface-structure changes in bioactive glass-ceramic A-W.* J Biomed Mater Res, 1990. **24**(6): p. 721-34.

111. Oyane, A., Kim, H.M., Furuya, T., Kokubo, T., Miyazaki, T., and Nakamura, T., *Preparation and assessment of revised simulated body fluids.* J Biomed Mater Res A, 2003. **65**(2): p. 188-95.

112. Rodriguez, I.A., Madurantakam, P.A., McCool, J.M., Sell, S.A., Yang, H., Moon, P.C., and Bowlin, G.L., *Mineralization potential of electrospun PDO-hydroxyapatite-fibrinogen blended scaffolds.* Int J Biomater, 2012. **2012**.

113. Madurantakam, P.A., Rodriguez, I.A., Cost, C.P., Viswanathan, R., Simpson, D.G., Beckman, M.J., Moon, P.C., and Bowlin, G.L., *Multiple factor interactions in biomimetic mineralization of electrospun scaffolds.* Biomaterials, 2009. **30**(29): p. 5456-64.

114. Kokubo, T. and Takadama, H., *How useful is SBF in predicting in vivo bone bioactivity?* Biomaterials, 2006. **27**(15): p. 2907-15.

115. Greenbaum, M.A. and Kanat, I.O., *Current concepts in bone healing. Review of the literature.* J Am Podiatr Med Assoc, 1993. **83**(3): p. 123-9.

116. Abarrategi, A., Moreno-Vicente, C., Martinez-Vazquez, F.J., Civantos, A., Ramos, V., Sanz-Casado, J.V., Martinez-Corria, R., Perera, F.H., Mulero, F., Miranda, P., et al., *Biological properties of solid free form designed ceramic scaffolds with BMP-2: in vitro and in vivo evaluation.* PLoS One, 2012. **7**(3): p. e34117.

117. Elshahat, A., *Correction of craniofacial skeleton contour defects using bioactive glass particles.* J. Plast. Reconstr. Surg., 2006. **30**(2): p. 113-119.

118. Ni, Z.L., Liu, H.S., Qu, Q.Y., Lu, H.L., Yan, B., and Zhang, Q.H., *Using of titanium mesh for the reconstruction of skull base defect.* Zhonghua Er Bi Yan Hou Tou Jing Wai Ke Za Zhi, 2006. **41**(5): p. 351-4.

119. Moioli, E.K., Clark, P.A., Xin, X., Lal, S., and Mao, J.J., *Matrices and scaffolds for drug delivery in dental, oral and craniofacial tissue engineering.* Adv Drug Deliv Rev, 2007. **59**(4-5): p. 308-24.

120. Barnes, C.P., Pemble, C.W., Brand, D.D., Simpson, D.G., and Bowlin, G.L., *Cross-linking electrospun type II collagen tissue engineering scaffolds with carbodiimide in ethanol.* Tissue Eng, 2007. **13**(7): p. 1593-605.

121. Sell, S.A., Francis, M.P., Garg, K., McClure, M.J., Simpson, D.G., and Bowlin, G.L., *Cross-linking methods of electrospun fibrinogen scaffolds for tissue engineering applications.* Biomed Mater, 2008. **3**(4): p. 045001.

122. Olde Damink, L.H., Dijkstra, P.J., van Luyn, M.J., van Wachem, P.B., Nieuwenhuis, P., and Feijen, J., *Cross-linking of dermal sheep collagen using a water-soluble carbodiimide.* Biomaterials, 1996. **17**(8): p. 765-73.

123. McClure, M., Sell, S., Barnes, C., Bowen, W., and Bowlin, G., *Cross-linking electrospun polydioxanone-soluble elastin blends: Material characterization.* Journal of Engineered Fibers and Fabrics, 2008. **3**(1): p. 1-10.

124. Ding, F., Liu, W., Diao, J.X., and Sun, Y., *Characterization of Alizarin Red S binding sites and structural changes on human serum albumin: a biophysical study.* J Hazard Mater, 2011. **186**(1): p. 352-9.

125. Sell, S., Barnes, C., Smith, M., McClure, M., Madurantakam, P., Grant, J., McManus, M., and Bowlin, G., *Extracellular matrix regenerated: tissue engineering via electrospun biomimetic nanofibers.* Polymer International, 2007. **56**(11): p. 1349-1360.

126. Duda, G.N., Haisch, A., Endres, M., Gebert, C., Schroeder, D., Hoffmann, J.E., and Sittinger, M., *Mechanical quality of tissue engineered cartilage: results after 6 and 12 weeks in vivo.* J Biomed Mater Res, 2000. **53**(6): p. 673-7.

127. Zhang, F., He, C., Cao, L., Feng, W., Wang, H., Mo, X., and Wang, J., *Fabrication of gelatin-hyaluronic acid hybrid scaffolds with tunable porous structures for soft tissue engineering.* Int J Biol Macromol, 2011. **48**(3): p. 474-81.

128. Nie, L., Chen, D., Suo, J., Zou, P., Feng, S., Yang, Q., Yang, S., and Ye, S., *Physicochemical characterization and biocompatibility in vitro of biphasic calcium phosphate/polyvinyl alcohol scaffolds prepared by freeze-drying method for bone tissue engineering applications.* Colloids Surf B Biointerfaces, 2012. **100**: p. 169-76.

129. Mansour, J.M., *Biomechanics of Cartilage.* Biomechanical Principles (Part I), 2003. **Ch. 5**: p. 66-79.

130. Tseng, H.J., Tsou, T.L., Wang, H.J., and Hsu, S.H., *Characterization of chitosan-gelatin scaffolds for dermal tissue engineering.* J Tissue Eng Regen Med, 2013. **7**(1): p. 20-31.

131. Hu, Y., Liu, L., Dan, W., Dan, N., Gu, Z., and Yu, X., *Synergistic effect of carbodiimide and dehydrothermal crosslinking on acellular dermal matrix.* Int J Biol Macromol, 2013. **55**: p. 221-30.

132. Xu, C., Lu, W., Bian, S., Liang, J., Fan, Y., and Zhang, X., *Porous collagen scaffold reinforced with surfaced activated PLLA nanoparticles.* ScientificWorldJournal, 2012. **2012**: p. 695137.

133. Myers, K.A., Rattner, J.B., Shrive, N.G., and Hart, D.A., *Osteoblast-like cells and fluid flow: cytoskeleton-dependent shear sensitivity.* Biochem Biophys Res Commun, 2007. **364**(2): p. 214-9.

134. Li, F.F., Chen, F.L., Wang, H., Yu, S.B., Cui, J.H., Ding, Y., and Feng, X., *Proteomics based detection of differentially expressed proteins in human osteoblasts subjected to mechanical stress.* Biochem Cell Biol, 2013. **91**(2): p. 109-15.

135. Gowen, M., Chapman, K., Littlewood, A., Hughes, D., Evans, D., and Russell, G., *Production of tumor necrosis factor by human osteoblasts is modulated by other cytokines, but not by osteotropic hormones.* Endocrinology, 1990. **126**(2): p. 1250-5.

136. Bharadwaj, S., Naidu, A.G., Betageri, G.V., Prasadarao, N.V., and Naidu, A.S., *Milk ribonuclease-enriched lactoferrin induces positive effects on bone turnover markers in postmenopausal women.* Osteoporos Int, 2009. **20**(9): p. 1603-11.

137. Shimizu, T., Akahane, M., Ueha, T., Kido, A., Omokawa, S., Kobata, Y., Murata, K., Kawate, K., and Tanaka, Y., *Osteogenesis of cryopreserved osteogenic matrix cell sheets.* Cryobiology, 2013.

138. Reinholt, F.P., Hultenby, K., Oldberg, A., and Heinegard, D., *Osteopontin--a possible anchor of osteoclasts to bone.* Proc Natl Acad Sci U S A, 1990. **87**(12): p. 4473-5.

139. Hans, S. and Mali, A.M., *Estimation and comparison of osteopontin levels in plasma in subjects with healthy periodontium and generalized chronic periodontitis and its assessment after scaling and root planing.* J Indian Soc Periodontol, 2012. **16**(3): p. 354-7.

140. Kawano, M., Yamamoto, I., Iwato, K., Tanaka, H., Asaoku, H., Tanabe, O., Ishikawa, H., Nobuyoshi, M., Ohmoto, Y., Hirai, Y., et al., *Interleukin-1 beta rather than lymphotoxin as the major bone resorbing activity in human multiple myeloma.* Blood, 1989. **73**(6): p. 1646-9.

141. Wu, L.Z., Duan, D.M., Liu, Y.F., Ge, X., Zhou, Z.F., and Wang, X.J., *Nicotine favors osteoclastogenesis in human periodontal ligament cells co-cultured with CD4(+) T cells by upregulating IL-1beta.* Int J Mol Med, 2013. **31**(4): p. 938-42.

142. Ishimi, Y., Miyaura, C., Jin, C.H., Akatsu, T., Abe, E., Nakamura, Y., Yamaguchi, A., Yoshiki, S., Matsuda, T., Hirano, T., et al., *IL-6 is produced by osteoblasts and induces bone resorption.* J Immunol, 1990. **145**(10): p. 3297-303.

143. Kurihara, N., Civin, C., and Roodman, G.D., *Osteotropic factor responsiveness of highly purified populations of early and late precursors for human multinucleated cells expressing the osteoclast phenotype.* J Bone Miner Res, 1991. **6**(3): p. 257-61.

144. Roodman, G.D., *Interleukin-6: an osteotropic factor?* J Bone Miner Res, 1992. **7**(5): p. 475-8.

145. Webb, S.J., McPherson, J.R., Pahan, K., and Koka, S., *Regulation of TNF-alpha-induced IL-6 production in MG-63 human osteoblast-like cells.* J Dent Res, 2002. **81**(1): p. 17-22.

146. Taguchi, Y., Yamamoto, M., Yamate, T., Lin, S.C., Mocharla, H., DeTogni, P., Nakayama, N., Boyce, B.F., Abe, E., and Manolagas, S.C., *Interleukin-6-type cytokines stimulate mesenchymal progenitor differentiation toward the osteoblastic lineage.* Proc Assoc Am Physicians, 1998. **110**(6): p. 559-74.

147. Bellido, T., Borba, V.Z., Roberson, P., and Manolagas, S.C., *Activation of the Janus kinase/STAT (signal transducer and activator of transcription) signal transduction pathway by interleukin-6-type cytokines promotes osteoblast differentiation.* Endocrinology, 1997. **138**(9): p. 3666-76.

148. Jiang, Z.L., Cui, Y.Q., Gao, R., Li, Y., Fu, Z.C., Zhang, B., and Guan, C.C., *Study of TNF-alpha, IL-1beta and LPS levels in the gingival crevicular fluid of a rat model of diabetes mellitus and periodontitis.* Dis Markers, 2013.

149. Boyce, B.F., Li, P., Yao, Z., Zhang, Q., Badell, I.R., Schwarz, E.M., O'Keefe, R.J., and Xing, L., *TNF-alpha and pathologic bone resorption.* Keio J Med, 2005. **54**(3): p. 127-31.

150. Garg, K., Pullen, N.A., Oskeritzian, C.A., Ryan, J.J., and Bowlin, G.L., *Macrophage functional polarization (M1/M2) in response to varying fiber and pore dimensions of electrospun scaffolds.* Biomaterials, 2013.

VITA

Isaac A. Rodriguez was born on April 29, 1985 in Fairfax, Virginia. He was raised in Fredericksburg, Virginia, graduated from Massaponax High School in June 2003, and was awarded a full scholarship to cover Bachelors, Masters, and Doctoral degrees through the Gates Millennium Scholarship (Bill and Melinda Gates Foundation). Isaac graduated from the University of Virginia (UVA) in May 2007 where he earned a Bachelors of Science in Biomedical Engineering and an Engineering Business Minor. During his time at UVA he served as President for the Society of Hispanic Professional Engineers, President for the UVA Tae Kwon Do Club, Treasurer for La Unidad Latina, Lambda Upsilon Lambda Fraternity, Inc., and a mentor for underclassmen in Biomedical Engineering. In 2007, Isaac attended Virginia Commonwealth University (VCU) for graduate school and in 2010 earned his Master's degree in Biomedical Engineering. His Master's thesis was entitled "Mineralization potential of electrospun PDO-nHA-Fibrinogen scaffolds intended for cleft palate repair". He is expected to graduate May 2013 from VCU with his Ph.D. in Biomedical Engineering as well. During his graduate career, Isaac worked in the Tissue Engineering Laboratory under the direction of Dr. Gary L. Bowlin conducting experiments in the field of bone tissue engineering. He is the author/co-author to 10 manuscripts, 2 book chapters, and 12 conference posters within the field of tissue engineering. During his tenure at VCU, Isaac was involved with several campus and community organizations. Some of which included: Student Today Alumni Tomorrow (President), Hispanic College

Fund University Chapter at VCU (Co-Founder and Alumni Advisor), the American Society of Artificial Internal Organs: for young innovators (Co-Founder and Vice President), the Alpha Psi Chapter of La Unidad Latina, Lambda Upsilon Lambda Fraternity, Inc. ((alumni advisor), VCU Latino Alumni Council (Co-Founder and Board Member), 2018 School of Engineering Strategic Planning Committee, 2012 HCF Greater Washington Hispanic Youth Institute (Assistant Director), 2012 VALHEN Hispanic College Institute (Assistant Director), and more. As a result of his dedication to the VCU and Richmond community, VCU's President, Dr. Michael Rao, awarded Isaac the Student Award for the Presidential Awards for Community and Multicultural Enrichment (PACME) in 2012. Within the PACME awards, Isaac was also awarded the capstone Riese-Melton Award (highest honor). Isaac has also won other University-wide Leadership and Service awards, VCU Alumni Association alumni service recognition, as well as the 2009-2010 Who's Who Among Students in American Universities and Colleges recognition at VCU. Isaac will continue his research in bone tissue engineering through a 2-year postdoctoral fellowship starting in the summer of 2013.